공학박사학위논문

양극 유로 개선을 통한 고분자 전해질 막 연료전지의 성능 향상에 관한 연구

Studies on the Performance Improvement of Polymer Electrolyte Membrane Fuel Cell by Modifying Cathode Flow Field

2018 년 2 월

서울대학교 대학원

기계항공공학부

신 동 규

양극 유로 개선을 통한 고분자 전해질 막 연료전지의 성능 향상에 관한 연구

Studies on the Performance Improvement of Polymer Electrolyte Membrane Fuel Cell by Modifying Cathode Flow Field

지도교수 김 민 수

이 논문을 공학박사 학위논문으로 제출함

2017 년 10 월

서울대학교 대학원

기계항공공학부

신 동 규

신동규의 공학박사 학위논문을 인준함

2017 년 12 월

위 원 장 : 민 경 덕

부위원장 : 김 민 수

위 원 : 송 한 호

위 원 : 도 형 록

위 원 : 주 현 철

Abstract

Studies on the Performance Improvement of Polymer Electrolyte Membrane Fuel Cell by Modifying Cathode Flow Field

Dong Kyu Shin
Department of Mechanical and Aerospace Engineering
The Graduate School
Seoul National University

Developing high performance polymer electrolyte membrane fuel cell (PEMFC) is now considered as the one of the most important key to make PEMFC commercialized. Although three losses which are activation losses, ohmic losses, and concentration losses occur when PEMFC operates, mitigating the concentration losses has a great effect on the overall performance of PEMFC because it is dominant losses in high load region. Since the concentration losses of PEMFC are caused by two factors oxygen depletion and flooding at the cathode side, keeping PEMFC away from those

problems can be a solution for reducing the concentration losses. PEMFC is composed of many components such as membrane electrode assembly (MEA), gas diffusion layer (GDL), gasket, bipolar plate, and end plate. Among the components, bipolar plate has a great effect on the performance related with concentration losses because it has a flow field where providing gases and produced water flow. Therefore, developing novel flow field on the bipolar plate should be conducted to make performance improved. In this study, two novel flow fields were suggested to get a better performance. The performance improvement was verified and the factors of enhancement were analyzed. The characteristics and analysis of those two flow fields will be discussed.

First of all, an inclined channel which has a gradually tapered depth was suggested as a new flow field. Unlike typical channel, the inclined channel has a different inlet and outlet depth. We designed three types of inclined channels which has the same inlet depth but different outlet depth. Therefore, the inclined channels which have different steepness level of channel depth were used as a new flow field at cathode side. Then, the performance of PEMFC was evaluated by using polarization curves and power curves. Moreover, electrochemical impedance spectroscopy (EIS) method also was used to investigate the losses of PEMFC when it operated with the inclined

channels. Pressure drop between inlet and outlet of fuel cell is one of parameters we should consider when fuel cell operates because it is related with power consumption of balance of plant (BOP) in PEMFC system. Therefore, pressure drop of PEMFC with inclined channels also measured and compared with conventional channel. Then, we verified that the performance of PEMFC was improved by about 27.9% with inclined channel. Furthermore, numerical analysis was conducted to investigate the effects of inclined channel to performance of PEMFC. To verify the effect of inclined channel on the mitigating flooding, numerical analysis for droplet dynamics was conducted. Moreover, numerical analysis for comparing oxygen concentration along the different channels was also done to explain the effect of inclined channel on the concentration losses decreasing. As a result, we could verify the effect of inclined channel on the PEMFC performance and explain how the inclined channel make PEMFC improved.

The other novel flow field suggested for developing high performance PEMFC is porous flow field by using metal foam as a cathode flow field. In case of conventional flow field, gases and liquid water are supposed to flow in certain channel. However, this conventional channel has problems such as flooding and oxygen depletion since produced liquid water can block the channel and diffusion area where gases diffuse to MEA. To solve these

problems, several types of metal foams ware inserted into cathode bipolar plate. Then, the effect of metal foam to the performance of PEMFC and characteristics of each metal foam were investigated. As a result, we found that the maximum power of PEMFC increased about 50.6% when we replaced conventional channel with proper metal foam as a cathode flow field for PEMFC. Moreover, operating characteristics of PEMFC with different metal foams was investigated by polarization curve, EIS method, and stability test. Eventually, novel flow field called mixed metal foam flow field was suggested through the results of investigation. The mixed metal was made by combining two different metal foams which have different cell size. Since metal foams show different advantage with respect to electric conductivity and oxygen diffusion, we placed a metal foam which has a large contact surface area to the upstream region of flow field. Then, metal foam which has a large diffusion region was placed to the downstream region. Finally, we could get about 60.1% of maximum power increase when novel mixed metal foam was used as a flow field to the cathode side of PEMFC. Furthermore, additional experiments were conducted to verify the effect of metal foam on the water management in PEMFC and compare diffusion between conventional channel and metal foam flow field.

Keyword: polymer electrolyte membrane fuel cell, proton exchange membrane fuel cell, PEMFC, high performance, performance improvement, inclined channel, porous flow field, metal foam, novel flow field

***Identification Number*: 2014-30290**

Contents

List of Figure

List of Tables

Nomenclature

A	drop area (mm^2)
A_c	area of channel (m^2)
C_P	specific heat (J/kg·K)
C	molar concentraion (mol/m^3)
c	chord length (mm)
D	diffusion coefficient (cm^2/s)
D_h	hydraulic diameter of channel
f	friction coefficient
H	hight (mm)
h	mass transfer convention coefficient (m/s)
J	current density (A/cm^2)
P	pressure (kPa)
Q	volmum flow rate (m^3/s)
R	gas constant (J/K·mol)
RH	relative humidity (%)
S	specific gravity of gas
SR	stoichiometric ratio (-)
Sh_F	Sherwood number
T	temperature (ºC)
U	air velcocity (m/s)
V	droplet volume (mm^3)

v	droplet velocity (m/s)
W	work (W)
X	molar fraction
Z	compressibility factor for gas

Greek

γ	heat capacity ratio
γ_{ST}	surface tension (N/m)
Δ	differential
η	efficiency
θ	contact angle (^{o})
μ	viscosity ($N \cdot s/m^2$)
ρ	density (kg/m^3)
τ	shear stress (N/m^2)

Subscript

A	advancing
an	anode
ca	cathode
cn	channel
conv	convention
comp	compressor

dp	droplet
p	presure
R	receding
ref	reference
S	static
ST	surface tension

Chapter 1. Introduction

1.1 Background of the study

Recently, improving the performance of PEMFC is one of the biggest issues in fuel cell research field because the demands of high performance and power are increasing gradually. Since PEMFC can generate electricity by converting chemical energy of hydrogen and oxygen to electrical energy and only pure water is emitted as a product, it is considered as one of the best renewable energy source able to substitute for fossil fuels. Fig. 1.1 shows how PEMFC operates. However, despite of its advantages such as relatively low operating temperature, fast response, high efficiency, and relatively cheap fuel cost, PEMFC should be more efficient and downsized to be commercialized. Therefore, improving the performance of PEMFC has been considered as one of the most important subject to many researchers.

Three losses are supposed to occur when PEMFC operates such as activation losses, ohmic losses, and concentration losses. Although all losses are inevitable when PEMFC is operated, dominant losses are different with operating current density region. Usually, the activation losses are dominant at low current density region and ohmic losses major overvoltage at

intermediate current density region. Moreover, the concentration losses are prevailing at high current density region. Even though reducing the losses to improve the performance of PEMFC is effective for all three losses, most important losses to develop high performance PEMFC are concentration losses because significant voltage drop occurs at the high current density region. Main factors causing the concentration losses can be divided into two aspects flooding and oxygen depletion. Hence, we should mitigate flooding and oxygen depletion problems to reduce the concentration losses and get performance improved.

Flooding and oxygen depletion are supposed to occur when PEMFC operates at high current density region because of a large amount of liquid water caused by electrochemical reaction. Since most liquid water is produced at the cathode side of PEMFC and has to be taken away by providing air, designing a novel flow fields which can mitigate flooding and oxygen depletion is able to be a solution for developing high performance PEMFC. In this study, two novel flow fields which can make PEMFC performance improved will be suggested. Moreover, their effects on the performance of PEMFC and characteristics will be discussed.

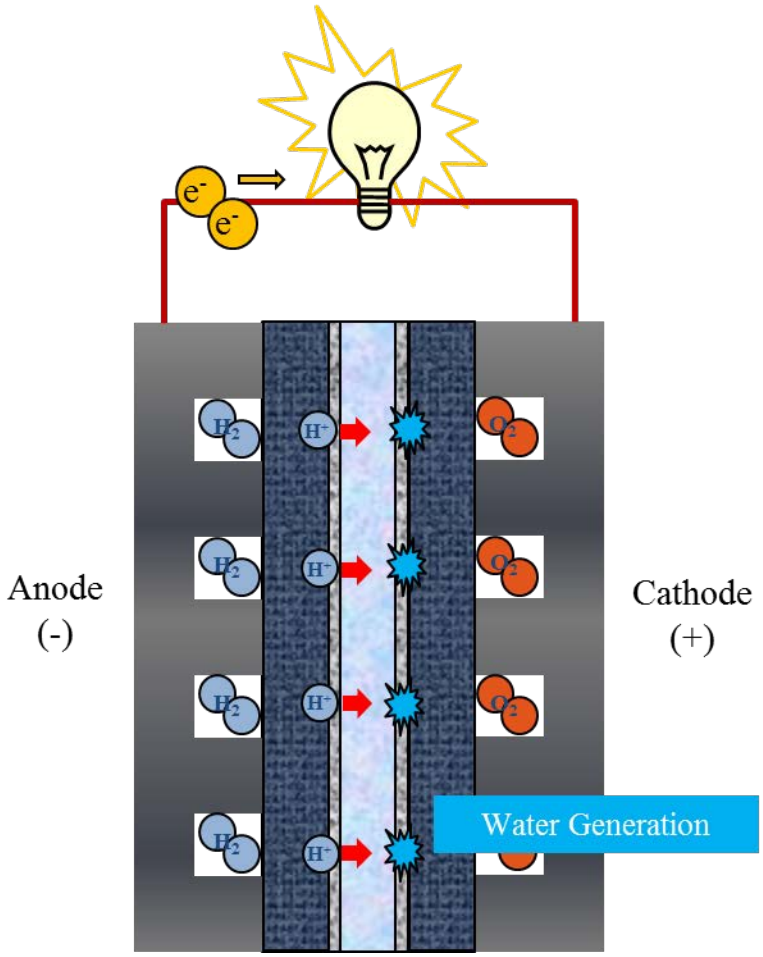

Fig. 1.1 Schematic diagram of chemical reaction in PEMFC

1.2 Literature survey

1.2.1 Water management in PEMFC

Liquid water must be produced in PEMFC because it operates under boiling point of water. Since this liquid water is directly related with performance of PEMFC, many researchers have studied about water management in PEMFC. First of all, it is essential to verify how liquid water is formed at cathode in PEMFC. Some researchers investigated how liquid water is formed inside PEMFC and transported to the flow field [1], [2]. They used a simulated fuel cell GFC with three transparent walls in conjunction with a high speed flouorescence photometry system to capture videos of dynamically deformed droplet. Then, plots were suggested to indicate the dominant horizontal and vertical deformation frequency component with the range of sizes of droplet from formation to detachment. The effect of a cross-flowing air is also investigated computationally and experimentally. CCD images were taken to reveal that the water produced within the PEMFC is forming droplets on the surface of the gas-diffusion later. Numerical model using volume of fluid (VOF) two-phase flow methodology was made to verify the formation and detachment of droplet inside PEMFC. Moreover, Tuber et al. [3] verified a water buildup in the

cathode side through the visualization experiment by using transparent PEMFC. The Effects of air stoichiometric ratio, operating temperature, relative humidity and different characteristics of diffusion layers were investigated. The influence of hydrophobicity and hydrophilicity on water transport was also verified. Subsequently, behaviors of water are also important. Hence, dynamics of droplet inside GDL and channel of PEMFC was investigated by several researchers [4]–[8]. They conducted experiment to investigate the liquid water and the flow dynamics within the transport channel with the channel acting as an optical window. Liquid water droplet movements were analyzed by considering the change of the contact angle with different air flow rates. Other research used high-resolution soft X-ray radiograph as an In-situ observation of liquid water transport in the micro porous layer (MPL) and gas diffusion layer of an operating PEMFC. Then, the dynamic liquid water transport from the cracks in the MPL to the interconnected pores in the GDL was observed. Moreover, numerical study was conducted by using 3-D CFD simulations with the VOF method for investigating water droplet dynamics in a low-temperature fuel cell microchannel. They conducted simulations for micro-channels with different cross sections such as rectangle, trapezoid, upside-down trapezoid, triangle, rectangle with a curved bottom wall, and semicircle. Eventually, they found

out that the upside-down trapezoid yields the maximum coverage ratio and water saturation, while the rectangle with a curved bottom wall results in the minimum values. Furthermore, theoretical and experimental study of the influence of controllable parameters such as surface condition, channel, geometry, droplet chord length and height, and air flow rate was conducted. They mentioned that operation conditions, droplet height, chord length, channel size and level of surface hydrophobicity directly affect the droplet instability.

Since produced liquid water has a diverse effects on the performance of PEMFC, many researchers studied about the effect of liquid water inside PEMFC. Rao et al. [9] conducted two-dimensional analysis for the effect of liquid water to the PEMFC. They concluded that a model that includes liquid water in all the layers with a flooded spherical agglomerate characterization for the reaction can predict the PEMFC behavior. Natarajan and Nguyen [10] did the similar work but they developed three-dimensional analysis and verified the effect of flooding for PEMFC system. In this study, they found out aht operating parameters have an effect on the water removal like higher temperature, and stoichiometric ratio of flow rates and lower inlet gas humidity at the high net current condition. Zhang and Gao [11] did more elaborate work for investigating the impact of liquid water on oxygen

reaction in PEMFC cathode. They made a model which has three parameters directly calculated from catalyst layer structure rather than by calibration. From this model, they can explain how to calculate the value of parameters under different water contents and analyze the effect of liquid water on the PEMFC performance. Lin et al. [12] made a model for verifying the effect of liquid water not only for catalyst layer but also GDL at cathode of PEMFC. The results of this study concluded that the water flooding situation in the catalyst layer is more severe than that in the backing layer because water is produced in the catalyst layer first. Therefore, they insisted that the catalyst layer should be considered as an individual domain. Then, they compare the results of simulation with experimental observations.

In addition, there are some studies about the way liquid water is placed in flow field and removed. Some researchers have studied about water distribution inside PEMFC because it is directly related with PEMFC performance [13]–[15]. X-ray computed tomography was used to investigate geometrical land and channel effects on spatial liquid water distribution in GDL of PEMFC under different clamping torques. Other study was focused on the formation and distribution of liquid water in GDL of PEMFC and its tendency to reduce the local effective mass diffusivity and to influence on the performance of PEMFC. Plus, soft X-ray radiography was used to

investigate the liquid water accumulation at the interface of a catalyst layer and gas diffusion media without an MPL also. Moreover, Wang et al. [16] did numerical analysis two phase flow and transport in cathode. Single and two phase regimes of water distribution and transport are classified by a threshold current density corresponding to first appearance of liquid water at the reaction site. Zhang et al. [17] conducted study on the liquid water removal in PEMFC by experimental and theoretical methods. In situ observations of the liquid water distribution on the GDL surface and inside the gas channel were made by transparent PEMFC. Theoretical methods were developed to determine what operating parameters and channel surface contact angles lead to sufficient liquid drainage from the PEMFC via corner flow. Furthermore, some studies were conducted to improve water management in PEMFC. Hassan et al. [18] verified water management in a single PEMFC with a serpentine flow field. The moisture profile models were investigated with the published data. Finally, they concluded that the strategy of saturating the hydrogen feed and using dry air has been shown to prevent water droplet formation in the cathode. Therefore, they suggested that strategy for preventing flooding phenomenon in PEMFC operation. Ge et al. [19] suggested using absorbent wicks to PEMFC to make water management enhanced. The performance of PEMFC with superabsorbent

sponge shows stable under high current density region, and also present less degradation over 120 h investigation period when both dry hydrogen and dry air were provide. Electroosmotic pumping was also proposed as a method for improving water management [20]. The results of study show that removing water from the cathode using integrated electroosmotic pumping structures improves performance and stability of PEMFC under certain operating conditions. Therefore they suggested the application of electroosmotic pumps for liquid water removal from PEMFC cathode. Turhan et al. [21] applied a passive control of liquid water storage and distribution by designing flow field of PEMFC. They suggested seven different flow field designs which have different land to channel ratio to investigate the effect of flow field to the performance of PEMFC. Eventually, they revealed that the impact of flow field geometry on stored liquid overhead is significant to the performance of PEMFC.

1.2.2 Effects of channel geometry on PEMFC

PEMFC is composed many component such as end plate, bipolar plate, MEA, gasket, GDL, and etc. Although all parts are important to operate PEMFC, bipolar plate is most important in terms of water management and gas providing because flow field is placed on the bipolar plate. Since

providing air and produced liquid water should flow in flow field of bipolar plate, designing a flow field is very important to make oxygen diffuse well to reaction site and take liquid water away efficiently. Hence, many studied have been conducted about flow field of PEMFC. Especially, many researchers studied geometry of channel because one of the typical types of flow field has a certain channel where gases and liquid water can flow. Some researchers conducted studies effects of channel geometry on the performance of PEMFC and its characteristics [22]–[27]. Different channel heights and widths were compared with the base flow field design of the serpentine flow field. Besides, numerical analysis was conducted to improve the performance of PEMFC by optimizing the channel dimensions and shape in the flow field. Single serpentine flow field was investigated to evaluate the effect of different channel shapes such as triangular and hemispherical and rectangular cross-section. Furthermore, simulation work was conducted to influence of the channel cross section aspect ratio on the performance of PEMFC with serpentine flow field. From the models, they suggested best geometrical ratio for the PEMFC in case of high operating voltages and low operating voltages. Plus parallel flow field design was also developed to eliminate the influence of other flow field design parameters like gas crossover effects at the turning point of the serpentine channel. They

concluded that narrow channel dimensions are preferred for high current densities while wider dimensions are better at low current densities. Other researchers conducted three dimensional numerical works to verify the effects of the cathode flow channel configuration on the local transport phenomena and performance for PEMFC with parallel and interdigitated flow field. They suggested proper geometric parameters for parallel and interdigitated flow field through the results of simulation. Moreover, Lin et al. [28] tried to change a height and width of channel to optimize a serpentine flow field for PEMFC. They changed the height of channel and compared the performance of PEMFC by conducting numerical analysis. Some researchers verified gas transport, flow distribution and cell performance with tapered channel geometry by using numerical analysis [29], [30]. Two-dimensional model was made to examine the reactant gas transport and the performance of PEMFC with a tapered flow channel design. Numerical predictions show that the possibility of performance improvement of PEMFC with tapered channel design. Moreover, thin stamped bipolar plate is suggested for PEMFC. They found that the aspect ratio and the base angle have significant influence on the resistance characteristics and flow distribution. Then, the result show that the homogeneity can be improved by increasing the proportion of flow resistance in the side channel. Yan et al.

[31] investigated effect of outlet channel contraction of serpentine channel on the performance of PEMFC. They conducted three-dimensional full-cell model to verify the effect of channel contraction on the performance of PEMFC. The performance improvement was predicted when the outlet channel was contracted. Moreover, they considered pressure losses to suggest optimal contraction design to the PEMFC channel. Wang et al. [32] verified an inverse geometry design problem while optimizing single serpentine flow field. They described an optimization approach that integrates the simplified conjugated-gradient scheme and a three-dimensional, two-phase, non-isothermal fuel cell model. As a result, they concluded that tapered channels can enhance sub-rib convention, local oxygen transport rate and local electrical current density.

In addition, many researchers studied not only parameters of geometry such as height, width and slope but also specific geometry which can affect the performance of PEMFC. Some researchers suggested a modified channel wall and investigated its effects [33], [34]. A turbulent channel flow with a smooth upper wall and lower wall consisting of square bars was investigated. Plus, numerical simulation of spherical dimple located on the wall of a narrow square channel was also conducted. Wang et al. [35] studied numerically to investigate local transport phenomena in PEMFC. They made

three-dimensional models of PEMFC with parallel and interdigitated flow field including the effects of liquid water formation on the reactant gas transport. The results of simulation revealed that the cell performance is independent of the flow channel designs and operating parameters at high operating voltages while both factors have significant influences on the cell performance at the low operating voltages. Turbulent flow inside a channel was a also investigated by some researchers [36], [37]. A numerical work to investigate the flow field in a model distribution header manifold of PEMFC was conducted. They concluded that the flow field and flow structures may impact the overall pressure drop along the header and the effective cross sectional area for the flow leaving the header. The LES simulation and PIV measurements was used to investigate the effect of header. Fontana et al. [38] studied effects of flow channel with non-uniform cross sectional area on PEMFC. They investigated the performance of PEMFC. They found out the effect of non-uniform cross sectional area on the performance of PEMFC by conducting numerical analysis. Furthermore, studied about optimum design of ratio between channel and rib were also conducted. Peng et al. [39] suggested optimum channel shape for metal bipolar plate. They used design of experiments methods and an adoptive simulated annealing optimization method to get an optimization model of flow channel section design for

hydroformed metal bipolar plate. They suggested an optimized channel dimension and PEMFC with optimized channel showed better performance.

1.2.3 Novel flow field for high performance PEMFC

Recently, many researchers try to design a novel flow field which can drastically improve the performance of PEMFC. Some researchers studied the way to make performance improved by modifying typical flow field such as serpentine, parallel, interdigitate channel [40]–[43]. Three-path serpentine and parallel-serpentine flow field with various depth were designed and investigated experimentally. Plus, die-sinking microelectrical discharge machining was used to fabricate bipolar plate. They concluded that a deep channel is required to leave sufficient space for reactant transportation and water removal. However, too deep channel can reduce the convective mass transport and cell performance because of its low flow velocity. Furthermore, novel style of straight flow channel tapered in height or width is proposed to improve the efficiency of PEMFC. They showed the relation between cell performance and channel height and width. Other researchers analyzed seven flow field and investigated PEMFC performance at the optimum channel to rib ratio. They showed the effects of flow field on current density, mass fraction of reactant gases, water distribution and flooding by

conducting numerical analysis. Also, the effects of stoichiometry, pressure and temperature on the performance of PEMFC are verified. Moreover, a blockage was inserted in channel to improve the performance of fuel cell [44]–[47]. A novel configuration of partially blocked channel with baffle plates transversely inserted in the channel. They investigated the effects of the blockage with various gap ratios and numbers of the baffle plates, the fuel flow Reynolds number and the porosity of the diffusion layer on the reactant gas transport, and the pressure drop across the channel length. The results showed that reducing the gap size and/or increasing the baffle number to improve the reactant gas transport can cause a high pressure drop. As a result, they suggested optimized condition with consideration of PEMFC performance and pressure drop. Other research was conducted to investigate the application of the baffle-blocked flow channel for reactant transport and PEMFC performance. They verified that the liquid water effect is significant and should be considered in the modeling at the low voltage conditions. Moreover, the performance of PEMFC can be enhanced at a higher air velocity on the cathode side because mass transport loss decreases. Other researchers conducted experimental work to investigate the effect of in-line and staggered blockage configurations within a parallel flow field by comparing the performance of PEMFC. The results showed that the

performance of PEMFC was improved by up to 28% with staggered configuration while in-line configuration improved cell performance by 18%. Furthermore, they mentioned that the performance of PEMFC was even improved when they considered a pressure drop increase with blockages. Han et al. [48] studied the performance of PEMFC with wave-like surface design in cathode channel. This wave shape was designed to increase the velocity gradient of the flow from the gas diffusion layers. As a results, they verified that the concentration losses induced by unstable mass transfer was delayed and the cell performance was improved by 5.76% with 25 cm^2 active area fuel cell and by 5.17% with 84 cm^2 unit-cell.

In addition, novel flow fields which have a no channel were applied to PEMFC. Porous metallic material was suggested as a flow field to PEMFC to improve the performance [49]–[51]. Porous media was suggested as a flow distributor of PEMFC. They compare the cell performance with different flow field design. Moreover, activated carbon air cathode was developed as an alternative to a platinum-catalyzed electrode for fuel cell. Srouji et al. [52], [53] obtained a ultra-high current density PEMFC by applying metallic element architecture as a flow field. They applied porous metallic flow field to the PEMFC. As the cell operating temperature increased, the effect of back diffusion was reduced due to the diminishing

liquid water content in the cathode catalyst layer, and at critical liquid water content, anode dry-out was triggered primarily through electro-osmotic drag. They showed that the trade-off between liquid water overshadowing cathode catalyst sites and its contribution in promoting back diffusion is a significant in systems with anode dry-oulet limited operation. Moreover, the performance of PEMFC with metallic element flow filed architecture was investigated comparing with PEMFC with conventional parallel flow field fuel cell. They found out that a heliox mixture at the cathode of both cells can improve mass transport for the parallel cell, but no oxygen gas phase transport limitation at high current density condition for the open metallic element architecture. Furthermore, Murata et al. Tanaka and Shudo studied about diffusion layer-less PEMFC [54]. They designed a gas diffusion layer-less fuel cell composed of a corrugated-mesh and found out that it showed low flooding performance even in the high current density region because the gases are provided more uniformly to the catalyst layer comparing with the conventional channel and GDL. Moreover, they measured the conductivities and the contact resistances of each material in the GDL-less fuel cell under various mechanical compression pressures, and a coupled mechanical-electric-electrochemical model was developed to investigate the effect of electrical resistance on the PEMFC performance. A Novel

corrugated mesh flow field was applied for reducing flooding to improve the performance of PEMFC [55]. They verified that the polarization curve of the corrugated-mesh fuel cell showed a lower flooding tendency at a high current density comparing with fuel cell which has conventional flow field. However, high frequency resistance of fuel cell increases with corrugated-mesh because of fewer contact point between mesh and micro porous layer. They also investigated the conductivity and rigidity of MPL to try to reduce the flow-channel pattern resistance. Furthermore, significant performance improvement of PEMFC was developed by using a stainless-steel microcoil gas flow field [56]. They used microcoil as the gas flow channel as well as the gas diffuser directly on the MPL without using the conventional GDL to improve the performance of PEMFC by mitigating the flooding phenomenon. However, high frequency resistance in this case is also slightly higher than PEMFC with conventional channel due to the differences in the electron conduction path. Therefore they suggested that the in-plain electron conductivity in the MPL as a key to improving the microcoil PEMFC performance.

1.3 Objective

In this study, novel flow field are suggested to mitigate the concentration losses in PEMFC because it causes drastic voltage drop at the high current density region. Since developing a high performance PEMFC is considered as one of the most important issues to make it commercialize, designing a new flow field which can improve the performance of PEMFC by reducing the concentration losses should be conducted.

The concentration losses are supposed to occur at any operating conditions, it becomes severe when PEMFC operates at high current density region. Since oxygen depletion and flooding are widely considered as a reason of concentration losses, the concentration losses should increase when PEMFC operates at the condition where lots of liquid water is produced as a product of electrochemical reaction. Meanwhile, the performance of PEMFC can be improved by reducing the effect of oxygen depletion and flooding.

Providing gases and produced liquid water flow in the flow field on the bipolar plate of PEMFC. Therefore, flow field is used not only as a place where providing gases can be fed to reaction site but also as a path for purging the liquid water came from the result of electrochemical reaction.

Hence, design of flow field is closely related with the concentration losses of PEMFC.

To mitigate the concentration losses of PEMFC, the flow field on the bipolar plate should be modified

Chapter 2. Experimental study on the PEMFC with inclined channel

2.1 Introduction

In this chapter, study on the PEMFC with inclined channel which is one of the novel flow fields suggested in this paper will be introduced. In general, we use a flow field such as serpentine, parallel, and interdigitate for PEMFC. For example, Fig. 2.1 shows design of serpentine flow path. Although all flow fields have different flow paths, we usually used a straight channel, which means that we used channel has a constant width and depth along with the length. However, we suggested a novel flow field where channel gets narrower from inlet to outlet and named it as an inclined channel. This inclined channel was designed for mitigating concentration losses in PEMFC. As described in chapter 1, concentration losses of PEMFC occur because of flooding and oxygen depletion at the cathode. Hence, inclined channel was applied to the cathode flow field and the effects on the performance were investigated by several methods. Moreover, we designed three types of inclined channels to investigate impact of inclination level on the performance of PEMFC.

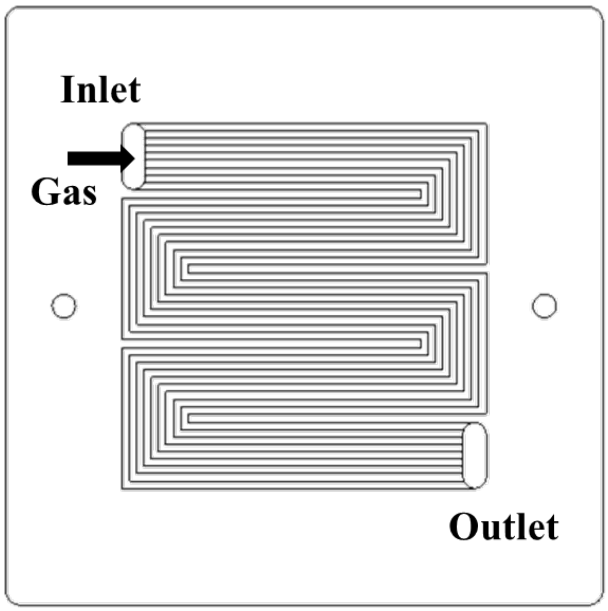

Fig. 2.1 Design of serpentine type flow path

2.2 Experimental setup

2.2.1 PEMFC components

A single unit cell which has an active area of 25 cm^2 (5 cm × 5 cm) was used in this study. Unit cell is composed of many components such as insulated end plate, carbon graphite bipolar plate, Teflon type gasket, GDL, and MEA. Fig. 2.2 shows how those components are assembled. All unit cells used in this study were assembled the same clamping torque of 9.04 N·m. The MEA (CNL Energy, KOREA) is made by using Nafion-211 which has a catalyst layer treated as 0.3 mg/cm^2 platinum loading for anode and 0.45 mg/cm^2 for cathode. Type of GDL (SIGRACET®, Germany) used in this study is SIGRACET 39BC which is a non-woven carbon paper type GDL with 5% PTFE treated micro porous layer (MPL).

2.2.2 PEMFC system apparatus

Since many BOPs are required to operate unit cell, some apparatuses were used to build an experimental setup. Fig. 2.3 presents the experimental setup for this study. It can be divided into four parts hydrogen providing system, air providing system, humidification system, and thermal management system. The flow rates of hydrogen and air were controlled by

mass flow controllers (EL-FlOW® Base, Bronkhorst, Netherlands). All mass flow controllers used in this study were calibrated before experiment. Moreover, we controlled a relative humidity (RH) of inlet gases by adjusting the temperature of bubbler humidifier. Humidity & temperature transmitter (MHT337, VAISALA, Finland) was used to verify the accuracy of RH control. Hence, hydrogen and air used as providing gases have 99.999% of purity. Moreover, they were humidified before being provided into PEMFC through bubbler type humidifier. Column type heater was used as thermal management system to maintain a cell temperature at certain value. Operation range and accuracy of equipment are presented in Table 2.1.

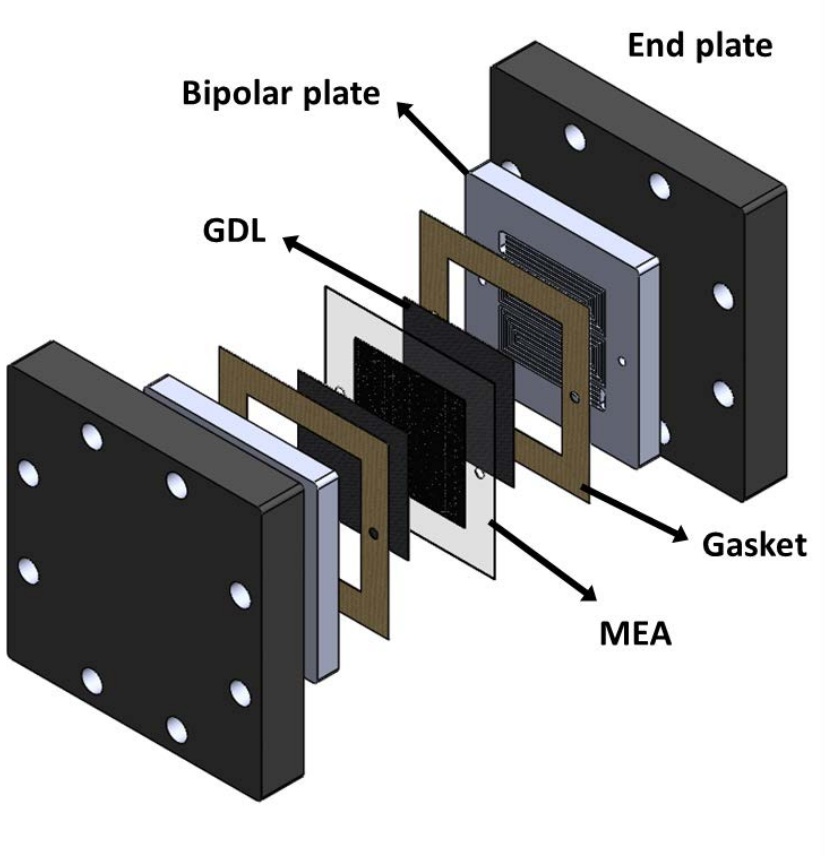

Fig. 2.2 Assembly diagram of PEMFC components

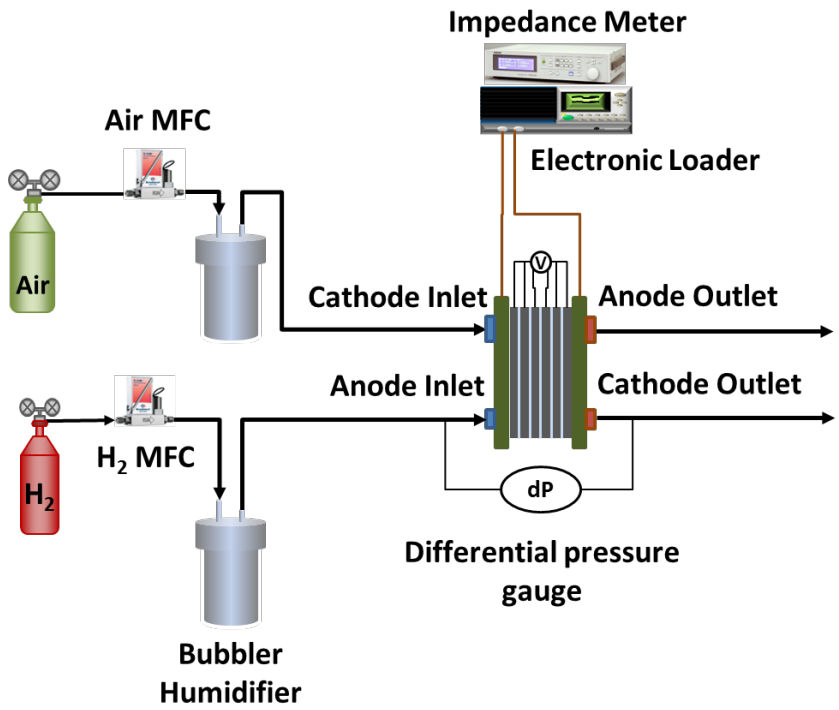

Fig. 2.3 Experimental setup

Table 2.1 Operation range and accuracy of apparatus

Apparatus	Range	Accuracy
Mass flow controllers (H_2)	0~2 lpm	±0.5% Rd plus ±0.1% FS
Mass flow controllers (Air)	0~2 lpm	±0.5% Rd plus ±0.1% FS
Humidity & temperature transmitter	0~100%	±0.3ºC (at 60ºC)

2.2.3 Measuring devices

In this study, many devices were used to measure experimental values for evaluating system. First of all, electric loader (PLZ1004W+PLZ2004WB, KIKUSUI, Japan) was used for investigating the performance of PEMFC. In addition, an impedance meter (KFM2150, KIKUSUI, Japan) was used for conducting EIS method. Electric loader and impedance meter are presented in Fig. 2.4. Moreover, we measured gas temperature and cell temperature by using thermocouples (T-type). Pressure drop between inlet and outlet of PEMFC was measured by differential pressure transmitter (DPDH0005R, Sensys, Korea). Data acquisition from sensors was handled by personal computer. Measuring range and accuracy of all equipment are presented in Table 2.2.

Fig. 2.4 Electric loader and impedance meter

Table 2.2 Measuring range and accuracy of equipment

Equipment	Range	Accuracy
Electric loader	1.5~150 V 0~200 A	±(0.2%+0.1% f.s)
Impedance meter	0.0001~9.9999 Ω	±(0.3%+0.3% f.s)
Thermocouples	-200~350ºC	±0.3ºC
Differential pressure transmitter	0~20 kPa	±0.5%

2.3 Preparation for experiment

2.3.1 Inclined channel design

Fig. 2.1 shows typical shape of serpentine flow field. In general, PEMFC channel has a constant width and depth for providing gases and purging liquid water generated from the electrochemical reaction at MEA. However, as described in Fig. 2.5 (b), depth of inclined channel gets narrower toward outlet while conventional channel has a constant channel depth represented in Fig. 2.5 (a). We designed three types of inclined channels which have a different level of inclination. The details of geometry of conventional channel and inclined channels are presented in Table 2.3. Although, conventional channel and inclined channels have the same channel depth, channel width, rib width, and rib height, inclined channels have a different channel depth comparing with conventional channel because of its tapered shape. Since the depth of inclined channels decrease gradually, inclined channel #3 has a highest inclination level among the inclined channels and level of inclination is the lowest when we use inclined channel #1. We applied these inclined channels to the cathode flow field of PEMFC because concentration losses of PEMFC are mostly happen at the cathode

side. Hence, as we adopt inclined channel to the cathode flow field, we can evaluated the effects of inclined channels on the performance of PEMFC.

2.3.2 Activation cycle

In general, PEMFC shows unstable performance when it is operated right after assembly. Since the MEA is supposed to be dehydrated condition after manufacturing, the MEA should be pre-operated in specific conditions called as activation cycle to show stable performance. The activation cycle was run to activate MEA by hydrating. After activation cycle, we can guarantee that PEMFC shows steady behavior. The details of activation cycle are as follows.

- Sequence 1 (constant voltage mode): 0.65 V (10 minutes) ➔ 0.50 V (10 minutes)
- Sequence 2 (constant voltage mode): 0.90V (1 minute) ➔ 0.89 V (1 minute) ➔ ⋯ ➔ 0.46 V (1 minute) ➔ 0.45 V (1 minute)

  Step voltage: 0.01 V

The activation cycle is composed of two sequences. Even though two sequences are under constant voltage mode, voltage values and their changes

are different. During the activation cycle, PEMFC operates under condition of sequence 1 first and moves on to condition of sequence 2. When PEMFC operated sequence 1 and 2, it is considered as operating a cycle of activation cycle. In this study, all PEMFCs were operated under 20 cycles of activation cycle before investigation. At the end of activation cycle, voltage of PEMFC was evaluated at certain current density (e.g. 1.0 A/cm^2) to verify whether PEMFC is fully activated or not.

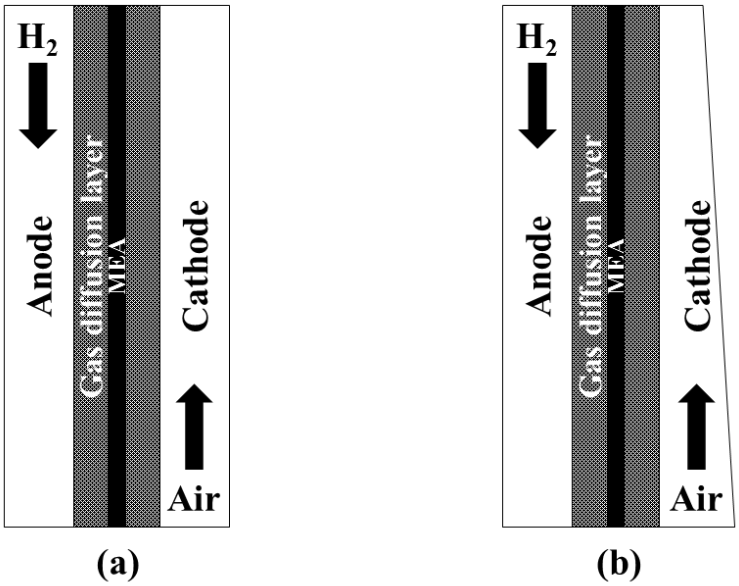

Fig. 2.5 Schematic diagram of cathode channel: (a) Conventional channel

(b) Inclined channel

Table 2.3 Specification of channels

Parameter \ Channel	Conventional	Inclined #1	Inclined #2	Inclined #3
Channel width (mm)	1.0	1.0	1.0	1.0
Inlet channel depth (mm)	0.9	0.9	0.9	0.9
Outlet channel depth (mm)	0.9	0.6	0.4	0.2
Rib width (mm)	0.9	0.9	0.9	0.9

Table 2.4 Experimental conditions

Parameter	Value
T_c (°C)	40/60
SR_{an}	1.5
SR_{ca}	2.0
RH_{an} (%)	100
RH_{ca} (%)	100

2.4 Results and discussion

2.4.1 PEMFC performance

2.4.1.1 Polarization curve

The polarization curves of PEMFC with different channels are presented in Fig. 2.6. There are two graphs presenting voltage change with respect to current density. Fig. 2.6 (a) presents polarization curves when PEMFC operates at 60ºC while Fig. 2.6 (b) shows the result at 40ºC. Each graph has four polarization curves showing the voltage of PEMFC with different channels. A circle mark represents the voltage of PEMFC with conventional channel, and others show that with inclined channels.

As described in Fig. 2.6, PEMFC with inclined channels shows higher voltage than PEMFC with conventional channel at the same current density. Hence, it can be said that the performance of PEMFC is improved with inclined channels. However, although all inclined channels make performance improved, the improvement levels are different with ratio between inlet and outlet depth. When PEMFC operates at 60ºC, inclined channel #3 which has the greatest inclination level shows the highest voltage. As mentioned in section 2.1., concentration losses of PEMFC usually occur

because of oxygen depletion and flooding. However, the effect of oxygen depletion can be mitigated when PEMFC operates with inclined channel because of channel decline. The details of effect of channel decline on the oxygen depletion will be discussed in Chapter 3. Moreover, flooding alleviation also can improve the performance of PEMFC. Since inclined channels make providing air gets fast along with channel because of its tapered shape, air can easily blow the liquid water produced from the electrochemical reaction. The details of effect of inclined channel on the removing liquid water also will be discussed in Chapter 3.

Meanwhile, PEMFC shows somewhat different behavior when it operates at 40ºC. As shown in Fig. 2.6 (b), despite all inclined channel show the better performance than conventional channel, inclined channel #3 no longer shows the highest voltage among the inclined channels. The inclined channel #2 and #3 show almost the same voltage in any current density region. Since temperature of PEMFC decreases, the amount of produced liquid water should increase. Although inclined channels have an advantage to remove liquid water inside PEMFC, this lots of water can block the narrow outlet. Hence, when PEMFC operates at lower operating temperature, inclined channel #3 which has the narrowest outlet no longer can manage the liquid water better than other inclined channel.

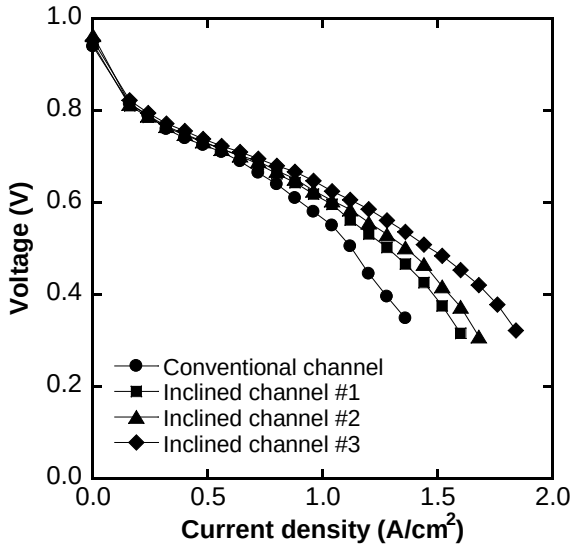

(a)

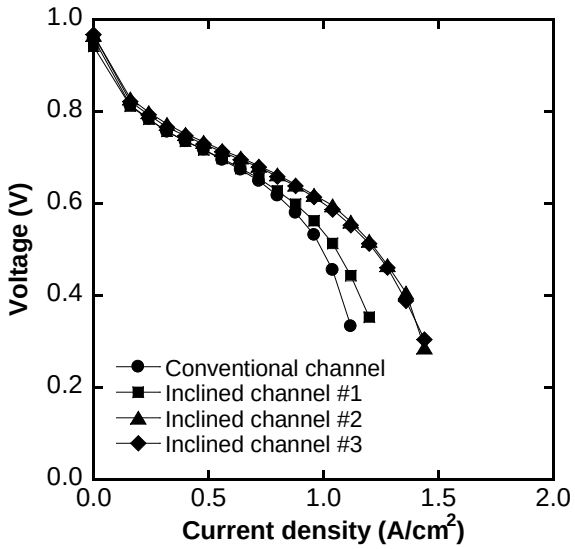

(b)

Fig. 2.6 Polarization curves of PEMFC with conventional and inclined channels conventional channel: (a) T_c = 60ºC (b) T_c = 40ºC

2.4.1.2 Power curve

Since comparing the power curves of PEMFC is the easiest way to investigate the performance, power values of PEMFC will be compared and discussed in this section. Fig. 2.7 shows the power of PEMFC with respect to current density. In Fig. 2.7 (a), as already mentioned in the section 2.4.1, PEMFC with inclined channel #3 shows the best performance among the different types of channels. The maximum power of PEMFC with inclined channel #3 is 18.4 W at 1.52 A/cm^2. The value of maximum power of PEMFC with inclined channel #3 is about 28.7% greater than that with conventional channel 14.3 W at 1.024 A/cm^2. However, the maximum power of PEMFC with inclined channel #3 is no longer greatest when it operates at 40ºC. PEMFC shows best performance with inclined channel #2, and maximum power of PEMFC with inclined channel #2 is 15.5 W at 1.12 A/cm^2. However, PEMFC with conventional channel only generates 12.8 W of maximum power at 0.88 A/cm^2. Hence, the maximum power of PEMFC is improved by about 21.1% at 40ºC when conventional channel of PEMFC is replaced with inclined channel #2.

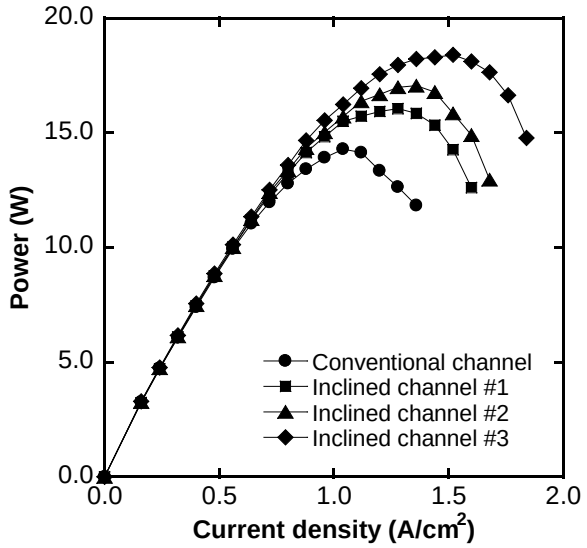

(a)

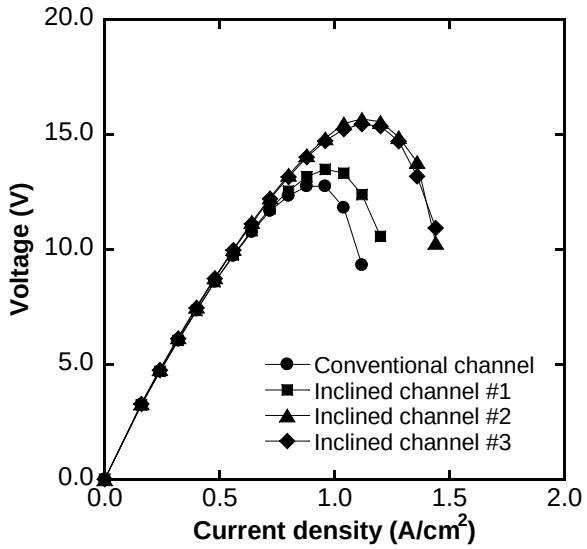

(b)

Fig. 2.7 Power curves of PEMFC with conventional and inclined channels

conventional channel: (a) T_c = 60ºC (b) T_c = 40ºC

2.4.2 Electrochemical impedance spectroscopy

EIS method is widely used technique to investigate the losses in PEMFC. As mentioned in previous chapters, three losses activation losses, ohmic losses, and concentration losses are supposed to occur in PEMFC. Although all losses occur at any operating conditions, dominant losses are different with current density region. The activation losses are dominant at low current density and the ohmic losses are the most significant at intermediate current density and lastly, the concentration losses of PEMFC have the greatest effect on the performance of PEMFC at high current density region. Hence, ETS method in this study was conducted at three current density region. Current density condition was chosen to 0.32 A/cm^2, 0.64 A/cm^2, and 1.28 A/cm^2 at 60ºC of operating temperature and 0.32 A/cm^2, 0.64 A/cm^2, and 0.96 A/cm^2 at 40ºC. Although two conditions are the same for both operating temperatures, high current density region is different with operating temperature because 1.28 A/cm^2 of current density is high enough to shut PEMFC down at 40ºC. To get a stability of experiment we chose different high current density region for PEMFC operating at 40ºC. The impedance spectra were recorded which frequency was swept from 4 kHz to 1.26 Hz with 32 moving average. The measuring AC current was fixed as 10% of the DC current magnitude.

Fig. 2.8 and 2.9 show the results of EIS method. First of all, high frequency resistance (HFR) is represented by the interception between kinetic loop and resistance axis at high frequency [57], and all graphs show that there are no differences in HFR. This result means that the ohmic losses of PEMFC are not that much varied with conventional and inclined channels. Therefore, we can neglect the effect of ohmic losses on the performance of PEMFC with inclined channels.

In terms of low frequency resistance (LFR), arc size at low frequency represents the concentration losses of PEMFC [58]. However, the concentration losses of PEMFC are dominant at the high current density region. Therefore, we can easily compare the concentration losses between PEMFC by verifying the arc size of low frequency in Fig. 2.8 (c) and Fig. 2.9 (c). In Fig. 2.8 (c), PEMFC with conventional channel shows the greatest size among the all graphs. Moreover, PEMFC with inclined channel #3shows the smallest arc size at low frequency, and this result can explain the result of polarization curve represented in Fig. 2.6 (a). Since PEMFC with inclined channel #3 has the smallest concentration losses, PEMFC shows the best performance when it operates with inclined channel #3. Meanwhile, Fig. 2.9 (c) shows different results with Fig. 2.8 (c). The arc size at low frequency of PEMFC with inclined channel #2 is the smallest among

the graphs. As mentioned before in section 2.4.1.2, PEMFC with inclined channel #3 is no longer shows the best performance when it operates at 40ºC. The result represented in Fig. 2.8 (c) can explain and support the results of polarization curves. PEMFC with inclined channel #2 shows the maximum power at 40ºC in section 2.4.1.1 because it has the smallest concentration losses verified in Fig. 2.8 (c).

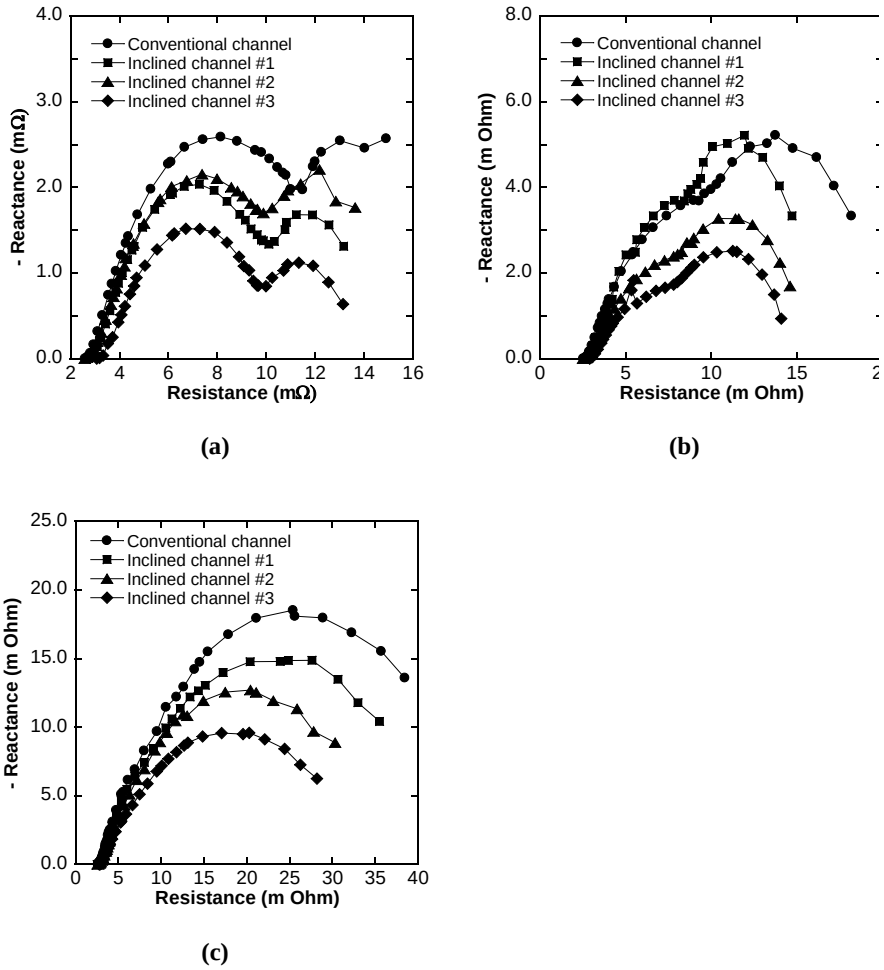

Fig. 2.8 Electrochemical impedance spectroscopy for PEMFC with conventional channel and inclined channels at 60ºC: (a) J = 0.32 A/cm^2 (b) J = 0.64 A/cm^2 (c) J = 1.28 A/cm^2

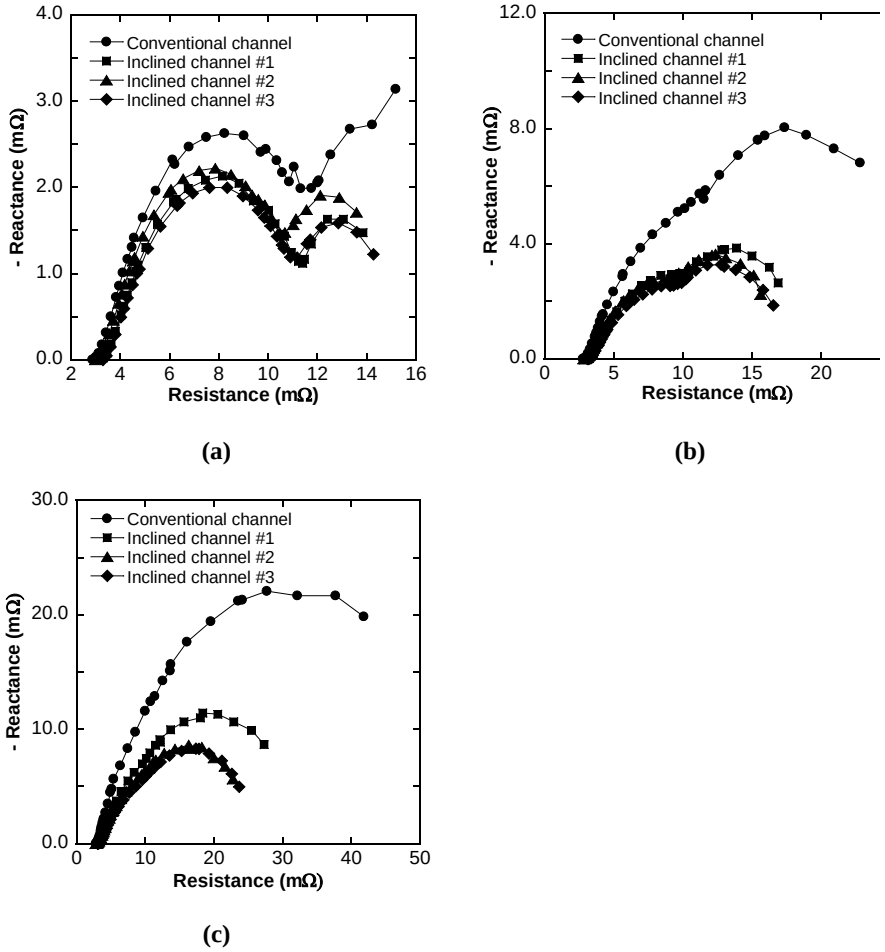

Fig. 2.9 Electrochemical impedance spectroscopy for PEMFC with conventional channel and inclined channels at 40ºC: (a) J = 0.32 A/cm^2 (b) J = 0.64 A/cm^2 (c) J = 0.96 A/cm^2

2.4.3 Pressure drop

In previous sections, remarkable performance enhancement is verified when conventional channel of PEMFC is replaced with inclined channels. However, still there is some concern about increase of pressure drop between inlet and outlet of cathode side because of tapered shape. Hence, pressure drop of PEMFC between inlet and outlet was investigated for conventional channel and inclined channels. The pressure drop was measured by using differential pressure transmitter. Fig. 2.10 shows the results of measurement. All PEMFCs with inclined channels shows higher pressure drop than that with conventional channel. Moreover, the inclined channel #3 shows the highest pressure drop among the inclined channels. This result is quite reasonable because the inclination level of inclined channel 3# is the greatest among the inclined channels.

Since magnification of pressure requires more compression work in BOP subsystem, calculating a compression work of PEMFC with different channels should be conducted to verify whether the inclined channel is adaptable to a real system or not. Eq. 2.1 was used for calculating the compression work [59].

$$W_{comp} = c_p \frac{T_c}{\eta_{comp}} \left[\left(\frac{P + \Delta P}{P} \right)^{\frac{\gamma - 1}{\gamma}} - 1 \right] \dot{m} \quad (2.1)$$

As a result of calculation, required compression works to provide air are presented in Fig. 2.11. As represented in both graphs of Fig. 2.11, the compression work for PEMFC system increases when inclined channel was used for PEMFC because pressure drop rises. However, this compression work is very small when it is compared with produced power from PEMFC represented in Fig. 2.7. For instance, the compression work is lower than 1% of produced power from PEMFC at any current density. Therefore, additional compression work by replacing conventional channel with inclined channel is quite negligible.

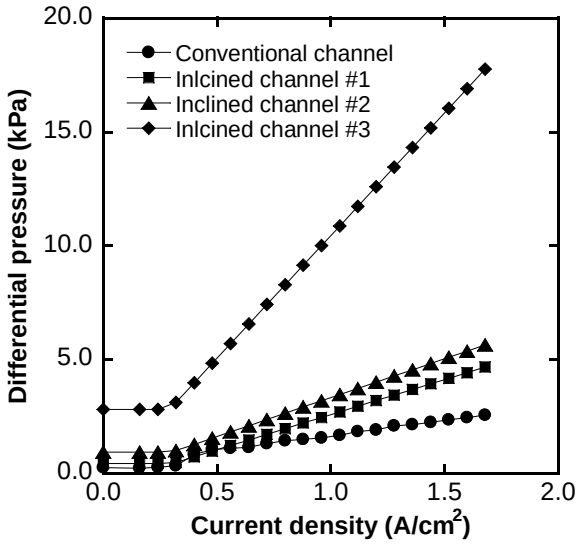

(a)

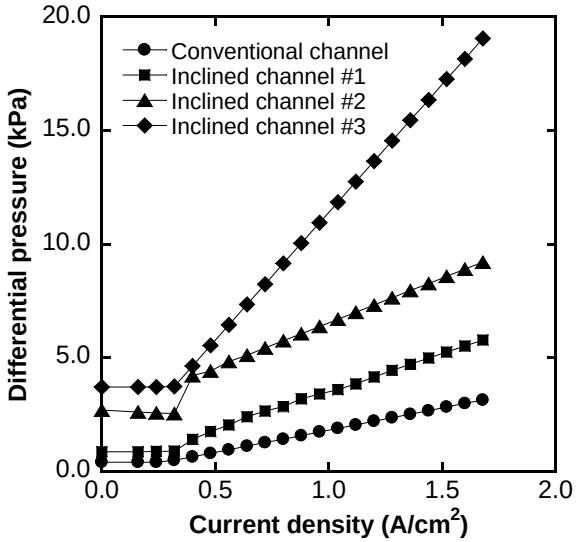

(b)

Fig. 2.10 Pressure drop between inlet and outlet of single cell with different cell temperatures: (a) 60ºC (b) 40ºC

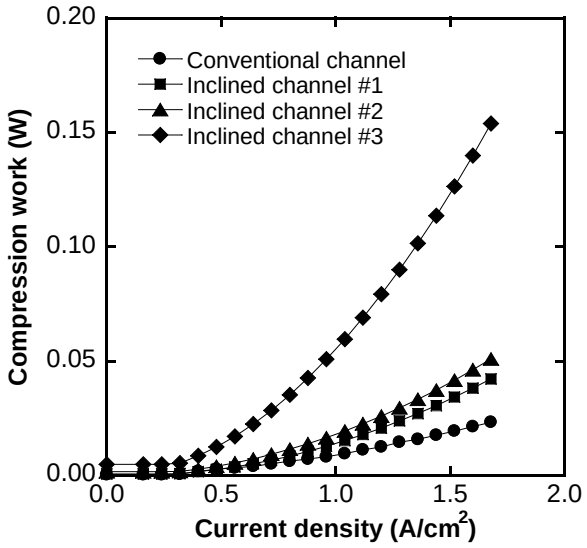

(a)

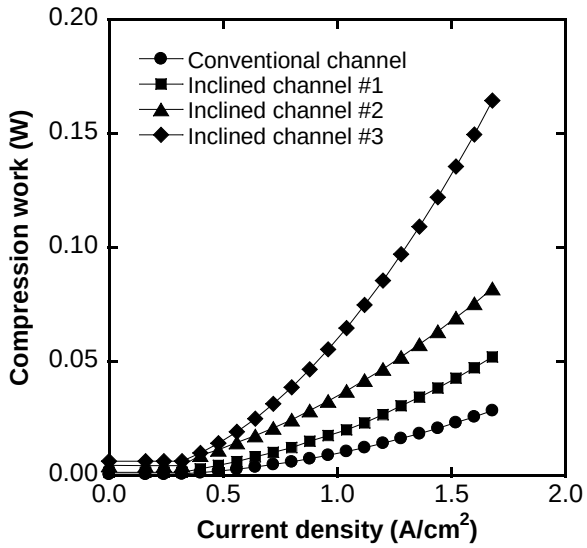

(b)

Fig. 2.11 Compression work calculated to provide required pressure drop with different cell temperatures: (a) 60ºC (b) 40ºC

2.4.4 Net power

In previous section 2.4.3, the results show that compression work for providing gas is negligible when conventional channel of PEMFC is replaced with inclined channels. However, net power of PEMFC with different channel shapes should be calculated and compared to evaluate the exact value of generated power. Eq. 2.2 was used for calculating the net power.

$$W_{net} = W_c - W_{comp} \quad (2.2)$$

Fig. 2.11 includes two graphs presenting the results of calculation. In Fig. 2.11 (a) shows calculated net power when PEMFC operates at 60ºC, and PEMFC with inclined channel #3 generates maximum net power enhanced by about 27.9% compared with maximum net power of PEMFC with conventional channel. Meanwhile, PEMFC with inclined channel #2 generated maximum power at 40ºC, and the enhancement is about 20.8% compared with PEMFC with conventional channel.

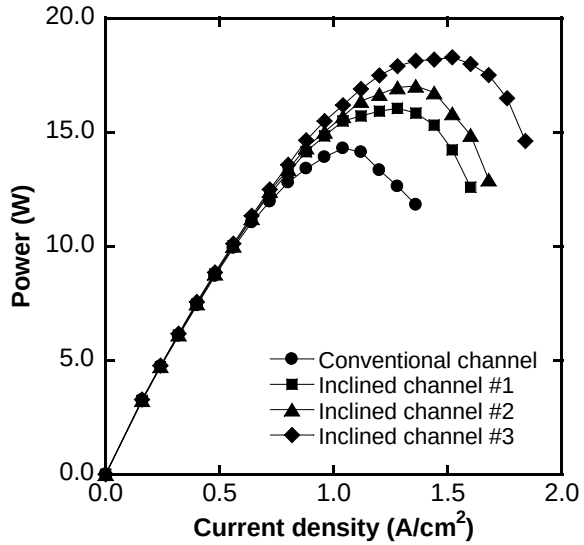

(a)

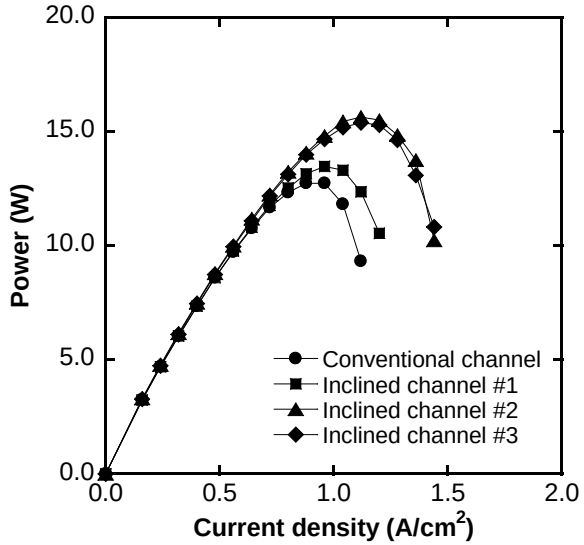

(b)

Fig. 2.12 Net power of PEMFC system with different channel shapes at different operating temperature: (a) 60ºC (b) 40ºC

2.5 Summary

In this chapter, three types of inclined channels were suggested as a flow field of PEMFC. The inclined channels were designed to have a tapered channel shape and three types of inclined channels have different levels of inclination. These different types of inclined channels were applied to the cathode side of PEMFC to evaluate the effects of inclined channel on the performance of PEMFC. As a result, the performance of PEMFC with inclined channels was improved and the results are verified through polarization curves and power curves. Furthermore, EIS method was conducted to investigate how inclined channel make performance improved. The results of EIS show that the concentration losses of PEMFC decrease when conventional channel is replaced with inclined channel. Hence, we can verify that inclined channels make PEMFC performance improved by reducing the concentration losses. Moreover, pressure drop of conventional channel and inclined channel was compared to evaluate the suitability of inclined channel to real PEMFC system and calculate net power. As a result, the results show that maximum net power of PEMFC in enhanced about 27.9% at operating temperature of 60ºC and 20.8% at 40ºC. Furthermore, suitability of inclined channel to PEMFC was also verified through the results of calculation of compression work.

Chapter 3. Numerical analysis of PEMFC with inclined channel

3.1 Introduction

In this chapter, numerical analysis for investigating the effect of inclined channel on the performance of PEMFC will be discussed. As verified experimentally in Chapter 2, the performance of PEMFC is enhanced with inclined channels. Moreover, EIS method shows that the concentration losses of PEMFC decrease when inclined channel is applied to the cathode flow field. Since the concentration losses of PEMFC are related with two factors oxygen depletion and flooding, analysis for investigating effect of inclined channel on those factors is fundamental to explain performance enhancement of PEMFC with inclined channel. Hence, there are two parts in this chapter, which are numerical studies on the oxygen depletion and behavior of liquid water in channel. As a result, experimental results of chapter 2 will be explained, and effect of inclined channel will be discussed.

3.2 Effect of inclined channel on the oxygen depletion

3.2.1 Governing equations

In Fig. 3.1, there are two figures representing conventional channel and inclined channel. Both figures are on the x-y coordinate and air flows from left to right while hydrogen flows right to left. In Fig. 3.1 (a), we assumed control volume which has a rectangular shape the same with real channel. Meanwhile, the inclined channel presented in Fig. 3.1 (b) has a trapezoid shape control volume and size of control volume is varied along the x-coordinate, and shapes of control volume are the same with inclined channels. In this numerical work, there are some assumptions. First of all, water exists only in the vapor form in channels, which means there is no liquid water produced by electrochemical reactions. Moreover, only y-directional convention and diffusion were considered. In addition, all oxygen which diffuses from channel to MEA is completely used up at the reaction site. Since both channels have the same channel width and length, the only difference between conventional channel and inclined channels is the channel depth. The depth of inclined channel gets narrower along with the flow path, which the depth of conventional channel is constant. This

different depth of channel affects to the velocity of the supplied air and the convention and diffusion rate along the y-direction. The governing equations for numerical analysis are as follows [60].

$$\frac{\partial \rho}{\partial t} = \nabla \cdot (\rho \mathrm{v}) \tag{3.1}$$

$$\mathrm{C_{O_{2,in}}} = \mathrm{X_{O_2}} \cdot \frac{\mathrm{P}}{\mathrm{RT}} \tag{3.2}$$

$$\mathrm{C_{O_{2,out}}} = \mathrm{C_{O_{2,in}}} \cdot \exp\left(-\frac{\mathrm{h} \cdot \mathrm{x}}{\mathrm{v} \cdot \mathrm{H_{cn}}}\right) \tag{3.3}$$

$$\mathrm{C_{O_{2,conv}}} = \mathrm{C_{O_{2,in}}} - \mathrm{C_{O_{2,out}}} \tag{3.4}$$

$$\mathrm{h} = \frac{\mathrm{Sh_F D_{O_2-N_2}(T)}}{\mathrm{H_{cn}}} \tag{3.5}$$

$$D_{O_2-N_2}(T) = D_{O_2-N_2} \cdot T_{ref} \cdot \left(\frac{T}{T_{ref}}\right)^{1.5} \tag{3.6}$$

Eq. 3.1 is continuity equations and used for calculate velocity of air along with the channels. Eq. 3.2 is the formula for calculating the concentration of the supplied air, which is dependent on the pressure, temperature, and molar fraction. Moreover, Eq. 3.3 is the formula for oxygen concentration of the air leaving the control volume. As a result, oxygen concentration of convention from control volume to the porous media can be described as Eq. 3.4. In process of analysis, oxygen concentration calculated

through the Eq. 3.3 becomes supplied oxygen concentration for the next control volume. Eq. 3.5 represents the mass transfer coefficient calculated by Sherwood number, binary gas diffusion coefficient and the depth of the channel. Binary gas diffusion coefficient can be calculated by using Eq. 3.6. The flow rate of supplied into single channel was assumed to 0.6 Lpm, and volume of air along the channel decreases as oxygen diffuses from channel to MEA.

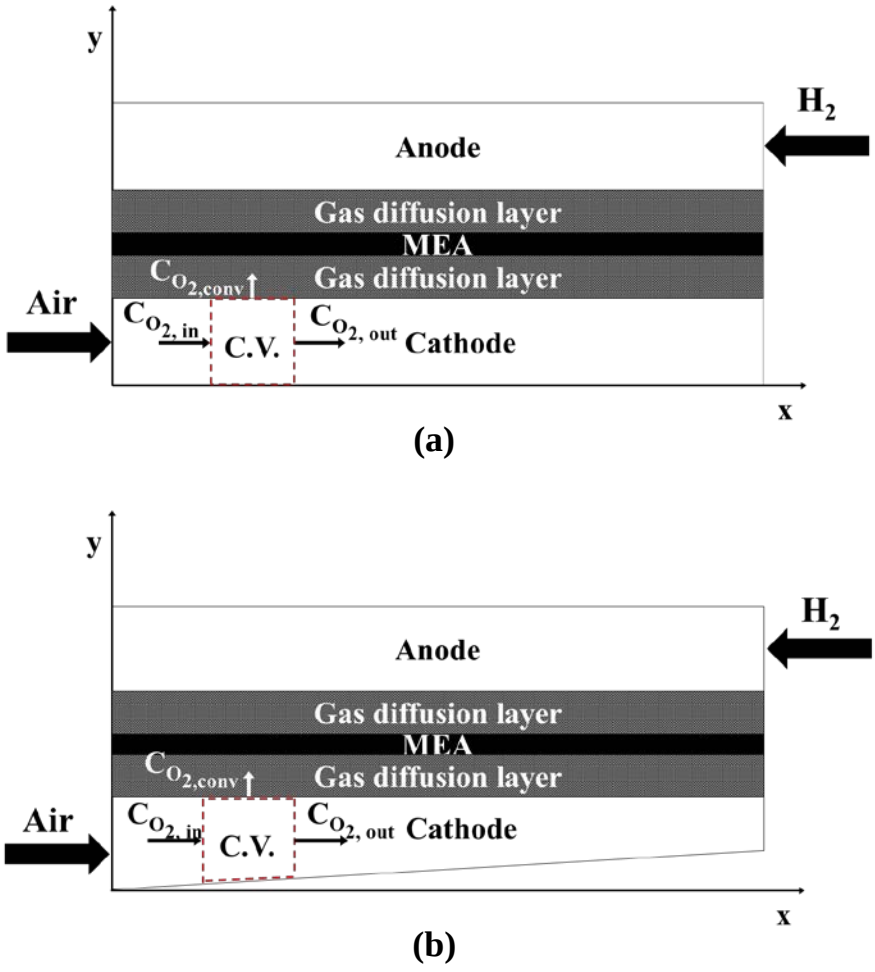

Fig. 3.1 Schematics of numerical analysis for different channel designs: (a) conventional channel (b) inclined channel

3.2.2 Air velocity analysis

Fig. 3.2 shows the result of calculation for air velocity in different types of channel. Since velocity is dependent on the depth of flow path as well as flow rate, the velocity of air in the inclined channels should increase along the channel. However, the velocity of air in conventional channel is supposed to decrease along the channel because oxygen diffuse to MEA and react with hydrogen. This increase of air velocity in the inclined channels has an advantage in terms of removing liquid water. Although liquid water is not considered in this numerical analysis, the effects of high air velocity in the inclined channels will be discussed in followed section 3.3.

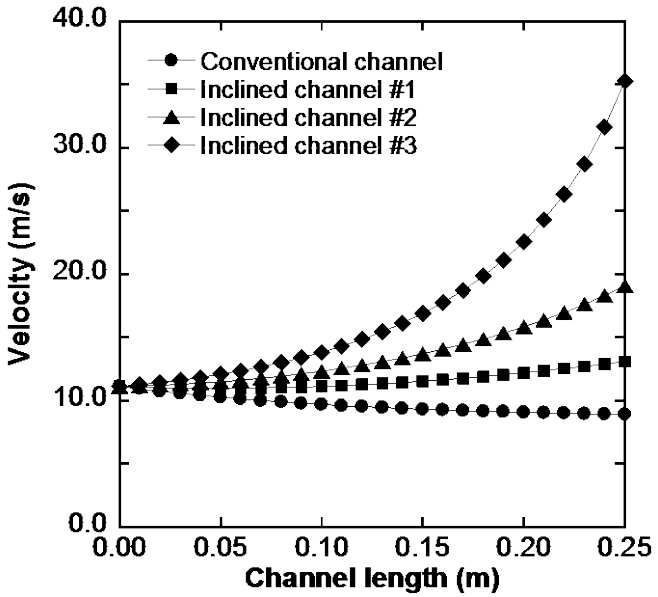

Fig. 3.2 Air velocity variation along the different types of channel

3.2.3 Oxygen diffusion analysis

In Chapter 2, we verified that the performance of PEMFC is enhanced when conventional channel is replaced with inclined channel. Moreover, the results show that the inclined channel makes performance improved by mitigating the concentration losses in PEMFC. Therefore, numerical analysis for oxygen diffusion was conducted in this chapter to verify the effect of inclined channel on the concentration losses of PEMFC.

Fig. 3.3 represents the results of analysis. The graph shows oxygen concentration in control volume along the channel. Since numerical analysis was conducted from inlet and outlet of channel, graph shows the oxygen concentration at the outlet of channel where the value of channel length is 0.25 m. In graph, the oxygen concentration in the inclined channels decreases sharper than the oxygen concentration in the conventional channel. Moreover, the value of oxygen concentration at the outlet of inclined channel is lower than that of conventional channel. This result means that oxygen is easier to diffuse from channel to MEA when air flows in inclined channel. The higher inclination level makes the more oxygen diffuse from channel to MEA. Since oxygen concentration is highly related with concentration losses of PEMFC, high oxygen concentration can reduce the concentration losses

of PEMFC. Hence, this result of analysis can explain the experimental result of Chapter 2.

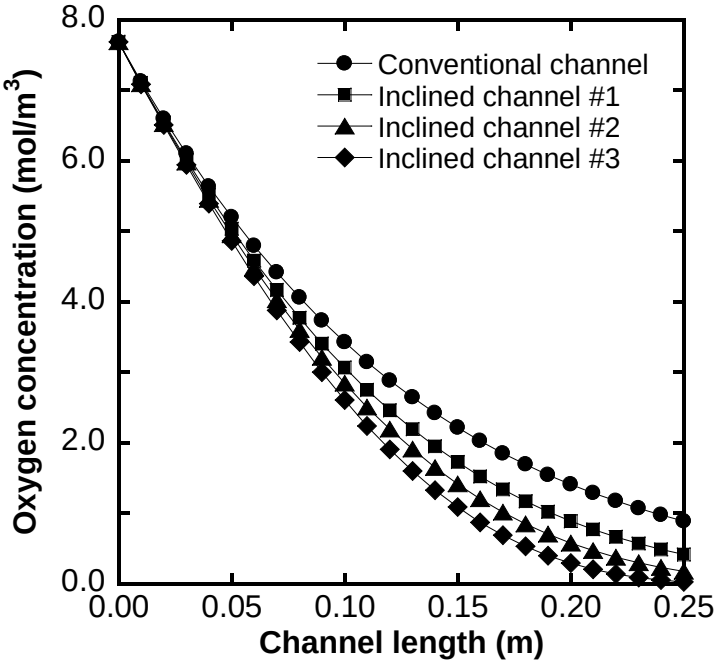

Fig. 3.3 Variation of oxygen concentration along the different types of channel

3.3 Effect of inclined channel on the liquid water

3.3.1 Governing equations

In this section, numerical analysis for investigating the effect of inclined channel on the liquid water. Especially, droplet dynamics in different shapes of channel was analyzed. Although liquid water flow can be divided into four types which are single-phase flow, droplet flow, film flow, and slug flow [4], analyzing the behavior of droplet is most important because it is a fundamental mechanism of removing water in PEMFC channel. Fig. 3.3 shows different shapes of droplet when it is in the channel where air flows. When liquid water is produced at the MEA, it moves from MEA to channel through the porous media. After moving to the channel, it forms droplet. Fig. 3.3 (a) represents a static condition of droplet which means that droplet is stable and not deformed. Fig. 3.3 (b) is deformed shape of droplet because of the forces exerting on droplet.

In Fig. 3.5, two forces exerting on the droplet are represented. When air flows in channel, drag exerts on the droplet. Meanwhile, surface tension force of droplet occurs opposite direction of shear force. Hence, equations

for both forces are necessary. First of all, drag force which can make droplet deformed and move will be discussed. The equations are as follows [7].

$$F_{drag} = F_p + F_{shear} \tag{3.7}$$

$$F_p = (p_a - p_b) \times H_{cn} \times 2R = \frac{48\mu B^2 U H_{dp}^2}{\left(H_{cn} - H_{dp}\right)^3 (1 - \cos\theta_A)^2} \tag{3.8}$$

$$F_{shear} = \tau_{xy} \times (2R)^2 = \frac{24\mu H_{cn} U H_{dp}^2}{\left(H_{cn} - H_{dp}\right)^2 (1 - \cos\theta_A)^2} \tag{3.9}$$

$$F_{drag} = \frac{24\mu H_{cn} U H_{dp}^2}{\left(H_{cn} - H_{dp}\right)^2 (1 - \cos\theta_A)^2} \left(\frac{4H_{cn}}{\left(H_{cn} - H_{dp}\right)^2} + 1 \right) \tag{3.10}$$

$$F_{drag} = f(U, H_{dp}, H_{cn}, \theta_A) \tag{3.11}$$

Eq. 4.1 represents that drag force on the droplet is composed of two forces pressure difference and shear. Hence, we can verify that drag force on the droplet is function of air speed, droplet height and advancing angle. On the other hand, equations for surface tension force exerting opposite direction to drag force are also needed. Fig. 3.6 shows surface tension exerting on the droplet. We assume that the advancing angle and receding

angle change linearly along the boundary of contact surface. The details of equations for surface tension force are as follows [7].

$$\theta = \frac{\theta_A - \theta_R}{\pi} \quad \alpha + \theta_A \tag{3.12}$$

$$dF_{ST} = \gamma_{ST} \frac{c}{2} d\alpha \cos(\pi - \theta) \cos\alpha \tag{3.13}$$

$$F_{ST} = 2\int_0^{\pi} dF_{ST} = -\gamma_{ST} c \int_0^{\pi} \cos\left(\frac{\theta_R - \theta_A}{\pi} + \theta_A\right) \cos\alpha d\alpha \tag{3.14}$$

$$\therefore F_{ST} = -\gamma_{ST} c \frac{\pi}{2}\left[\frac{\sin(\theta_R) + \sin(\theta_A)}{\theta_A - \theta_R - \pi} + \frac{\sin(\theta_R) + \sin(\theta_A)}{\theta_A - \theta_R + \pi}\right] \tag{3.15}$$

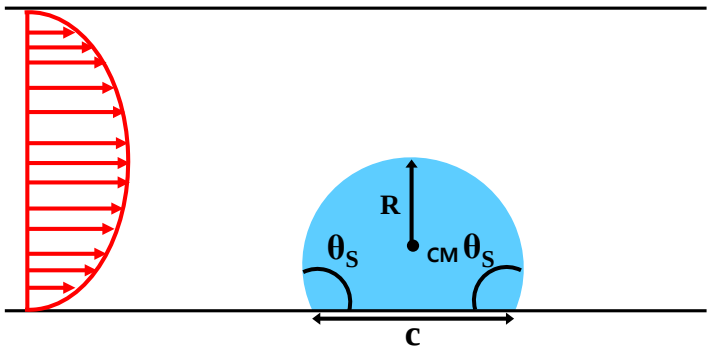

(a)

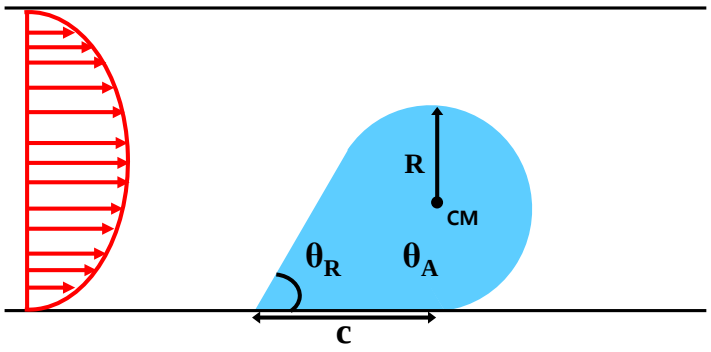

(b)

Fig. 3.4 Shapes of droplet in air flow channel: (a) static droplet (b) deformed droplet

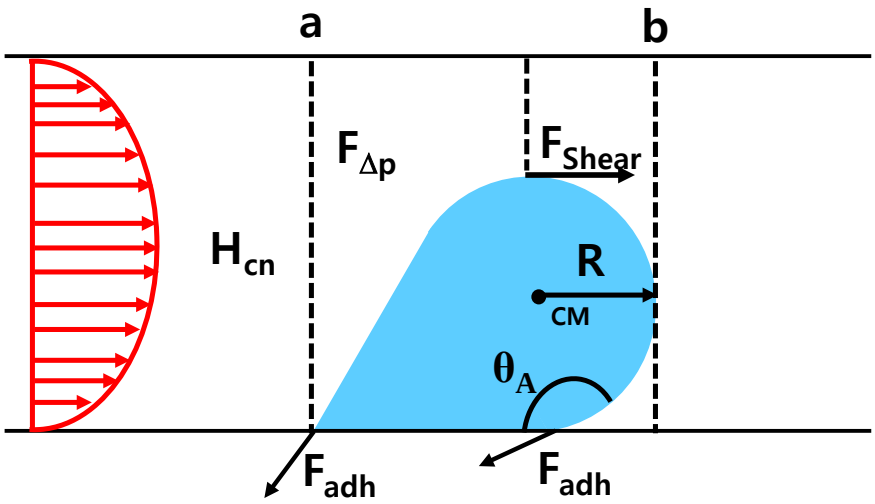

Fig. 3.5 Forces exerting on the deformed droplet

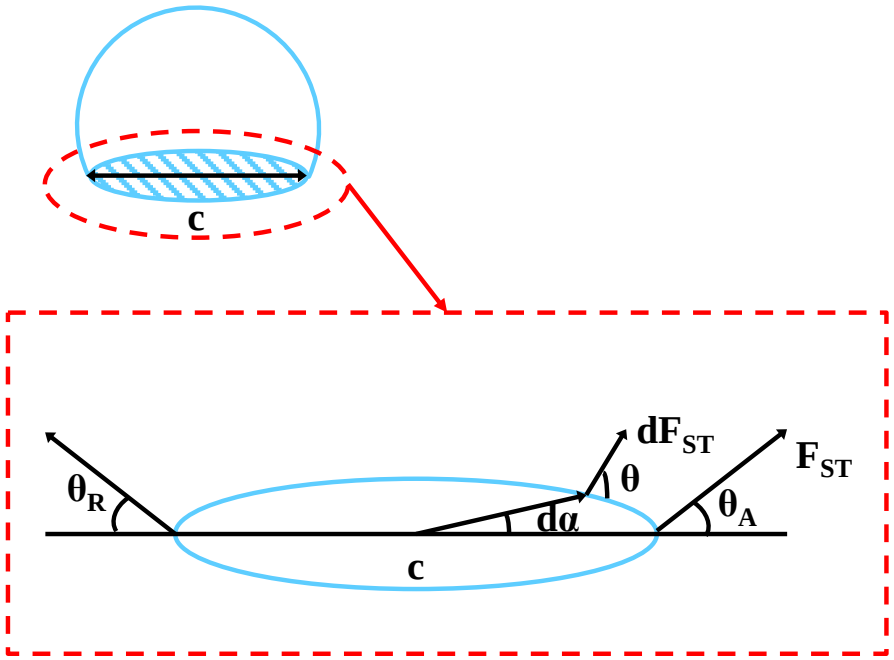

Fig. 3.6 Surface tension force exerting on the droplet

3.3.2 Droplet deformation

3.3.2.1 Contact angle relationship

As described in previous section, there are two forces exerting on the droplet, which are drag force and surface tension force. When these two forces are exerted on the droplet, the shape of droplet should be deformed. Although droplet remains stable when surface tension force is larger than drag force, droplet is supposed to be deformed when drag force becomes larger than surface tension force as represented in Fig. 3.7. Since surface tension force increases when droplet is deformed, two forced get equilibrated at certain point. Hence, before all, the relationship between advancing contact angle and receding contact angle should be calculated to verify how contact angle changes. Moreover, we made a two assumption which are constant chord length verified by previous works [61] and biunique correspondence between advancing contact angle and receding contact angle. The equations for calculation are as follows.

$$c_s = 2\sin\theta_s \left[\frac{3V}{\pi(4-(1+\cos\theta_S)^2(2-\cos\theta_S))}\right]^{\frac{1}{3}} \tag{3.16}$$

$$H_{dp} = R(1-\cos\theta_A) \tag{3.17}$$

$$A = \frac{R^2}{2}\left[\theta_A + \theta_R - \sin(2\theta_A) + \sin(\theta_A - \theta_R) + \frac{4\sin^3\left(\frac{\theta_A - \theta_R}{2}\right)}{\sin\theta_R}\sin\left(\frac{\theta_A + \theta_R}{2}\right)\right] \quad (3.18)$$

$$c = 2R\sin\theta_A + \frac{2R\sin^2\left(\frac{\theta_A - \theta_R}{2}\right)}{\sin\theta_R} \quad (3.19)$$

$$f(\theta_A, \theta_R) = c - c_s \quad (3.20)$$

$$\forall\theta_A^*, \theta_R^* | f(\theta_A^*, \theta_R^*) = 0 \quad (3.21)$$

Fig. 3.8 represents the results of calculation using above equations. In this calculation we used some parameters such as static contact angle, volume of droplet, and chord length which are 130º, $133 \cdot 10^{-3}$ mm^3, and 0.5 mm respectively. Those values were adapted from previous study [62]. From the result represented in Fig. 3.8, the equation for relationship between receding contact angle and advancing contact angle can be made, and it is as follows.

$$\theta_R = 5.7663{\theta_A}^4 - 64.548{\theta_A}^3 + 270.66{\theta_A}^2 - 504.63\theta_A + 354.92 \quad (3.22)$$

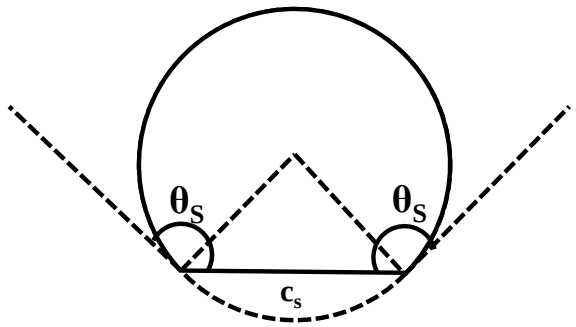

(a)

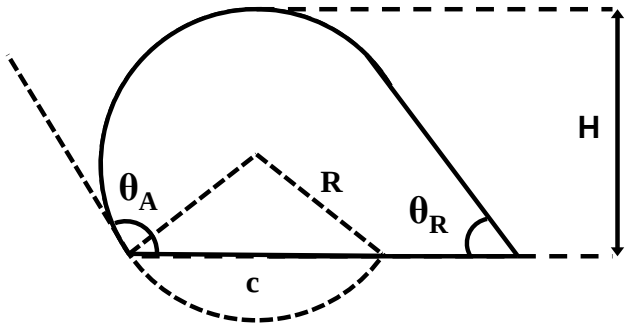

(b)

Fig. 3.7 Surface tension force exerting on the droplet: (a) static (b) deformed

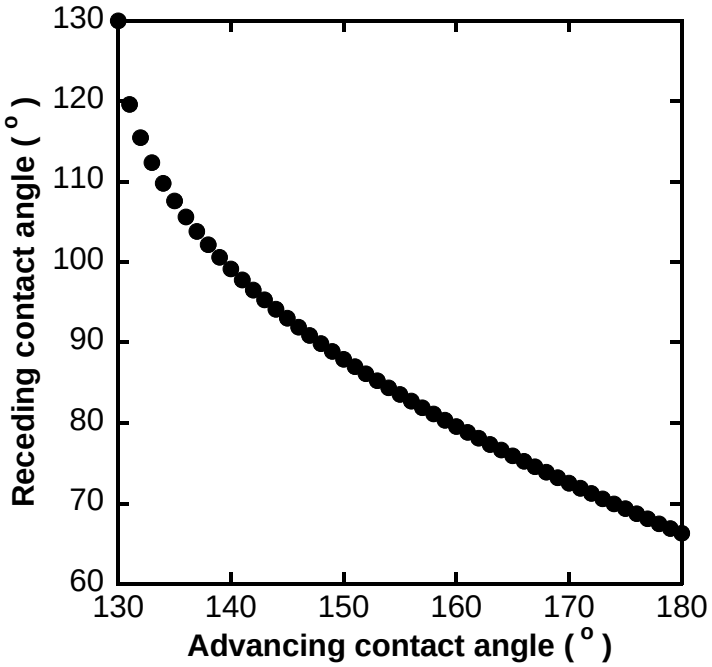

Fig. 3.8 Receding contact angle variation with advancing contact angle

3.3.2.2 Center of mass

Since center of mass of droplet should be changed when droplet is deformed, it is necessary to calculate the variation of center of mass. Fig. 3.9 shows droplet on the x-y coordinate. The center of mass of droplet is on the x-y coordinate and changed as described in Fig. 3.9 (b). Moreover, center of mass was calculated as follows.

$$y_{CM} = \frac{R^3}{A}\left[\frac{4}{3\sin^2\theta_R}\sin^4\left(\frac{\theta_A-\theta_R}{2}\right)\sin^2\left(\frac{\theta_A+\theta_R}{2}\right)\right.$$
$$-\frac{2}{3}\sin^3\left(\frac{\theta_A-\theta_R}{2}\right)\cos\left(\frac{\theta_A+\theta_R}{2}\right)+\frac{2}{3}\sin^3\theta_A+\cos\theta_A$$
$$\left.+\cos\theta_A\left(\frac{\sin(2\theta_A)}{2}-\frac{\theta_A+\theta_R}{2}-\frac{\sin(\theta_A-\theta_R)}{2}\right)\right] \qquad (3.23)$$

if $\theta_R > \frac{\pi}{2}$

$$x_{CM} = \frac{R^3}{A}\left[\frac{8}{3\sin^2\theta_R}\sin^5\left(\frac{\theta_A-\theta_R}{2}\right)\sin^3\left(\frac{\theta_A+\theta_R}{2}\right)-\frac{16\cot\theta_R}{3}\left[\sin\left(\frac{\theta_A-\theta_R}{2}\right)\sin\left(\frac{\theta_A+\theta_R}{2}\right)\right]\right.$$
$$-\frac{4\cot\theta_R}{3\sin\theta_R}\left[\sin^2\left(\frac{\theta_A-\theta_R}{2}\right)\sin\left(\frac{\theta_A+\theta_R}{2}\right)\right]^2$$
$$+2\left[\frac{2\sin\theta_A}{\sin\theta_R}-\frac{1}{3}\right]\sin^3\left(\frac{\theta_A-\theta_R}{2}\right)\sin\left(\frac{\theta_A+\theta_R}{2}\right)$$
$$\left.+\sin\theta_A\left[\frac{\theta_A+\theta_R}{2}+\frac{\sin(\theta_A-\theta_R)-\sin(2\theta_A)}{2}\right]\right] \qquad (3.24)$$

if $\theta_R < \frac{\pi}{2}$

$$x_{CM} = \frac{R^3}{A}\left[\frac{8}{3\sin^2\theta_R}\sin^5\left(\frac{\theta_A-\theta_R}{2}\right)\sin\left(\frac{\theta_A+\theta_R}{2}\right) + 4\cot^2\theta_R\left[\sin\left(\frac{\theta_A-\theta_R}{2}\right)\sin\left(\frac{\theta_A+\theta_R}{2}\right)\right]^3\right.$$
$$+\frac{4\cot\theta_R}{3\sin\theta_R}\left(1-\frac{2}{\sin\theta_R}\right)\left[\sin^2\left(\frac{\theta_A-\theta_R}{2}\right)\sin\left(\frac{\theta_A+\theta_R}{2}\right)\right]^2$$
$$+2\left[\frac{2\sin\theta_A}{\sin\theta_R}-\frac{1}{3}\right]\sin^3\left(\frac{\theta_A-\theta_R}{2}\right)\sin\left(\frac{\theta_A+\theta_R}{2}\right)$$
$$+4\sin\theta_A\cot\theta_R\left(1-\frac{1}{\sin\theta_R}\right)\left[\sin\left(\frac{\theta_A-\theta_R}{2}\right)\sin\left(\frac{\theta_A+\theta_R}{2}\right)\right]^2$$
$$\left.+\sin\theta_A\left[\frac{\theta_A+\theta_R}{2}+\frac{\sin(\theta_A-\theta_R)-\sin(2\theta_A)}{2}\right]\right] \qquad (3.25)$$

As a result, the center of mass of droplet can be represented in Fig. 3.10. We used the same assumption for the parameters of droplet represented in section 3.3.2.1. The graph shows that center of mass of x-coordinate gets smaller with increase of advancing contact angle while center of mass of y-coordinate gets bigger. The results of center of mass are very important to analyze dynamics of droplet. Hence, these results will be used in section 3.3.3.

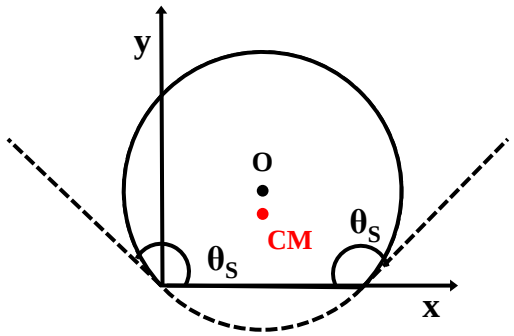

(a)

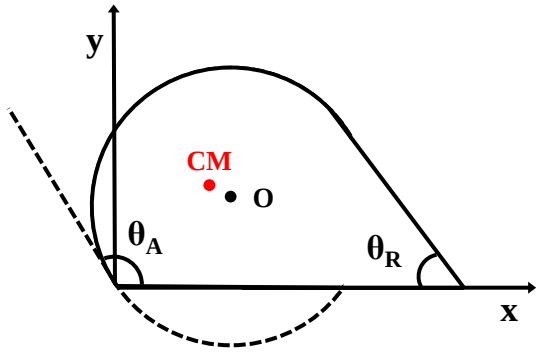

(b)

Fig. 3.9 Center of mass of droplet at different conditions: (a) static (b) deformed

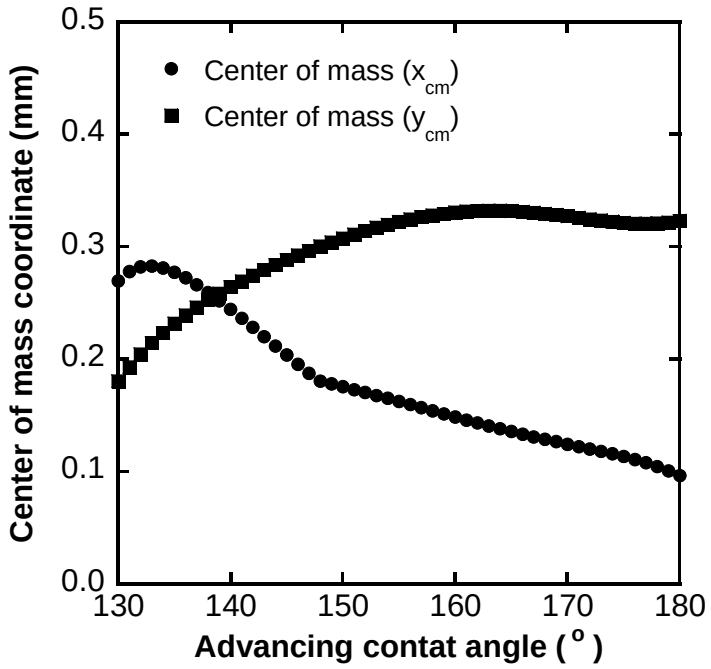

Fig. 3.10 Center of mass of droplet with different advancing contact angle

3.3.3 Droplet movement in channel

3.3.3.1 Droplet detachment

The size of droplet on the GDL is getting bigger and bigger because produced liquid water is accumulated on the GDL through the porous media. Fig. 3.11 shows how droplet is accumulated and moves in channel. Since forces on the droplet are changed with the shape of droplet especially with a volume of droplet, we can calculate the volume when droplet starts moving on the GDL by comparing the drag force and surface tension force on the droplet. Eq. 4.4 and 4.9 were used to calculate drag and surface tension force on the droplet. Moreover, deformation of droplet was also considered by using Eq. 4.17, 4.18 and 4.19. Fig. 3.12 shows the result of calculation. The graph represents drag force and surface tension force on the droplets which have a different volume. Fig. 3.12 (a) present forces on the droplet which has a volume of $100 \cdot 10^{-3}$ mm^3, and droplet in Fig. 3.12 (b) has a volume of $130 \cdot 10^{-3}$ mm^3. As verified in Fig. 3.12 (a), drag force is not big enough to overcome the surface tension force exerting on the droplet. However, drag force gets bigger than surface tension force when droplet grows. In Fig. 3.12 (b), drag force is larger than surface tension force at static condition, and it makes droplet move. Hence, we can verify that the volume of droplet is one

of the most important factors that determine droplet in the channel moves or not. Although the velocity of air in channel and channel shape also can affect the droplet detachment, it is not considered in this section. The effects of air velocity and channel shape will be discussed in section 3.3.3.2 to investigate the droplet speed in channel.

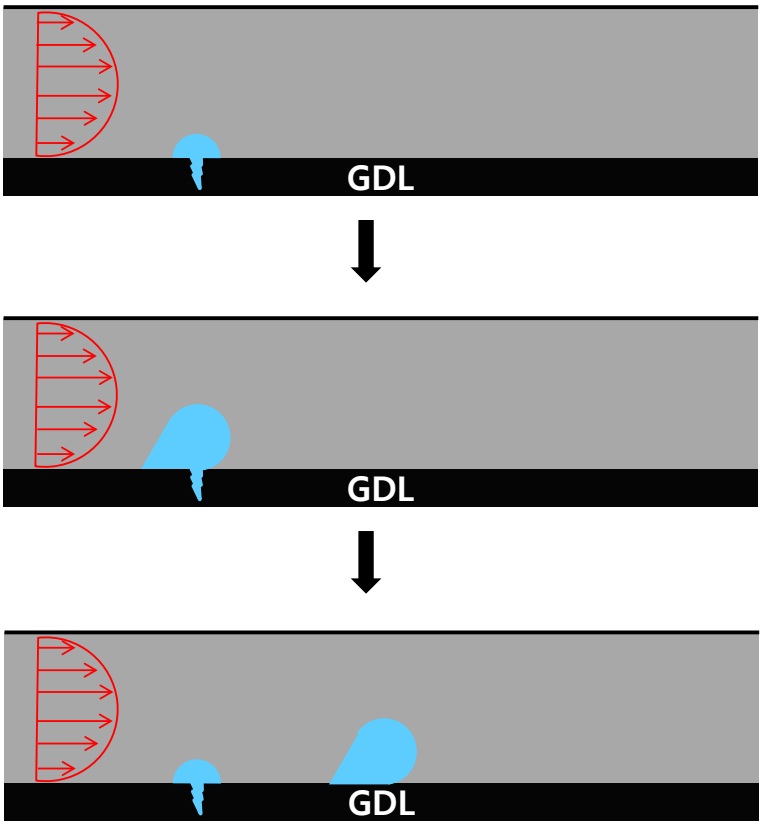

Fig. 3.11 Process of droplet formation and shift in channel

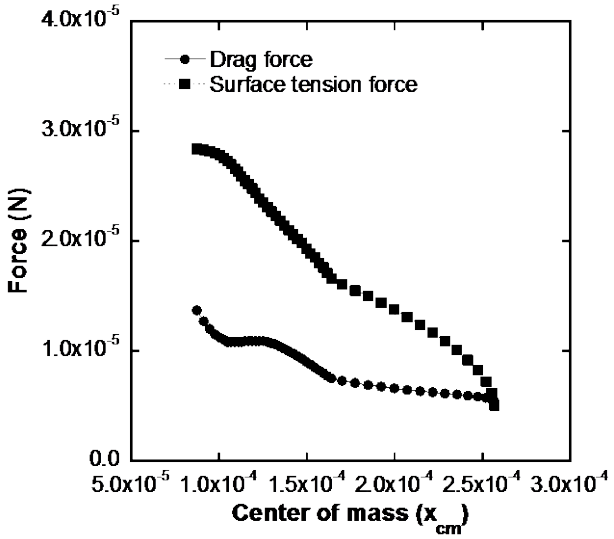

(a)

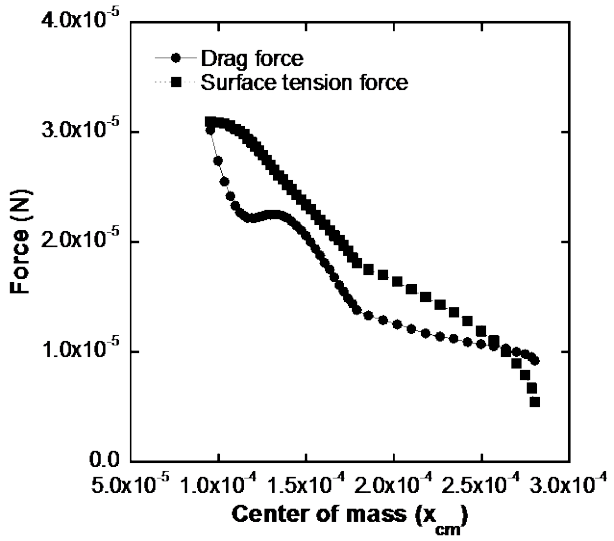

(b)

Fig. 3.12 Drag force and surface tension force with x-coordinate center of mass: (a) $V=100\cdot10^{-3}$ mm^3 (b) $V=130\cdot10^{-3}$ mm^3

3.3.3.2 Droplet velocity

In this section, numerical analysis for calculating the speed of droplet in channel will be discussed. As described in section 3.3.3.1, droplet starts moving when drag force is larger than surface tension force. In this condition, droplet is deformed to where drag force and surface tension force are equilibrated while droplet is shifting. Fig. 3.13 (a) represents the situation when droplet grows to $130 \cdot 10^{-3}$ mm^3. As mentioned in section 3.3.3.1, droplet is deformed and detached at the same time. Fig. 3.13 (b) shows the net power exerting on the droplet while it is deformed and detached. Hence, we can calculate the impulse on the droplet by using net power on the droplet.

$$P = \int F_{net} dt = mv = \rho V v \tag{3.26}$$

Eq. 4.20 represents the impulse on the droplet and we already calculated the net power exerting on the droplet. However, it is very hard to determine how long net power exerts on the droplet. Therefore, exerting time of impulse is determined by adapting the results of previous work, which is 0.02 s [8]. As a result, we can calculate the detachment speed of droplet. The result of calculation is 0.24 m/s. On the other hands, we need to compare the

droplet velocity in conventional channel and inclined channel. Since air velocity in inclined channel increases along the channel, the effect of air speed on the net force should be calculated first. Fig. 3.14 shows the result of analysis. Since drag force on the droplet is supposed to increase when velocity of air gets fast, net force on the droplet also should increase. Hence, the velocity of droplet can be calculated when it moves in inclined channel. Fig. 3.15 shows the result of calculation for the velocity of droplet in conventional channel and inclined channel. As represented in graph, the velocity of droplet increases continuously in inclined channel while the velocity of droplet gets constant at certain value. As a result, droplet in inclined channel is more easily escape the channel compared with droplet in conventional channel. This is why concentration losses of PEMFC decreases when conventional channel is replaced with inclined channel.

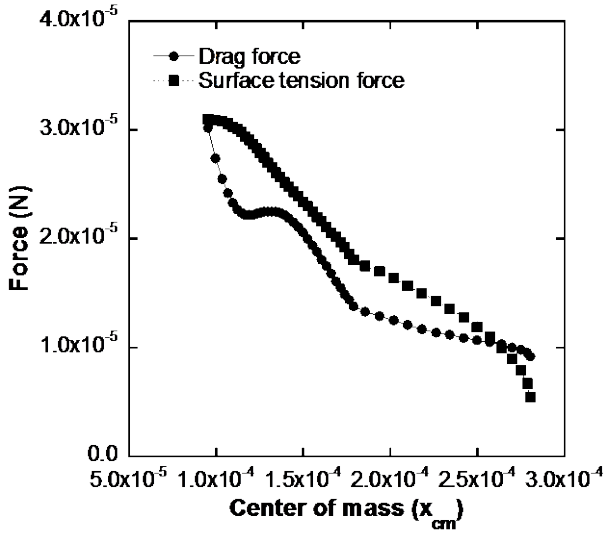

(a)

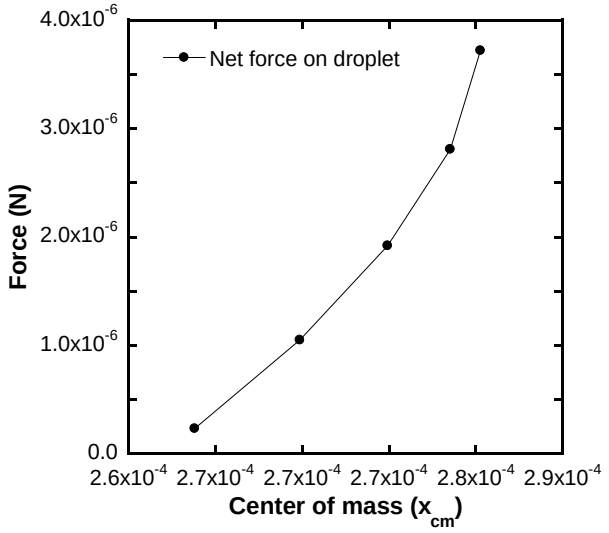

(b)

Fig. 3.13 Variation of force on the droplet (a) Drag and surface tension force (b) Net force on the droplet

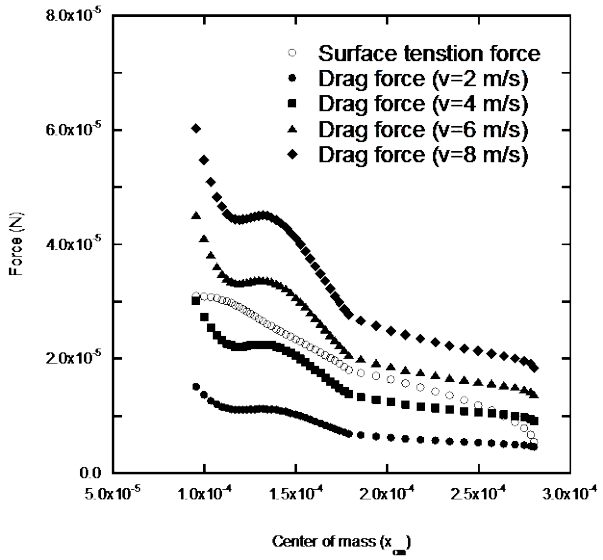

(a)

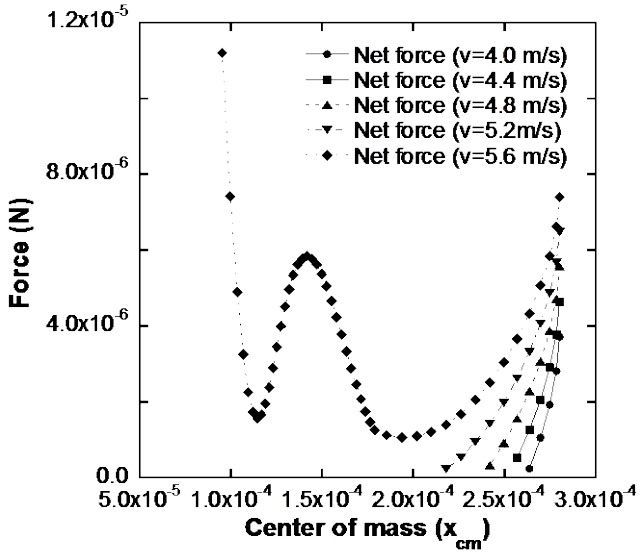

(b)

Fig. 3.14 Effect of air speed in channel on the drag force and net force: (a) drag force variation (b) net force variation

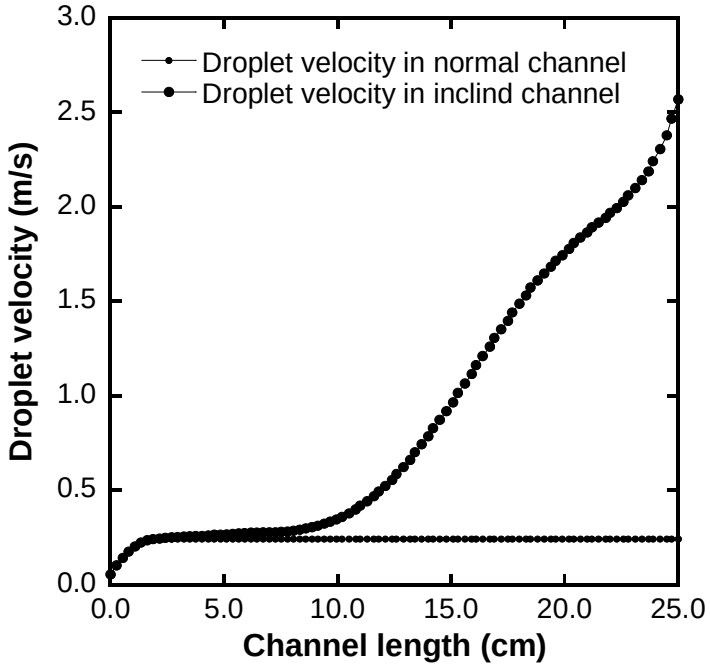

Fig. 3.15 Droplet velocity along the different channels

3.3.4 Pressure drop

3.3.4.1 Pressure drop analysis

Since pressure drop should occur when provided gases flow into both conventional channel and inclined channel, it is very important to verify the effects and characteristics of pressure drop in both channels. Therefore, we conducted experiments to evaluate how channel shape effects on the pressure drop in section 2.4.3. However, we still need to analyze the change of pressure drop with respect to the geometry of channel.

$$\mathrm{dP} = \frac{R}{T}\left(\frac{Q \cdot \rho}{A\_c}\right)^2 \frac{f}{D\_h} \tag{3.27}$$

$$P_{in}^2 - P_{out}^2 = 25.2\left[\frac{SQ^2ZTfL}{D\_h^5}\right] \tag{3.28}$$

The result of numerical analysis for pressure drop is presented in Fig. 3.16. The pressure of gases along the cathode channel was calculated when 1 Lpm of fully humidified air was supplied into a conventional channel and inclined channels. As we can easily verify in the graph, the pressure of air decreases gradually along the all channels. However, the value of pressure drop is varied with the shape of channels. Since outlet pressure of cathode is constant at atmospheric pressure, different pressure drop causes increasing

of inlet pressure. Therefore, inclined channel #3 shows the highest inlet pressure among the channels. Although all tapered channels get pressure drop increase, inlet pressure drastically rise when the inclined channel #3 was used. This phenomenon also can be found in the experimental result presented in Fig. 2.10. The velocity of air in inclined channel gets fast along the channel length, and velocity increment gets severe at the later part of inclined channel #3. Hence, pressure drop increases especially at the end of the inclined channel #3 because of high friction loss.

To investigate the accuracy of numerical analysis, we need to compare the pressure drop values measured in experiment and calculated from the numerical analysis. Fig. 3.17 shows the results of comparison. Although the tendency of pressure drop increment of each channel is quite similar, the difference of values becomes bigger and bigger from inclined channel #1 to inclined channel #3. The reason of this difference between experiment and numerical analysis will be discussed in the next section.

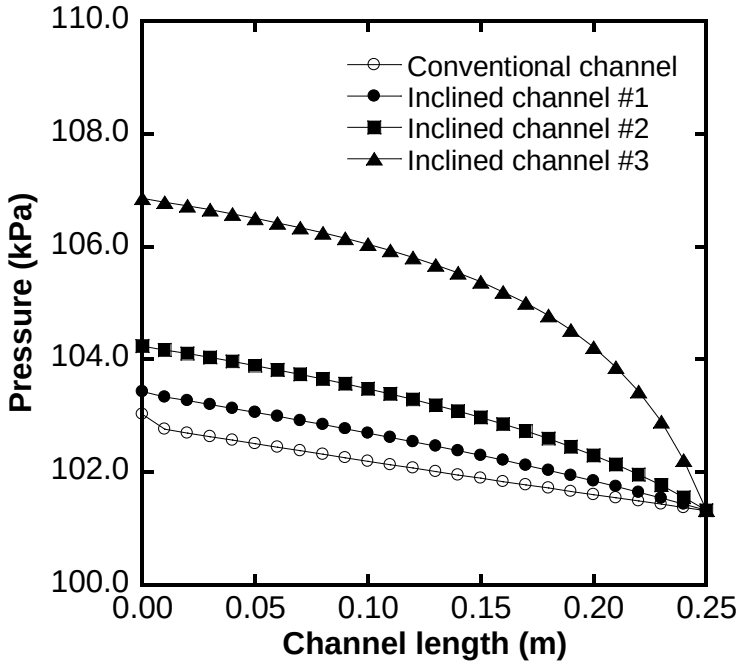

Fig. 3.16 Pressure drop calculation along the different types of channels

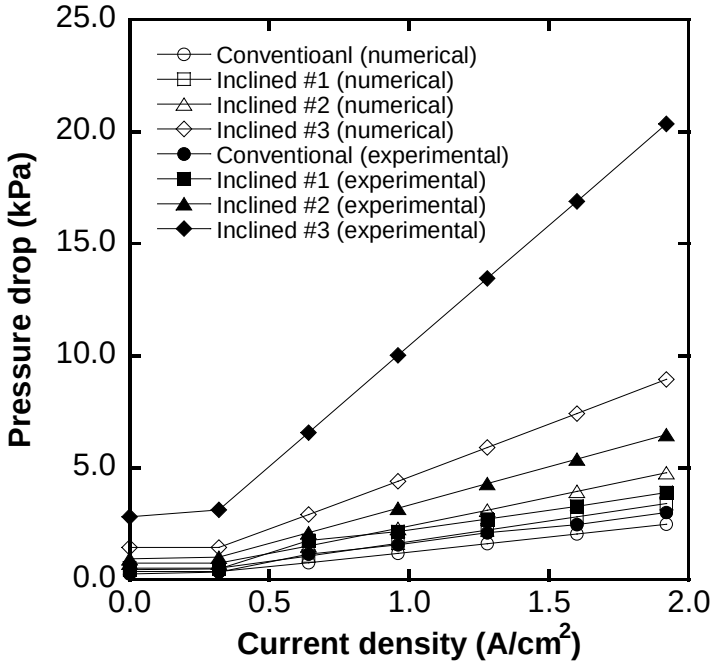

Fig. 3.17 Pressure drop comparison between experiment and numerical analysis

3.3.4.2 Water film effect

In the previous section, we found that the difference of pressure drop between experiment and numerical analysis becomes larger especially when inclined channel #2 and #3 were used. Therefore, the reason of this difference will be discussed in this section.

Since all droplets produced in the reaction comes out from the reaction site and moves along the flow channel, the water film problem can arise when droplet size gets bigger than the height of channel. Therefore, we investigated the volume and height of detached droplet at different air velocity. The results of calculation is presented in Fig. 3.18. As we can verify in graph, the detachment volume and height of droplet is supposed to decrease with increment of air velocity. Then, we found out the size of droplet for all types of channel. As a result, we verified that the droplets moving in inclined channel #2 and #3 must bump the channel and cause a water film. The average height of droplet in inclined channel #2 and #3 is 0.47 mm and 0.44 mm, respectively. As a result, the spot where water film start generating can be assumed, and the length of water film is 35 mm in inclined channel #2 and 86 mm in #3 as Fig. 3. 19 shows the schematics of water film inside the inclined channel #2 and #3.

Since we already verified that there are differences of pressure drop between experiment and numerical analysis when the inclined channel #2 and #3 were used, the effects of water film on the pressure drop can be calculated inversely. The generated water film can block the inclined channel, and it can cause the high pressure drop comparing with numerical condition because of narrowed channel. Hence, the thickness of water film in inclined channel #2 and 3# at different current density can be calculated through the results of pressure drop differences between experiment and numerical analysis, and the values are presented in Table 3.1. Even though the water film make channel outlet narrowed in both inclined channel #2 and #3, it is not that critical to make fuel cell shut down. However, the water film generated in inclined channel #3 is quite thick to make channel narrowed. Therefore, the difference of pressure difference gets severe when we used inclined channel #3 comparing with the result of inclined channel #2.

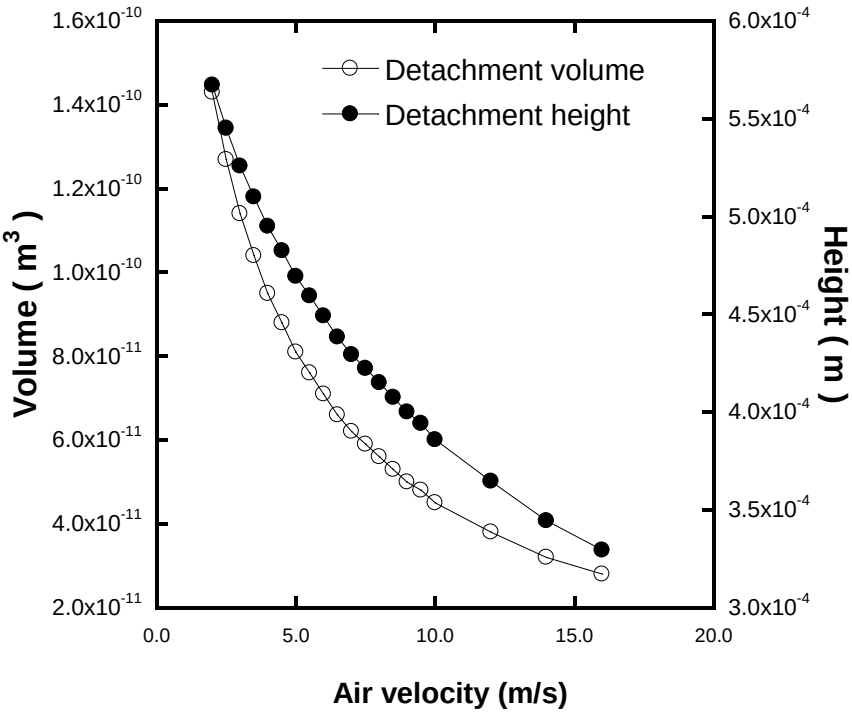

Fig. 3.18 Detachment volume and height of droplet in different air velocity

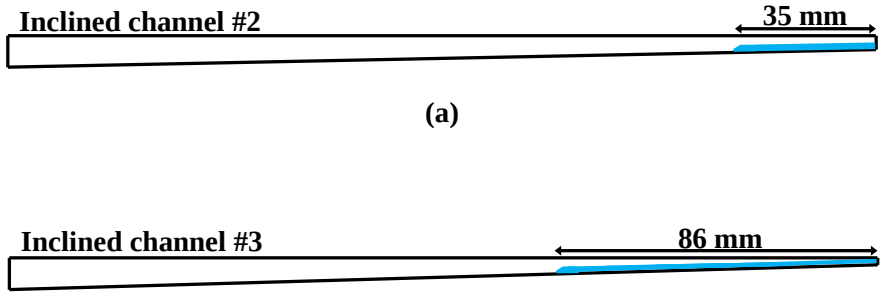

Fig. 3.19 Schematics of water film generation in inclined channel #2 and #3

Table 3.1 Water film thickness

Current density (A/cm^2)	Water film thickness in inclined channel #2 (mm)	Water film thickness in inclined channel #3 (mm)
0.8	0.1504	0.0991
1.2	0.1506	0.1011
1.6	0.1491	0.1024
2.0	0.1473	0.1034
2.4	0.1456	0.1041

3.4 Summary

In this chapter, numerical analysis for investigating the effect of inclined channel on the PEMFC was conducted. Since we verified the performance enhancement of PEMFC when conventional channel was replaced with inclined channel, the factors that improve the performance of PEMFC were investigated in this chapter. First of all, the effect of inclined channel on the oxygen depletion of PEMFC was analyzed. The concentration losses of PEMFC were mitigated when inclined channel was applied. Hence, numerical analysis for calculating the oxygen diffusion from the channel to MEA with different channel shape was conducted. As a result, we found that oxygen diffuses more easily at the inclined channel comparing with conventional channel, and these results can explain the results of experimental work. Furthermore, numerical analysis was conducted for investigating the droplet behavior in conventional channel and inclined channel. Drag force and surface tension force are exerting on the droplet in the channel, and their values were calculated. Moreover, the effect of inclined channel on the net power exerting on the droplet also investigated, and velocity of droplet in channel also was calculated. As a result, we found that the droplet moves faster in inclined channel than conventional channel because of its shape. Therefore, this result means that liquid water is more

easily removed from the channel, and it can explain the mitigation of concentration losses of PEMFC when it operates with inclined channel.

Chapter 4. Experimental study on performance improvement of PEMFC with metal foam flow field

4.1 Introduction

In this chapter, experimental study on the effects of metal foam as a flow field of PEMFC will be introduced. Metal foam is a porous material which has lots of pore. In general, PEMFC uses a flow field which has a channel and rib. Since produced liquid water is easily accumulated under rib, oxygen is hard to diffuse from channel to MEA at high current density region when conventional channel is used as a flow field for PEMFC. Therefore, we suggested a novel flow field which uses metal foam replacing with conventional channel and rib. The experimental work was conducted to verify the performance and characteristics of PEMFC with metal foam flow field. Moreover, the characteristics of metal foams which have a different cell size was investigated by several methods such as polarization curve, power curve, EIS method, pressure drop measurement, and stability comparison.

4.2 Preparation for experiment

4.2.1 Metal foam

In Fig. 4.1, there are four types of metal foam used in the experiment. These metal foams have different cell size of 450 μm, 580 μm, 800 μm, and 1200 μm respectively. All metal foams are made of nickel and coated by gold. Since metal foam should take a role as a path of electrons in PEMFC, the electrical resistance is very important to make PEMFC operate normally [63]. This is why metal foam was coated by gold before it applied as a flow field. All metal foams were compressed to the same thickness to set an equal test condition. Then, they were cut to 5 cm × 5 cm size of square shape to put them into cathode bipolar plate. Fig. 4.2 shows conceptual diagram of how PEMFC with different flow field is assembled. Moreover, Fig 4.3 contains a picture of cathode bipolar plate with conventional and metal foam flow field. In this study, we used metal foam only for the cathode because the concentration losses of PEMFC usually occur at cathode. Hence, metal foam flow field was applied to cathode of PEMFC and investigated its effects on the mitigating concentration loss and enhancing the performance of PEMFC.

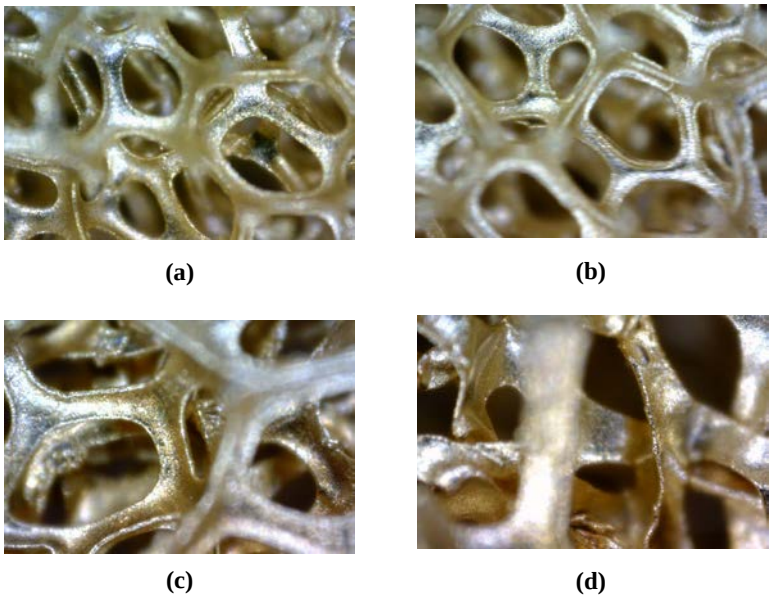

Fig. 4.1 Types of metal foam with different cell size: (a) 450 µm (b) 580 µm (c) 800 µm (d) 1200 µm

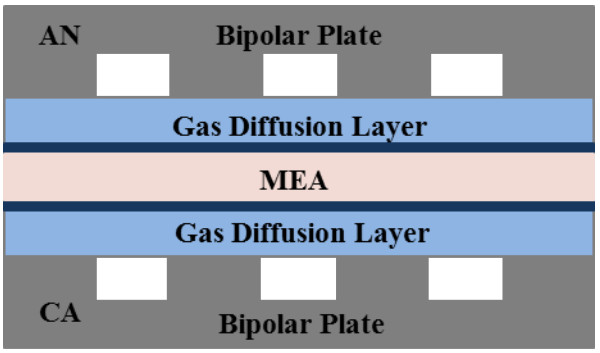

(a)

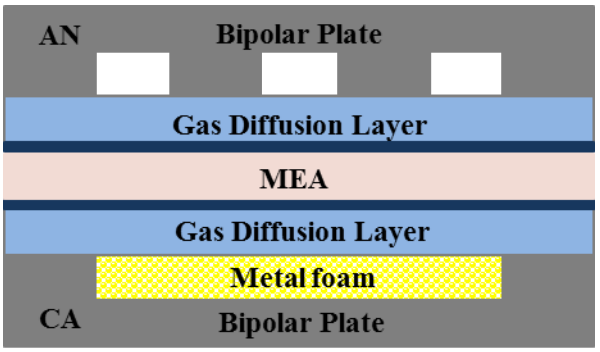

(b)

Fig. 4.2 Conceptual diagram of side view of different flow field: (a) conventional flow field (b) metal foam flow field

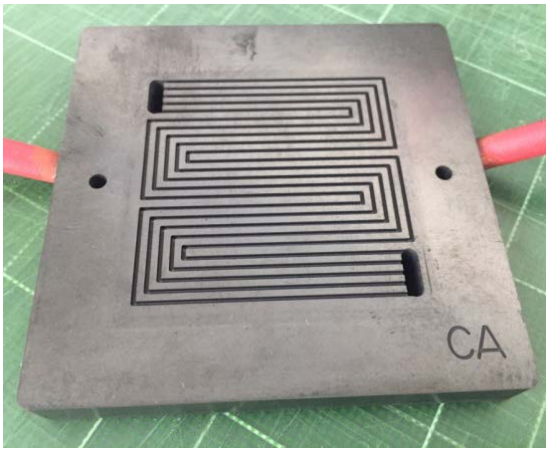

(a)

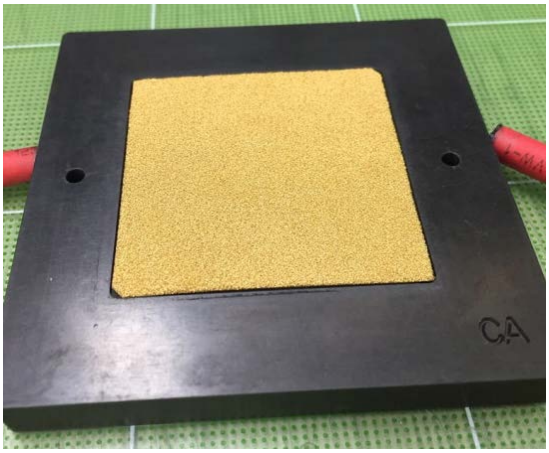

(b)

Fig. 4.3 Cathode bipolar plate with different flow fields: (a) conventional flow field (b) metal foam flow field

4.2.2 Experimental setup

Fig. 4.4 represents the experimental setup used for this study. Measuring devices and apparatuses are almost the same with things already described in chapter 2. The purity of 99.999% of hydrogen and oxygen are supplied to PEMFC after humidified by using bubbler humidifier. The flow rate of provided gases was controlled by mass flow meter. Moreover, voltage and current were measured by electric loader. The impedance meter was used for measuring the losses of PEMFC while it operates. All components for single unit cell is the same with those in chapter 2 except for the cathode bipolar plate which has a flow field replaced with metal foam. Furthermore, all PEMFCs operated under activation cycle explained in previous chapter before they are used for experiment.

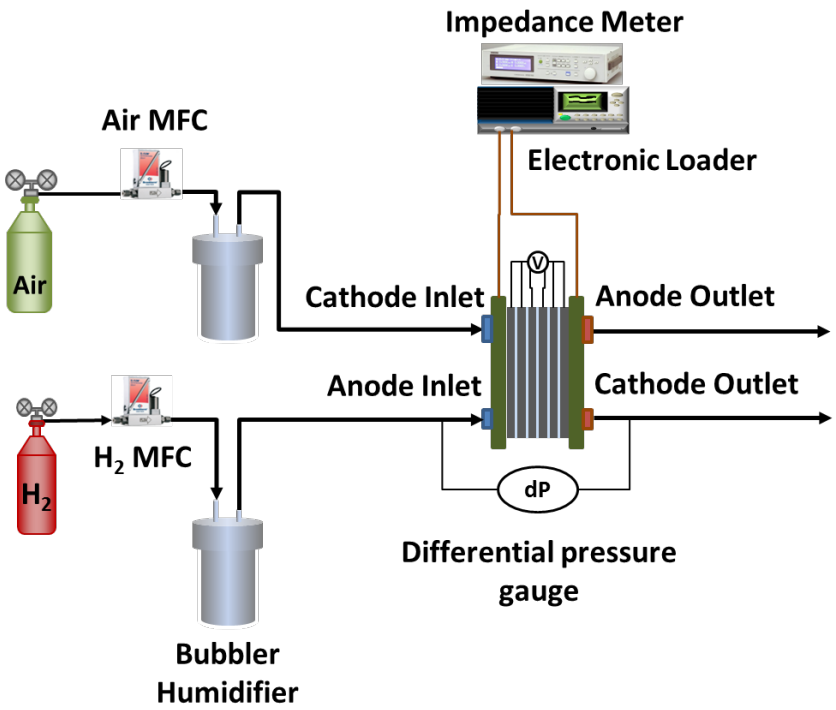

Fig. 4.4 Experimental setup

4.2.3 Experimental conditions

In table 4.1, the experimental conditions for this study are presented. The performance, stability and losses were investigated at two operating temperatures 40℃ and 60℃. Stoichiometric ratio of anode side and cathode side were fixed at 1.5 and 2.0, respectively. All gases were fully humidified before they were supplied to PEMFC.

Table 4.1 Experimental conditions

Parameter	Value
T_c (°C)	40/60
SR_{an}	1.5
SR_{ca}	2.0
RH_{an} (%)	100
RH_{ca} (%)	100

4.3 Results and discussion

4.3.1 PEMFC performance

4.3.1.1 Polarization curve

In Fig.5, there are two graphs representing the polarization curves of PEMFC with conventional flow field and metal foam flow field at different operating temperatures. Each graph has five polarization curves. As we can easily verify in the graphs, the voltage of PEMFC with metal foam flow fields is higher than that of PEMFCE with conventional flow field at the same current density. Hence, metal foam flow field make PEMFC enhanced. When the performance of PEMFC is compared, we usually verify the current density of PEMFC at certain voltage (0.6 V). A typical current density of PEMFC with conventional flow field at 0.6 V under operating temperature of 60°C is about 1.0 A/cm^2, and it can be verified in Fig. 4.5 (a). Meanwhile, every PEMFC using metal foam flow field show higher current density than 1.0 A/cm^2 at 0.6 V. Especially, PEMFC shows the best performance when it operates with metal foam flow field which has the cell size of 800 μm.

Although all metal foam flow fields showed better performance than conventional flow field, the effect of metal foam can be shown clearly when

PEMFC operates at low operating temperature represented in Fig. 4.5 (b). The difference of the performance between PEMFC with conventional flow field and metal foam flow field get significant at low operating temperature. This result can be explained by the reduction of concentration losses of PEMFC. Since the concentration losses of PEMFC are dominant at the high current density region because of flooding and oxygen depletion, the voltage of PEMFC with conventional flow field drops suddenly at high current density. However, the voltage of PEMFC with metal foam flow field decreases smoothly at the high current density region. Hence, we can verify the effect of metal foam flow field on the mitigation of the concentration losses. The details of effects will be discussed in section 4.3.2.

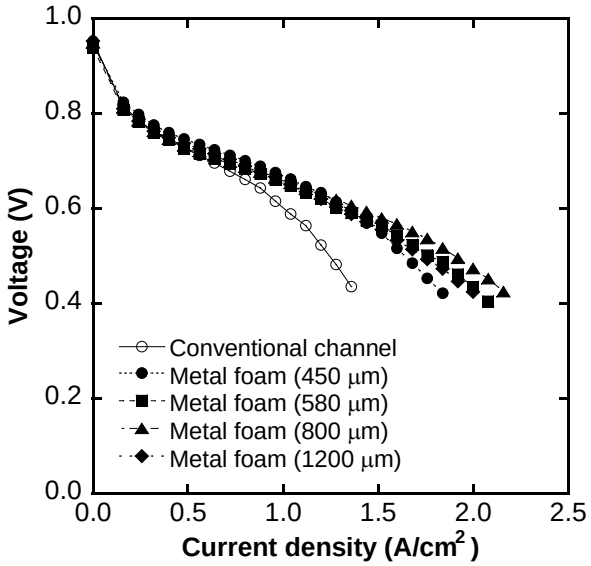

(a)

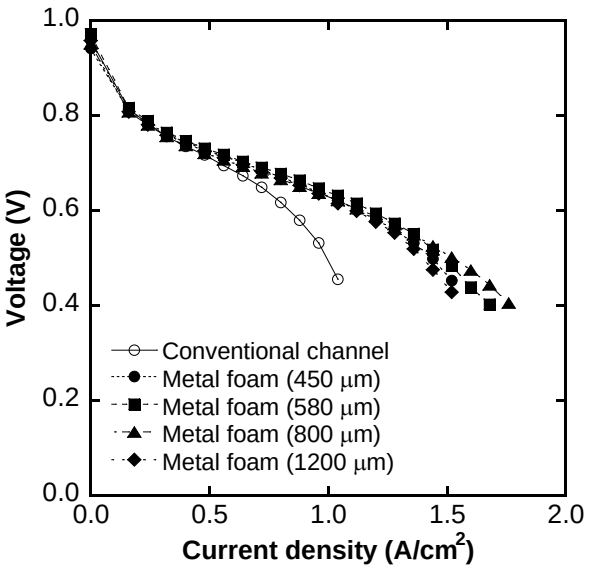

(b)

Fig. 4.5 Polarization curve of PEMFC with conventional and metal foam flow field: (a) T_c=60°C (b) T_c=40°C

4.3.1.2 Power density curve

Investigation of power density curve is the easiest way to compare the performance of PEMFC with different flow fields because it represents the power capacity of PEMFC. In Fig. 4.6, there are two graphs representing the power density with respect to current density at operating temperature of 60°C and 40°C. Both graphs show that PEMFC with metal foam flow field generate more power density than that with conventional flow field. When it comes to maximum power density at the operating temperature of 60°C, PEMFC generates maximum power density about 0.952 W/cm^2 at 1.92 A/cm^3 with metal foam flow field which have 800 μm cell size while PEMFC with conventional flow field produced only 0.632 W/cm^2 at 1.12 A/cm^2. As a results, the maximum power density of PEMFC is improved 50.6% by replacing conventional flow field with proper metal foam flow field. Moreover, PEMFC with metal foam flow field shows better performance at operating temperature of 40°C. PEMFC with 800 μm metal foam flow field shows the highest maximum power density of 0.764 W/cm^2 at 1.52 A/cm^2, which means that maximum power density of PEMFC is enhanced by 50.4% comparing with the maximum power density of PEMFC with conventional flow field, which is 0.508 W/cm^2 at 0.88 A/cm^2. Therefore,

this results show that PEMFC can generate more power density by replacing conventional flow field with suggested metal foam flow field.

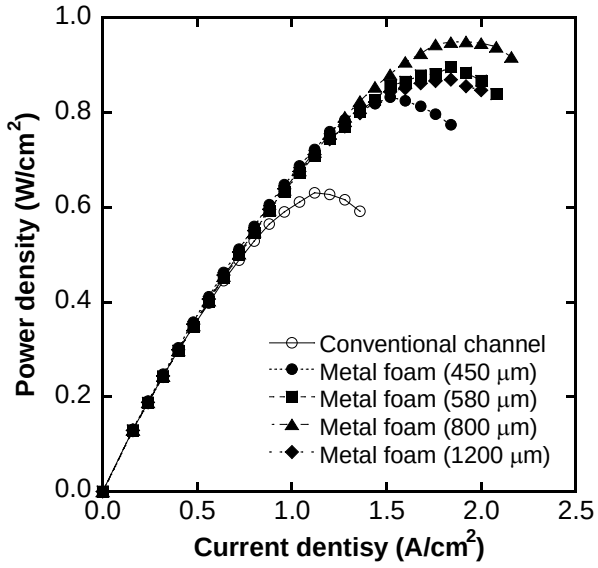

(a)

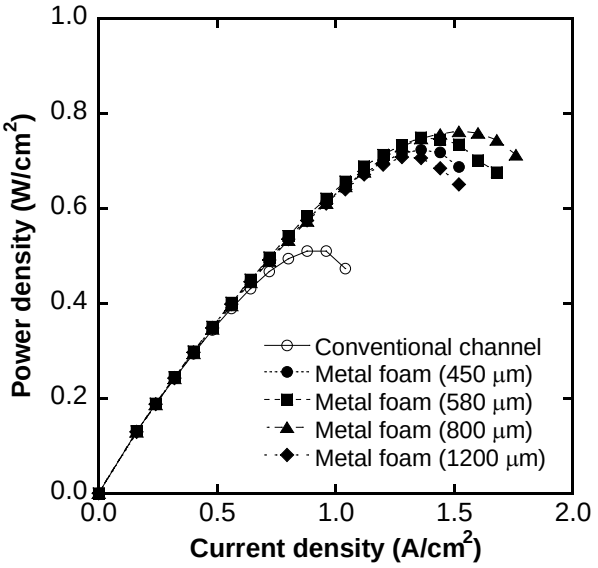

(b)

Fig. 4.6 Power density curve of PEMFC with conventional and metal foam flow field: (a) T_c=60°C (b) T_c=40°C

4.3.2 Electrochemical impedance spectroscopy

In this section, the results of EIS method will be introduced. To investigate the losses in PEMFC, EIS method was conducted at low current density region, intermediate current density region, and high current density region. Therefore, EIS was conducted when PEMFC operates under three constant current density 0.32 A/cm^2, 0.64 A/cm^2, and 1.28 A/cm^2 at 60°C. However, the value of high current density region was changed from 1.28 A/cm^2 to 0.96 A/cm^2 when EIS was conducted at operating temperature of 40°C because current density of 1.28 A/cm^2 is high enough to make PEMFC shut down at 40°C with conventional flow field. The impedance spectra were recorded while frequency was swept from 4 kHz to 1.26 Hz with 32 moving average. The measuring AC current was fixed as 10% of the DC current magnitude.

Fig. 4.7 and 4.8 show the results of EIS measurement for PEMFC with different flow field at operating temperature of 60°C and 40°C respectively. First of all, as we investigate the high frequency resistance (HFR), PEMFC with metal foam flow field shows lower HFR than that of PEMFC with conventional flow field. Especially, it can be found more easily at the low current density region represented in Fig 4.7 (a) and 4.8 (a) because ohmic losses relatively get smaller and smaller when fuel cell operates at high

current density. These results mean that there is no conductivity problem when we replace conventional flow field with metal foam flow field. Among the metal form flow fields, there are some differences in ohmic losses. The details and characteristics of metal foam flow fields on the ohmic losses will be discussed in chapter 5 later.

In terms of mass transfer resistance, the size of arc at low frequency represents the concentration losses. Even though there is a charge transfer resistance, that is not that big. Moreover, mass transfer resistance caused drastic voltage drop at intermediate current density region and high current density region. In Fig. 4.7 and 4.8, arc size of PEMFC with conventional flow field is the largest among the PEMFCs with different flow fields. This result means that mass transfer resistance is reduced when conventional flow field is replaced with metal foam flow field. Furthermore, the results represented in Fig. 4.7 (c) and 4.8 (c) can explain the performance enhancement of PEMFC with metal foam flow field. As verified in section 4.3.1, the performance of PEMFC is enhanced with metal foam flow fields especially at the high current density region. In general, drastic voltage drop happens as a result of concentration losses coming from flooding and oxygen depletion. However, PEMFC with metal foam flow field has a small concentration losses at the high current density region, and this advantage

can make PEMFC enhanced. Therefore, one of the important factors that metal foam flow field make PEMFC performance improved is reducing the concentration losses of PEMFC by mitigating the flooding and oxygen depletion problems in PEMFC.

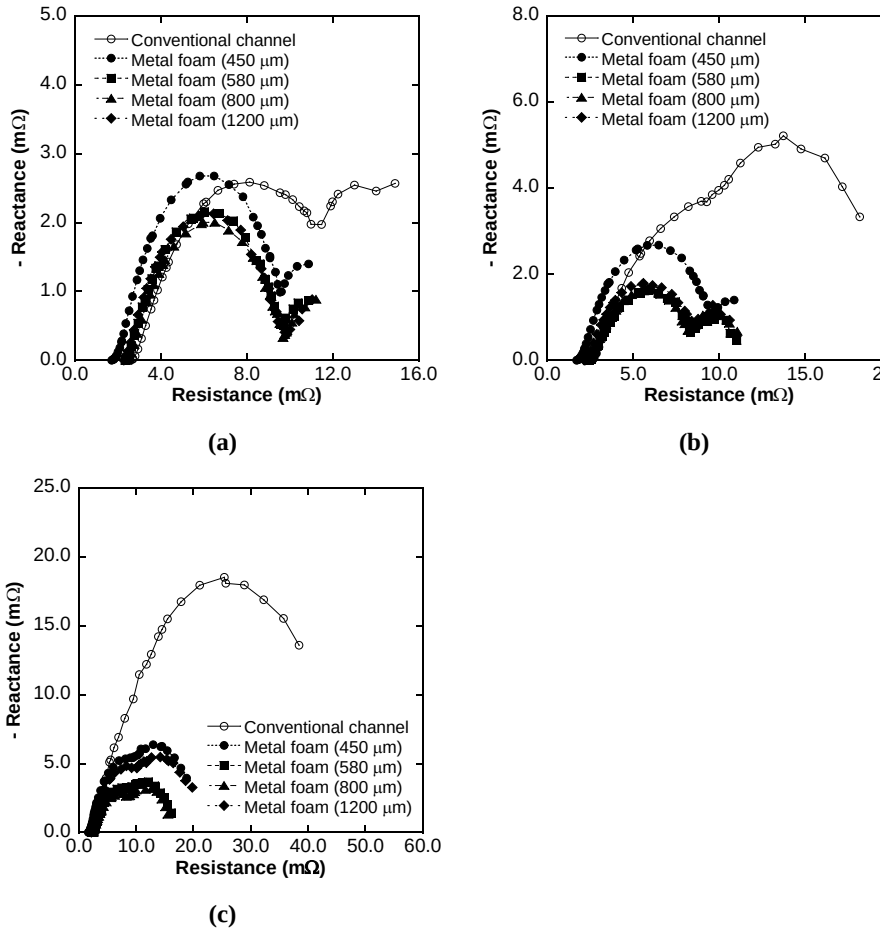

Fig. 4.7 Electrochemical impedance spectroscopy for PEMFC with conventional and metal foam flow field at 60°C: (a) J=0.32 A/cm^2 (b) J=0.64 A/cm^2 (c) 1.28 A/cm^2

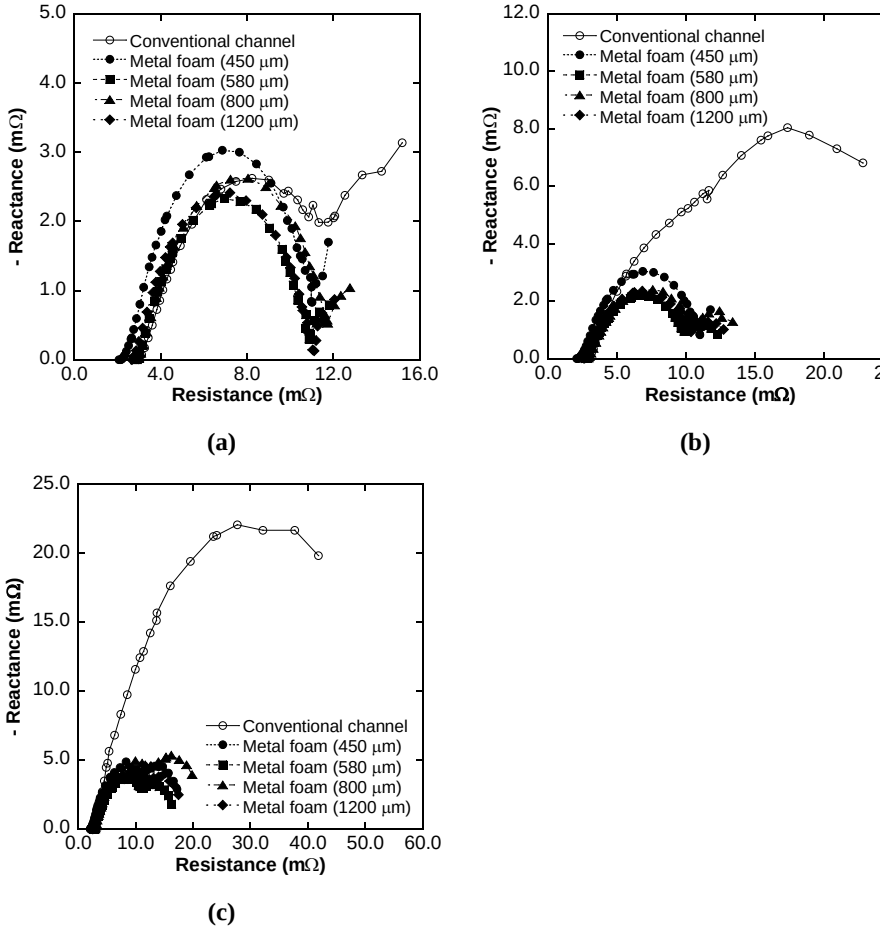

Fig. 4.8 Electrochemical impedance spectroscopy for PEMFC with conventional and metal foam flow field at 40°C: (a) J=0.32 A/cm^2 (b) J=0.64 A/cm^2 (c) 0.96 A/cm^2

4.3.3 Pressure drop

In this section, investigation of pressure drop between the inlet and outlet of cathode will be introduced. As verified in section 4.3.1, the performance of PEMFC is improved drastically when conventional flow field is replaced with metal foam flow field. However, operating condition like pressure drop in the flow field of PEMFC has to be considered to determine whether metal foam flow field can be applied to the real system or not. Since high pressure drop in the flow field needs more compression work to the BOP, it can cause a high power consumption for providing air. Hence, we measured a pressure drop between inlet and outlet of conventional flow field and metal foam flow field by using differential pressure gauge. Operating conditions are the same with the values presented in Table 4.1.

Fig. 4.9 shows the results of pressure drop measurement. Two graphs show that pressure drop even decreases when metal foam flow field was used for PEMFC. As current density of PEMFC increases, pressure drop is supposed to increase because produced liquid water can block the flow path and the amount of gas also increases. However, the pressure drop of PEMFC with metal foam flow field is always lower than that of PEMFC with conventional flow field. Hence, metal foam flow field not only make the performance of PEMFC enhanced, but also can reduce the power

consumption of BOP by reducing the pressure drop between inlet and outlet of flow field.

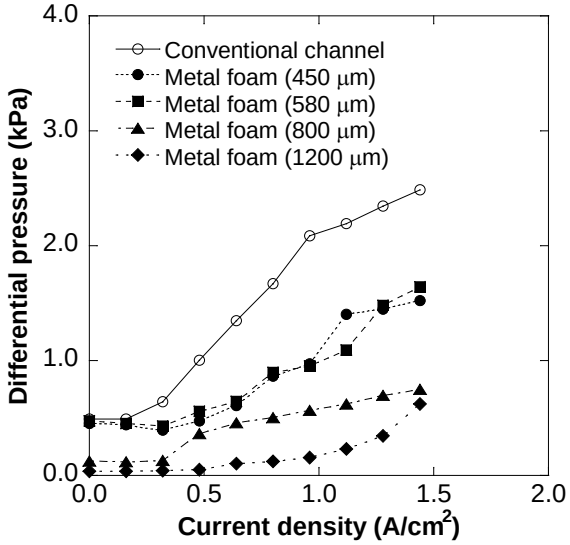

(a)

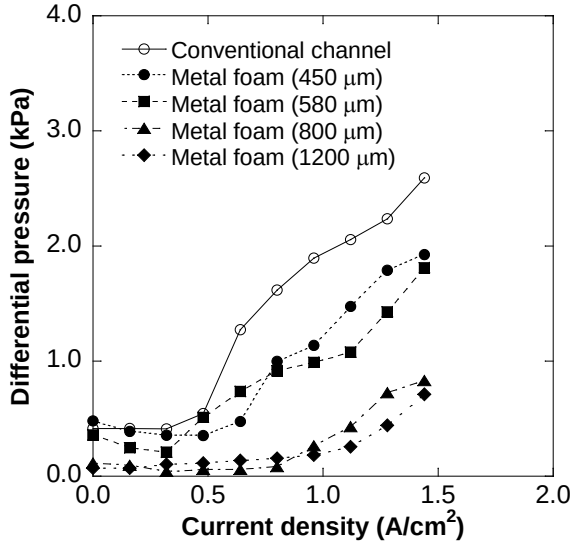

(b)

Fig. 4.9 Pressure drop between inlet and outlet of PEMFC cathode: (a) T_c=60°C (b) T_c=40°C

4.3.4 Stability comparison

In this section, the stability of PEMFC with conventional flow field and metal foam flow field will be discussed. In previous sections, the performance improvement of PEMC is verified when conventional flow field is replaced with metal foam flow field. However, stability of PEMFC is also important as well as the performance of PEMFC. Stability is usually verified by measuring the voltage of PEMFC at the constant current density. Since voltage of PEMFC is varied at the constant current density because of instability of electrochemical reaction, the variation of voltage is normally compared to investigate how stable PEMFC is. Experimental conditions for stability comparison are presented in Table 4.2. The PEMFC with conventional flow field and metal foam flow field operate at the same conditions. The voltage of PEMFC was measured at 1.12 A/cm^2 when PEMFC operates at 40°C, and 1.28 A/cm^2 at operating temperature of 60°C. The values were chosen to make voltage of PEMFC be about 0.6 V. The experiment for stability comparison was conducted for an hour and the voltage of PEMFC was measured.

The experimental results are represented in Fig. 4.10. Since the graphs show the changes of voltage when PEMFC operates at constant current density, fluctuation of voltage can represent the instability of power

generation of PEMFC. Even though it is a little difficult to distinguish the exact value of voltage in Fig 4.10, it is clear that PEMFC with metal foam flow fields show not only higher voltage but also less fluctuation comparing with PEMFC with conventional flow field. Nevertheless, the fluctuation of voltage was investigated by calculating the standard deviation of its values. Fig. 4.11 shows standard deviation of voltages in Fig. 4.10. Since the standard deviation shows how far the values are away from the average value, the bigger standard deviation means the more unstable state. As represented in Fig. 4.11, the standard deviation of voltage of PEMFC with conventional flow field is always higher than that of PEMFC with metal foam flow field. Especially the instability of PEMFC with conventional flow field get worse at the low operating temperature because PEMFC with conventional flow field is hard to remove liquid water at the condition that can make more liquid water in flow field. According to the results in Fig. 4.11, voltage of PEMFC with metal foam flow field which has cell size of 800 μm shows the lowest standard deviation among the different types of flow fields. Hence, we can verify that metal foam flow field of 800 μm cell size has an advantage in managing liquid water in PEMFC and it makes not only performance improved but also power generation of PEMFC stable.

Table 4.2 Experimental conditions for stability comparison

Parameter	Value
T_c (°C)	40/60
SR_{an}	1.5
SR_{ca}	2.0
J (A/cm^2)	1.12/1.28

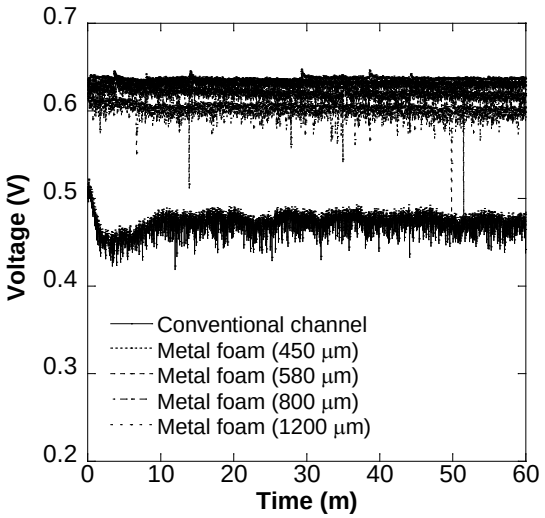

(a)

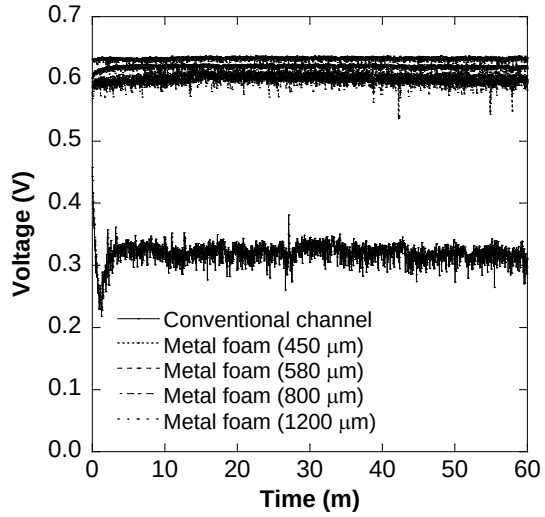

(b)

Fig. 4.10 Voltage measurement for 1 hour period for PEMFC with conventional and metal foam flow field at the constant current density: (a) T_c=60°C, J=1.28 A/cm^2 (b) T_c=40°C, J=1.12 A/cm^2

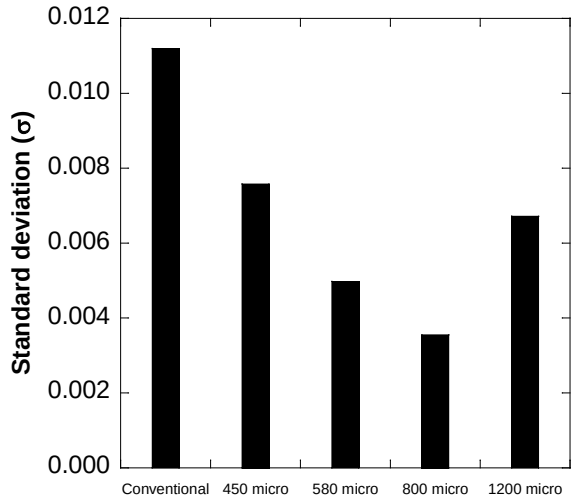

(a)

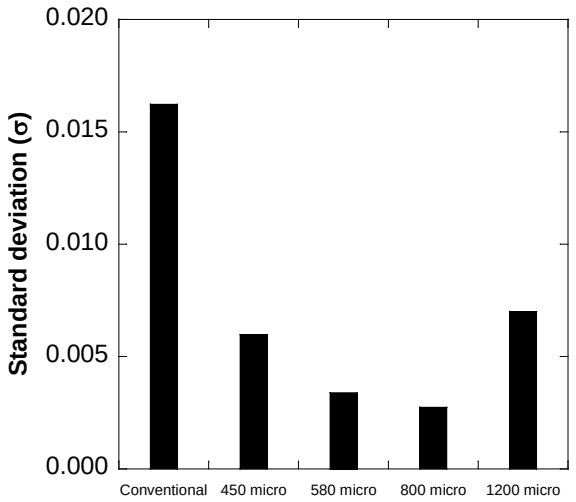

(b)

Fig. 4.11 Standard deviation of 1 hour measurement of voltage for PEMFC with different flow field at the constant current density: (a) T_c=60°C, J=1.28 A/cm^2 (b) T_c=40°C, J=1.12 A/cm^2

4.4 Summary

In this chapter, the effects of metal foam flow field on the performance of PEMFC was investigated. The performance of PEMFC was enhanced when conventional flow field was replaced with proper metal foam flow field. The maximum power density of PEMFC is improved by about 50.6% with metal foam flow field which has a cell size of 800 μm, Moreover, pressure drop and stability of PEMFC was also verified. In the results of experiment for measuring pressure drop, metal foam flow field showed even lower pressure drop between inlet and outlet compared with that of conventional flow field. This results mean that power consumption of BOP can be reduced by replacing conventional flow field with metal foam flow field. Furthermore, experiment for investigating stability of PEMFC show that fluctuation of voltage get less with metal foam flow field. The calculation of standard deviation of voltage values also represents that metal foam flow field make PEMFC operate more stably. As a results of experiments, we can conclude that the PEMFC with metal foam flow field has an advantage in performance, pressure drop and stability comparing with the PEMFC with conventional flow field.

Chapter 5. Advanced experimental study on the investigation of metal foam flow field

5.1 Introduction

In this chapter, the experiments for investigating the characteristics of metal foam flow field in water management will be discussed. In previous chapter, we verified that the performance of PEMFC was improved when we replaced conventional flow field with metal foam flow field. However, the characteristics of metal foam flow field should be investigated more to understand how metal foam flow field works in PEMFC. Hence, we designed mixed metal foam which has a two different metal foam arrayed on the different region of bipolar plate. We used the results of experiment in chapter 4, and chose two metal foams which had a proper cell size to front region and back region of flow field. Then, the performance of PEMFC with mixed metal foam was investigated. Moreover, experiment for visualizing the liquid water movement in conventional flow field and metal foam flow field was also conducted. We made a transparent apparatus which can show the liquid water flow inside PEMFC. Furthermore, experiment for

comparing the air diffusivity of conventional flow field and metal foam flow field was conducted to investigate why PEMFC with metal foam flow field showed better performance.

5.2 Mixed metal foam flow field

5.2.1 Characteristics of metal foam cell size

In this section, the characteristics of metal foam cell size when it used as a flow field in PEMFC will be discussed. As discussed in chapter 4, the performance of PEMFC showed drastic improvement with metal foam flow field. Fig. 5.1 shows the polarization curve of PEMFC with metal foam flow fields and extended figure of polarization curve especially at the low current density region and high current density region. In case of low current density region, the difference is not that big, PEMFC with metal foam flow field which has cell size of 450 μm shows the best performance among the metal foam flow fields. Meanwhile, PEMFC with metal foam flow field which has cell size of 800 μm shows the best performance at the high current density region among the metal foam flow field.

These results can be explained the contact surface area and diffusion area of metal foam flow field. Since contact surface area and diffusion area influence on the performance of PEMFC [58], [64], the values of each area should be investigated. To verify the differences of metal foam flow fields, we compare the contact surface area of all meatal foam flow field. First of all,

microphotograph was used to measure the thickness of support of metal foam. Fig. 5.2 shows the microphotograph of all metal foams. Hence, we can obtain the thickness of metal foam through the microphotograph. However, shapes of pores are little bit uncertain. Although they look like polygonal shape, we need to make it clear. Therefore, we assumed four shapes square, hexagon, octagon and circle for metal foam shape. Moreover, we assumed that all polygonal figures have the same shape and size, and contact GDL evenly. In Table 5.1, the parameters of metal foam and results of calculation for contact surface area are presented. The contact surface of metal foam which has cell size of 800 μm is always the lowest in calculation. Meanwhile, cell size of 450 μm shows the greatest value of contact surface area. These results can explain the characteristics of PEMFC with metal foam flow field presented in Fig 5.1. Since large contact surface area can guarantee the high electric conductivity, metal foam flow field with cell size of 450 μm at low current density region where the ohmic losses of PEMFC is more dominant than the concentration losses of PEMFC. On the other hand, metal foam flow field with cell size of 800 μm has the smallest contact surface area, which means that it has a largest diffusion area among the all metal foam flow fields. Hence, this large diffusion area can make oxygen diffuse well at high current density region even though the problems of flooding and

oxygen depletion happen. As a result, we can conclude that the characteristics of metal foam flow fields occur because they have a different contact surface area and diffusion area when they applied to the PEMFC.

However, we still need to investigate the characteristics of diffusion area and contact surface area attaching with the resistance of fuel cell. Therefore, we investigated the effect of both areas on the resistance of fuel cell. First, Fig. 5.4 shows the values of diffusion area and contact surface area for different types of metal foams. As represented in Fig. 5.4, metal foam #3 which has cell size of 800 μm shows the highest diffusion area among the metal foams while metal foam #1 which has 800 μm represents the lowest diffusion area. Moreover, we investigated the high frequency resistance of fuel cell with contact surface area at the current density of 0.32 A/cm^2. As described in Fig. 5.5 (a), metal foam #1 has the smallest high frequency because it has the largest contact surface area which can guarantee the high electric conductivity. Meanwhile, the tendency get opposite when we measured the low frequency resistance at the current density of 1.28 A/cm^2. The metal foam #3 shows the smallest low frequency resistance since it has the lowest contact surface area, which means the space where air can diffuse is the largest among all metal foams. As a result, we could verify the effect of diffusion area and contact surface area on the fuel cell resistance.

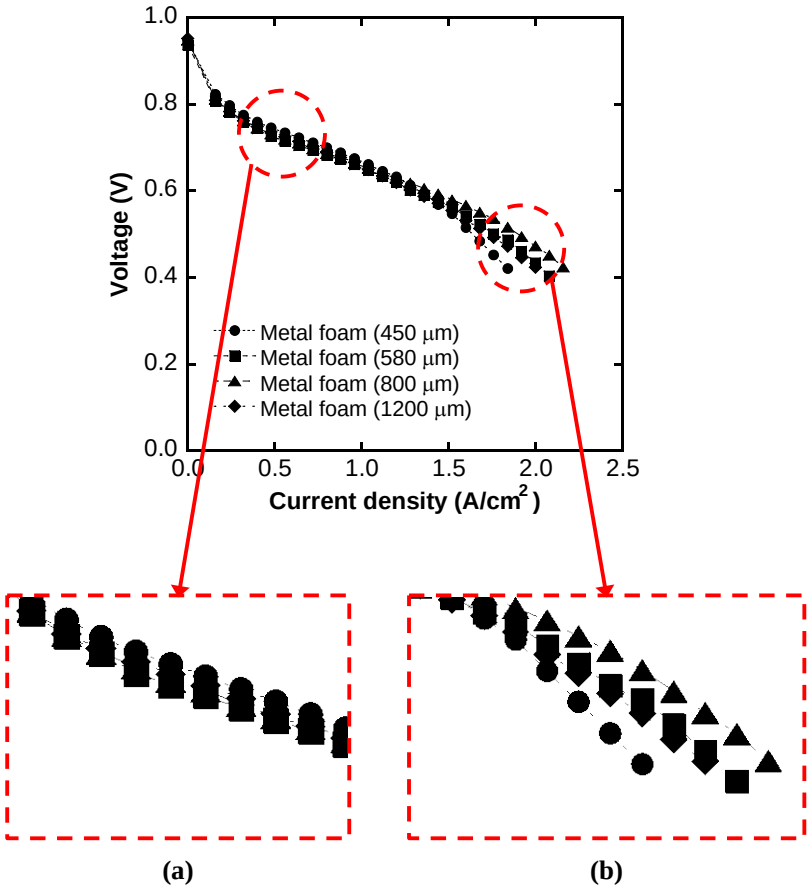

Fig. 5.1 Voltage of PEMFC with metal foam flow field at different current density region: (a) low current density region (b) high current density region

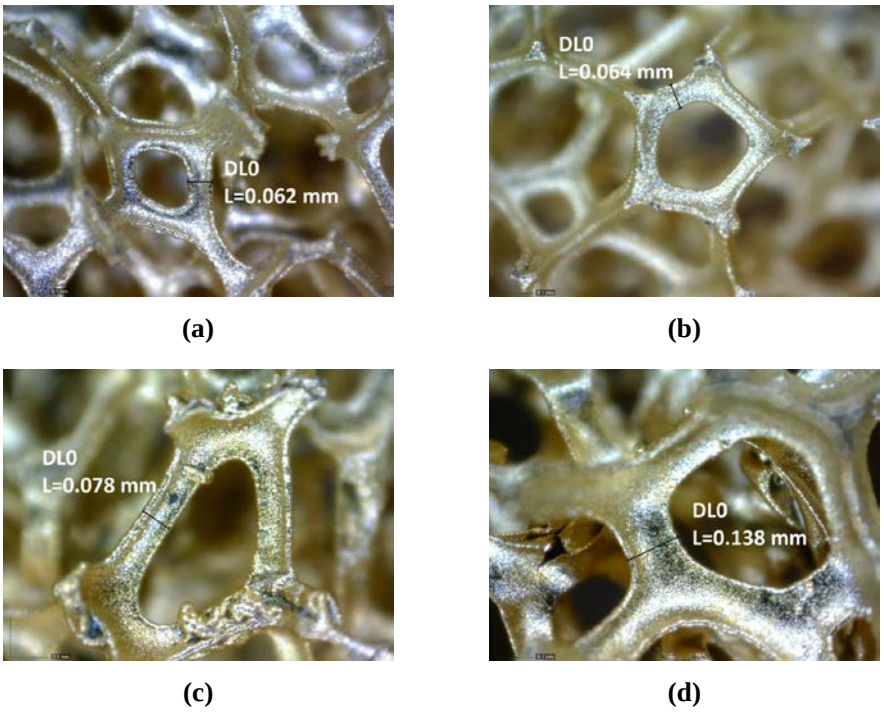

(a) **(b)**

(c) **(d)**

Fig. 5.2 Microphotograph for measuring the thickness of metal foam structure: (a) 450 μm (b) 580 μm (c) 800 μm (d) 1200 μm

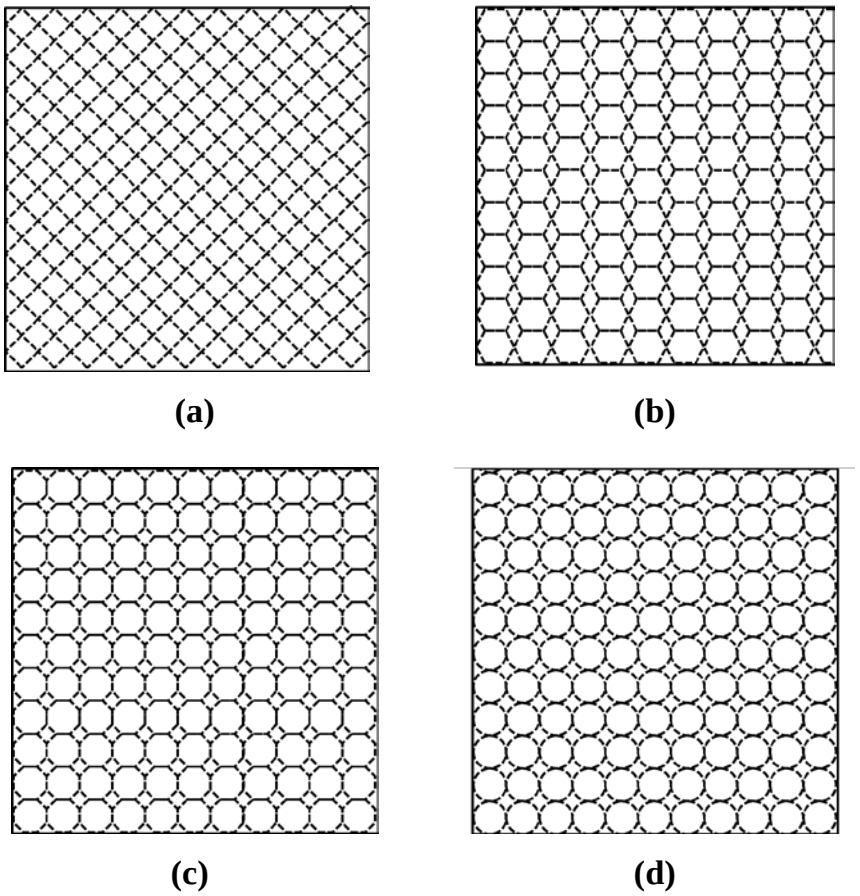

Fig. 5.3 Schematics of assumed shapes of metal foam: (a) square (b) hexagon (c) octagon (d) circle

Table 5.1 Results of calculating the contact surface area of metal foams

Cell size (μm)	Pore size (μm)	Support thickness (μm)	Contact surface area ($\times 10^{-3}$ m^2)			
			Square	Hexagon	Octagon	Circle
450	225	63	1.219	1.327	1.511	1.594
580	290	64	1.062	1.129	1.259	1.351
800	400	78	0.959	1.005	1.106	1.199
1200	600	138	1.088	1.155	1.296	1.381

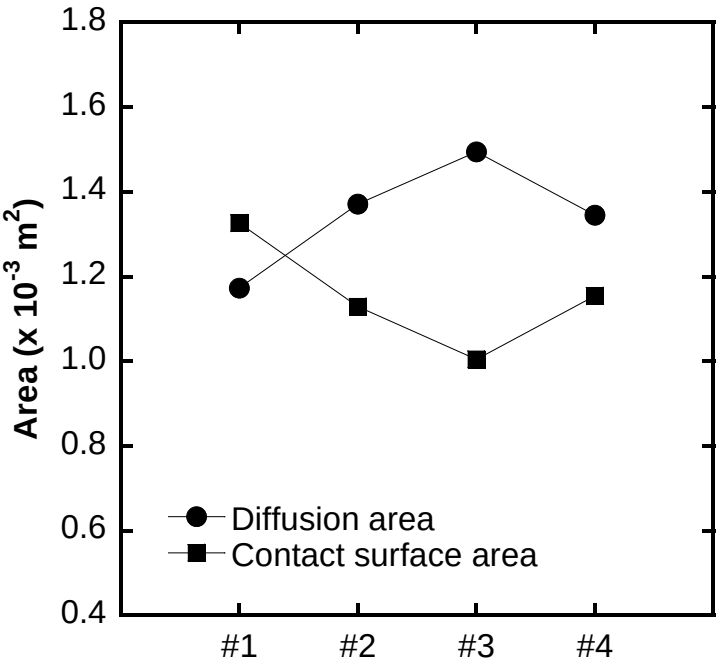

Fig. 5.4 Diffusion area and contact surface area of different metal foams

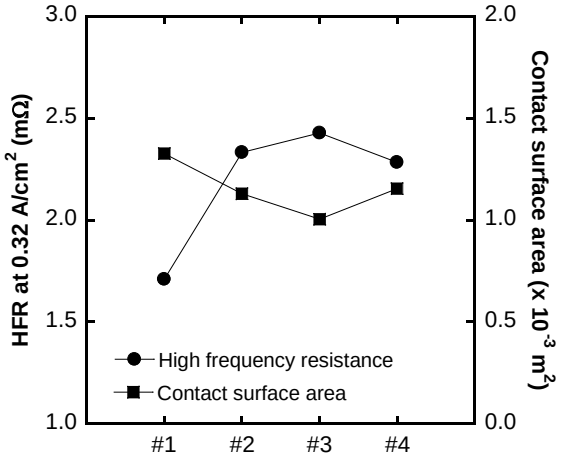

(a)

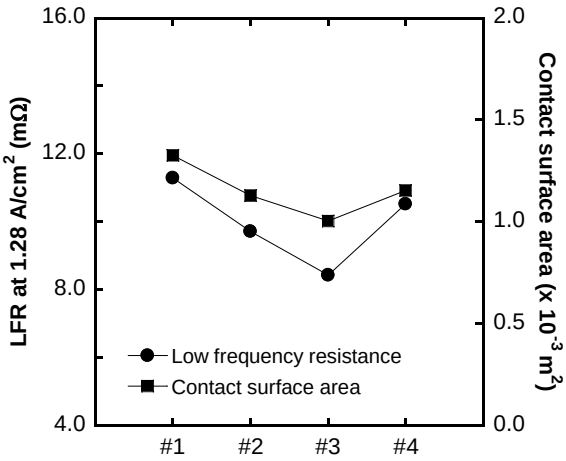

(b)

Fig. 5.5 Relation between contact surface area and resistance: (a) high frequency resistance (b) low frequency resistance

5.2.2 Fabrication of mixed metal foam

In this section, design of mixed metal foam will be introduced. In previous section 5.2.1, we found that each metal foam flow field has characteristics when it is applied to PEMFC because of its relationship contact surface area and diffusion area. Since liquid water move from inlet to outlet of flow field, most liquid water is supposed to remain at the region nearby outlet. Therefore, metal foam flow field which has large diffusion area is appropriate to the outlet area. Meanwhile, the front area of flow field retains less liquid water than outlet. Hence, we can conceive that contact surface area is important for front area. As a result, we designed mixed metal foam which contains two different metal foams. The metal foam which has cell size of 450 μm was used for the front triangle of flow filed to enhance contact surface area, and metal foam which has cell size of 800 μm was used for the rest triangle of flow field to improve the oxygen diffusion. Fig. 5.4 shows how mixed metal foam is assembled in cathode flow field. This mixed metal foam flow field was made and investigated their effect on the performance of PEMFC. The results will be discussed in the next section.

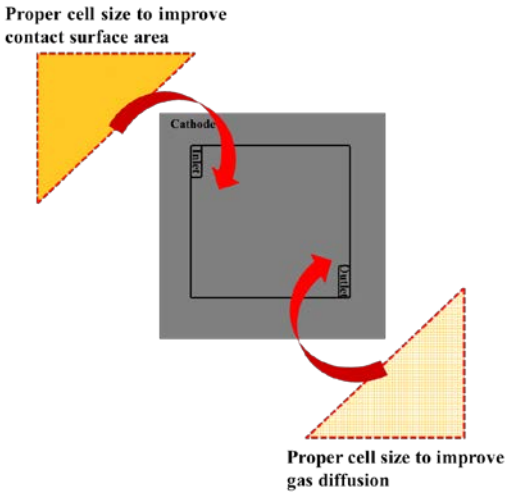

(a)

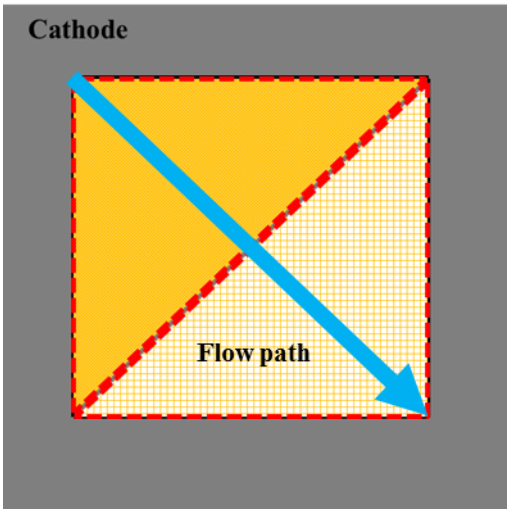

(b)

Fig. 5.6 Schematics of mixed metal foam: (a) assembly view (b) flow path

5.2.3 Performance of PEMFC with mixed metal foam flow field

In this section, the effect of mixed metal foam flow field on the performance of PEMFC will be introduced. The fabrication of mixed metal foam flow field is already shown in section 5.2.2. This mixed metal foam was applied to PEMFC and the performance was investigated. The experimental conditions are presented in Table 5.2. We will compare the performance of PEMFC with conventional, 450 μm metal foam flow field, 800 μm metal foam flow field, and mixed metal foam flow field to verify the effect of mixed metal foam on the performance of PEMFC.

Fig. 5.5 and Fig. 4.6 represent the polarization curve and power density curve of PEMFC with different types of flow fields at 60ºC and 40ºC of operating temperature. The results show that the PEMFC with mixed metal foam shows the better performance comparing with 450 μm metal foam flow field and 800 μm metal foam flow field. The PEMFC with mixed metal foam has advantage of 450 μm and 800 μm metal foam flow field. Even though its voltage is slightly lower that that with 450 μm at low current density region, it generates better performance at high current density even higher than PEMFC with 800 μm metal foam flow field. Large contact surface area of the 450 μm metal foam flow filed can reduce the ohmic losses of PEMFC while large diffusion area of 800 μm metal foam flow field enhance the

water management in PEMFC. As a result, the PEMFC with mixed metal foam generates the best performance among the different types of flow fields. When it comes to maximum power density, the PEMFC with mixed metal foam generates about 1.01 W/cm^2 at 1.92 A/cm^2, which means that maximum power density of PEMFC is improved about 60.1% comparing with that of PEMFC with conventional flow field. Furthermore, the maximum power density of PEMFC with mixed metal foam flow field is enhanced about 21.6% and 6.3% comparing with 450 μm metal foam flow field and 800 μm metal foam flow field respectively.

Table 5.2 Experimental conditions

Parameter	Value
T_c (°C)	40/60
SR_{an}	1.5
SR_{ca}	2.0
RH_{an} (%)	100
RH_{ca} (%)	100
Types of flow field	Conventional/ 450 μm metal foam/ 800 μm metal foam/ mixed metal foam

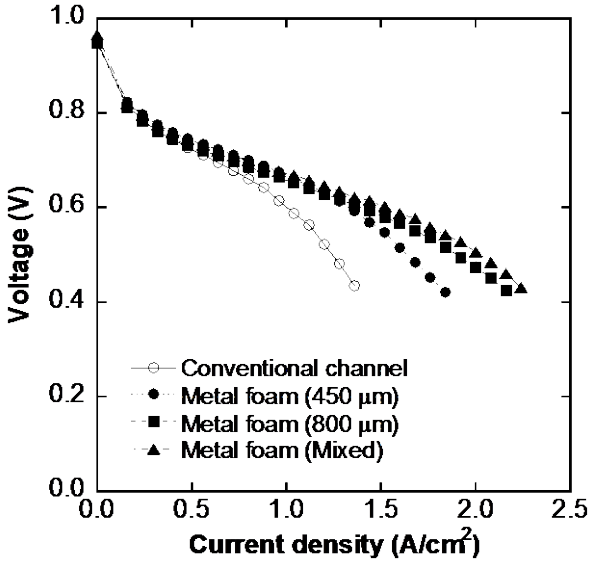

(a)

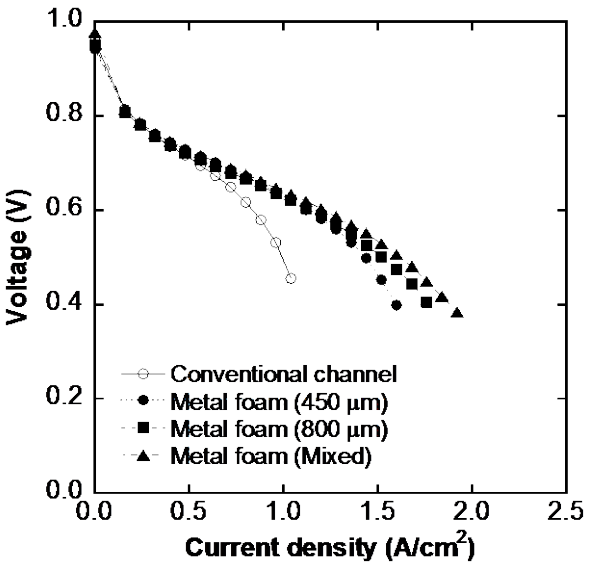

(b)

Fig. 5.7 Polarization curve of different types of flow fields: (a) T_c=60ºC (b) 40ºC

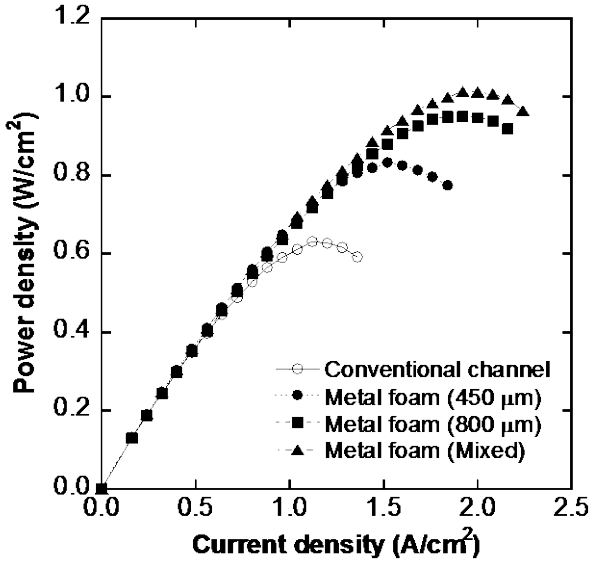

(a)

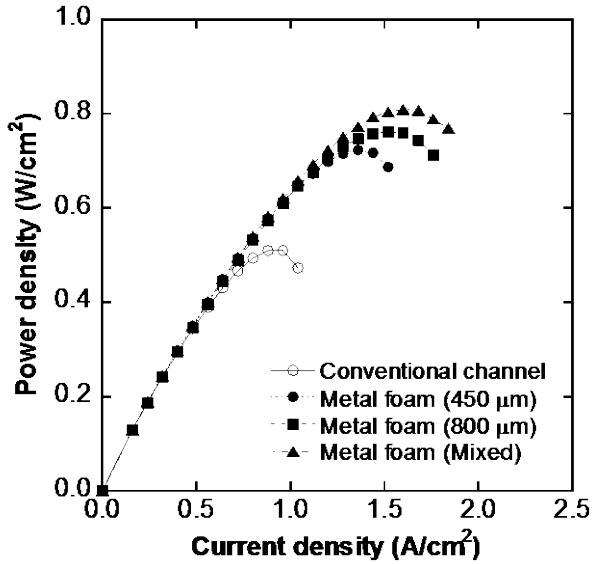

(b)

Fig. 5.8 Power density curve of different types of flow fields: (a) T_c=60ºC

(b) 40ºC

5.3 Visualization of metal foam flow field

5.3.1 Design of transparent cell

In this section, design of transparent cell will be introduced. The transparent cell was made for investigating the behavior of liquid water in conventional flow field and metal foam flow field. In Fig. 5.7, there are two pictures of transparent cell with conventional flow field and metal foam flow field. The flow field area is 9 cm^2 (3 cm × 3 cm). Moreover, conventional flow field has serpentine channel and metal foam flow field used metal foam which has cell size of 800 μm. At the inlet of flow field, humidified air was supplied and liquid water was provided into opposite side of flow field. Hence, liquid water penetrates into GDL, and was purged by providing air. This situation copied the liquid water behavior inside real PEMFC.

(a)

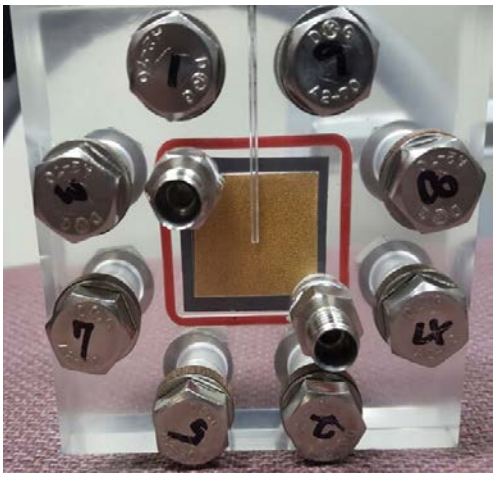

(b)

Fig. 5.9 Pictures of transparent cell with different types of flow fields: (a) conventional channel (b) metal foam flow field

5.3.2 Experimental conditions

Fig. 5.8 shows method of experiment for visualization. The transparent cell is used to investigate the behavior of liquid water in different flow fields. Liquid water is provided into opposite side of flow field and penetrated into GDL and flow field. Then, it is removed by the providing air. Moreover, a digital camera was used to verify the circumstance of liquid water in flow field. We used 39BC SIGRACET® GDL which is the same with used in chapter for investigating the performance of PEMFC. The conventional flow field has a serpentine shape channel and cell size of 800 μm metal foam flow field is used to compare the difference between conventional and metal foam flow field. The air was supplied as 2.0 Lpm to inlet of flow field, and 0.5 Lpm of liquid water was provided into opposite side of flow field. The flow path for liquid water is shape of serpentine channel.

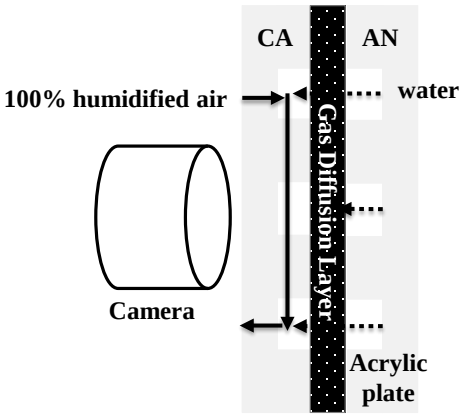

(a)

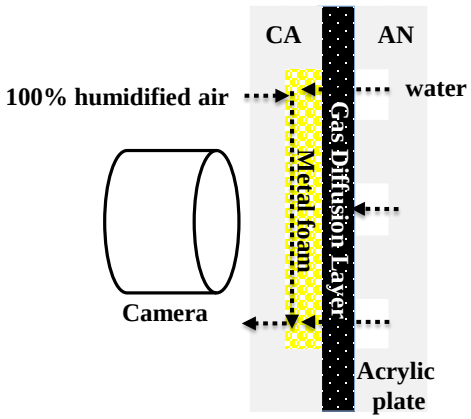

(b)

Fig. 5.10 Schematics of experimental process: (a) conventional channel (b) metal foam flow field

5.3.3 Result and discussion

In Fig. 5.9, there are two pictures showing the conventional flow field and metal foam flow field. Since penetrated liquid water from the GDL to flow field should be purged through the flow path of flow field, we can verify how produced water is removed in the different flow fields. In case of conventional channel, penetrated liquid water should be removed along the channels. Hence liquid water has to move long way from the penetrated site to outlet of flow field. Moreover, some liquid water remains on the channel forming liquid water film. Therefore, this liquid water film can be an obstacle for oxygen to diffuse to MEA. Furthermore, significant blockage problem also happens when liquid water grows and blocks the channel. Meanwhile, as verified in Fig. 5. 9 (b), liquid water in metal foam flow field should not move along the certain channel because there is no channel shape in metal foam flow field. Although some liquid water is accumulated at the bottom region of flow field, blockage is not that significant. As a result, we can verify that metal foam flow field has advantage in water management comparing with conventional flow field.

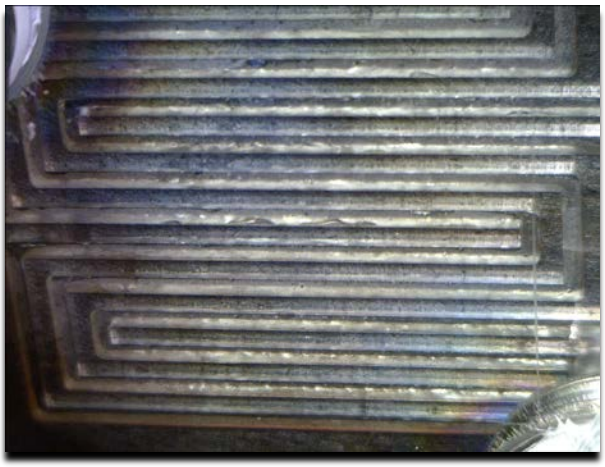

(a)

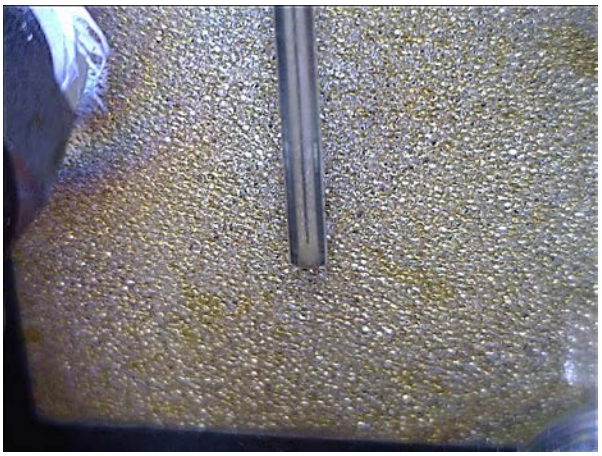

(b)

Fig. 5.11 Pictures of water behavior in different flow filed: (a) conventional channel (b) metal foam flow field

5.4 Summary

In this chapter, experiments for verifying the characteristics of metal foam flow field in PEMFC were introduced. The mixed metal foam flow field was suggested by the results of investigation for verifying the characteristics of metal foam flow fields. We found that metal foam flow field which has 450 μm cell size has an advantage on the mitigating the ohmic losses of PEMFC. Meanwhile metal foam flow field which has 800 μm cell size can improve the performance of PEMFC by mitigating the concentration losses. To combine the advantages of two metal foam flow field, we designed novel flow field made by using two metal foams to proper flow field region. As we divided the flow field and applied proper metal foam to the divided region, the maximum power density of PEMFC is enhanced by about 60.1% comparing with that of PEMFC with conventional flow field. Furthermore, transparent cell was designed to investigate the behavior of liquid water in conventional and metal foam flow field. As a result, we verified that metal foam flow field has an advantage in water management comparing with conventional flow field because there are no problems such as liquid water film, blockage, and long path for purging.

Chapter 6. Concluding remarks

In this study, two novel flow fields were suggested to improve the performance of PEMFC by mitigating the concentration losses. Since the needs of high performance and efficiency for PEMFC increases, reducing the concentration losses is one of the most important issues in research because the concentration losses cause drastic voltage drop of PEMFC when it operates at high operating region. Hence, the inclined channel and metal foam flow field were suggested and applied to PEMFC as a novel flow field and their effects and characteristics were investigated.

In chapter 2, three types of inclined channels were designed and applied to the cathode of PEMFC. As a result, the performance of PEMFC with inclined channels was improved and the results are verified through polarization curve, power curve, and EIS method. The results of EIS showed that the concentration losses of PEMFC decrease drastically when conventional channel was replaced with inclined channels. Moreover, pressure drop of conventional channel and inclined channels to evaluate the suitability of inclined channel to real PEMFC system. Although the pressure drop in inclined channel was larger than that in conventional channel, the difference is not enough to affect the net force of PEMFC. Finally the

PEMFC with proper inclined channel show about 27.9% of improvement in maximum power at operating temperature of 60ºC, and 20.8% at 40ºC.

In chapter 3, numerical analysis for investigating the effects of inclined channel on the performance of PEMFC was introduced. The results of numerical analysis for calculating the oxygen diffusion form the channel to MEA with conventional channel and inclined channel showed that inclined channel make oxygen diffuse well from channel to MEA comparing with conventional channel. This result can explain the mitigation of concentration losses in inclined channels. Furthermore, the droplet behavior in conventional channel and inclined channel was analyzed numerically. We calculated the forces exerting on the droplet in conventional channel and inclined channel. As a result, we obtained the net power on the droplet, and we found that droplet moves faster in inclined channel comparing with conventional channel. Hence, we concluded that the inclined channel make oxygen diffuse better from channel to MEA and easily removed the produced liquid water in flow channel.

In chapter 4, the metal foam flow field was introduced. We suggested four types of metal foam flow field which have the different cell sizes, and the performance of PEMFC with them was investigated. As a result, the maximum power density of PEMFC was improved by about 50.6% when

conventional flow field was replaced with metal foam flow field which has a cell size of 800 μm. Moreover, we verified that metal foam flow field make pressure drop decreased. The experiment for stability of PEMFC verified that PEMFC with metal foam flow field even showed better stability than that of PEMFC with conventional flow field.

In chapter 5, advanced experiment was discussed. We conducted experiment for verifying the characteristics of metal foam flow field in PEMFC. As a result, we suggested novel mixed metal foam flow field made by combining two different metal foam flow field. Through the investigation of characteristics of PEMFC with different metal foam flow fields, we found that 450 μm metal foam flow field improved the electrical conductivity of PEMFC, and metal foam flow field which has 800 μm cell size can mitigate the concentration losses drastically. Hence, we verified that the maximum power density of PEMFC with mixed metal foam is enhanced by about 60.1% comparing with the maximum power density of PEMFC with conventional flow field. Furthermore, transparent cell was designed to investigate the behavior of liquid water in conventional and metal foam flow field. We verified that metal foam flow field has an advantage in water management because it can solve the problems in conventional flow field such as liquid water film, blockage, and long path for purging.

To enhance the performance of PEMFC, two different flow fields were designed and suggested. Through the results of experiment for evaluating the performance of PEMFC with different flow fields, we verified that both inclined channel and metal foam flow field can improve the performance of PEMFC intensely. Moreover, we investigated the reason of performance improvement of PEMFC by conducting numerical analysis and advanced experiments. Hence, this study is meaningful since it suggested novel directions for improving the performance of PEMFC and parameters we have to consider.

References

[1] D. Spernjak, A. K. Prasad, and S. G. Advani, “Experimental investigation of liquid water formation and transport in a transparent single-serpentine PEM fuel cell,” *J. Power Sources*, vol. 170, no. 2, pp. 334–344, 2007.

[2] A. Bazylak, D. Sinton, and N. Djilali, “Dynamic water transport and droplet emergence in PEMFC gas diffusion layers,” *J. Power Sources*, vol. 176, no. 1, pp. 240–246, 2008.

[3] K. Tüber, D. Pócza, and C. Hebling, “Visualization of water buildup in the cathode of a transparent PEM fuel cell,” *J. Power Sources*, vol. 124, no. 2, pp. 403–414, 2003.

[4] S. Shimpalee and V. Lilavivat, “Study of Water Droplet Removal on Etched-Metal Surfaces for Proton Exchange Membrane Fuel Cell Flow Channel,” *J. Electrochem. Energy Convers. Storage*, vol. 13, no. 1, p. 11003, 2016.

[5] P. Deevanhxay, T. Sasabe, S. Tsushima, and S. Hirai, “Observation of dynamic liquid water transport in the microporous layer and gas diffusion layer of an operating PEM fuel cell by high-resolution soft X-ray radiography,” *J. Power Sources*, vol. 230, pp. 38–43, 2013.

[6] X. Zhu, Q. Liao, P. C. Sui, and N. Djilali, “Numerical investigation of

water droplet dynamics in a low-temperature fuel cell microchannel: Effect of channel geometry," *J. Power Sources*, vol. 195, no. 3, pp. 801–812, 2010.

[7] E. C. Kumbur, K. V. Sharp, and M. M. Mench, "Liquid droplet behavior and instability in a polymer electrolyte fuel cell flow channel," *J. Power Sources*, vol. 161, no. 1, pp. 333–345, 2006.

[8] J. G. Carton, V. Lawlor, a. G. Olabi, C. Hochenauer, and G. Zauner, "Water droplet accumulation and motion in PEM (Proton Exchange Membrane) fuel cell mini-channels," *Energy*, vol. 39, no. 1, pp. 63–73, 2012.

[9] R. M. Rao, D. Bhattacharyya, R. Rengaswamy, and S. R. Choudhury, "A two-dimensional steady state model including the effect of liquid water for a PEM fuel cell cathode," *J. Power Sources*, vol. 173, no. 1, pp. 375–393, 2007.

[10] D. Natarajan and T. Van Nguyen, "Three-dimensional effects of liquid water flooding in the cathode of a PEM fuel cell," *J. Power Sources*, vol. 115, no. 1, pp. 66–80, 2003.

[11] X. Zhang and Y. Gao, "Impact of liquid water on oxygen reaction in cathode catalyst layer of proton exchange membrane fuel cell: A simple and physically sound model," *J. Power Sources*, vol. 318, pp.

251–263, 2016.

[12] G. Lin, W. He, and T. Van Nguyen, “Modeling Liquid Water Effects in the Gas Diffusion and Catalyst Layers of the Cathode of a PEM Fuel Cell,” *J. Electrochem. Soc.*, vol. 151, no. 12, p. A1999, 2004.

[13] I. V. Zenyuk, D. Y. Parkinson, G. Hwang, and A. Z. Weber, “Probing water distribution in compressed fuel-cell gas-diffusion layers using X-ray computed tomography,” *Electrochem. commun.*, vol. 53, pp. 24–28, 2015.

[14] J. H. Nam and M. Kaviany, “Effective diffusivity and water-saturation distribution in single- and two-layer PEMFC diffusion medium,” *Int. J. Heat Mass Transf.*, vol. 46, no. 24, pp. 4595–4611, 2003.

[15] P. Deevanhxay, T. Sasabe, S. Tsushima, and S. Hirai, “Effect of liquid water distribution in gas diffusion media with and without microporous layer on PEM fuel cell performance,” *Electrochem. commun.*, vol. 34, pp. 239–241, 2013.

[16] Z. H. Wang, C. Y. Wang, and K. S. Chen, “Two-phase flow and transport in the air cathode of proton exchange membrane fuel cells,” *J. Power Sources*, vol. 94, no. 1, pp. 40–50, 2001.

[17] F. Y. Zhang, X. G. Yang, and C. Y. Wang, “Liquid Water Removal from a Polymer Electrolyte Fuel Cell,” *J. Electrochem. Soc.*, vol. 153,

no. 2, p. A225, 2006.

[18] N. S. M. Hassan, W. R. W. Daud, K. Sopian, and J. Sahari, “Water management in a single cell proton exchange membrane fuel cells with a serpentine flow field,” *J. Power Sources*, vol. 193, no. 1, pp. 249–257, 2009.

[19] S.-H. Ge, X.-G. Li, and I.-M. Hsing, “Water Management in PEMFCs Using Absorbent Wicks,” *J. Electrochem. Soc.*, vol. 151, no. 9, pp. B523–B528, 2004.

[20] C. R. Buie *et al.*, “Water management in proton exchange membrane fuel cells using integrated electroosmotic pumping,” *J. Power Sources*, vol. 161, no. 1, pp. 191–202, 2006.

[21] A. Turhan, K. Heller, J. S. Brenizer, and M. M. Mench, “Passive control of liquid water storage and distribution in a PEFC through flow-field design,” *J. Power Sources*, vol. 180, pp. 773–783, 2008.

[22] K. Choi, H. Kim, and S. Moon, “Numerical studies on the geometrical characterization of serpentine flow-field for efficient PEMFC,” *Int. J. Hydrogen Energy*, vol. 36, no. 2, pp. 1613–1627, 2010.

[23] A. Kumar and R. G. Reddy, “Effect of channel dimensions and shape in the flow-field distributor on the performance of polymer electrolyte membrane fuel cells,” *J. Power Sources*, vol. 113, no. 1, pp. 11–18,

2003.

[24] A. P. Manso, F. F. Marzo, M. G. Mujika, J. Barranco, and A. Lorenzo, “Numerical analysis of the influence of the channel cross-section aspect ratio on the performance of a PEM fuel cell with serpentine flow field design,” *Int. J. Hydrogen Energy*, vol. 36, no. 11, pp. 6795–6808, 2011.

[25] A. P. Manso, F. F. Marzo, J. Barranco, X. Garikano, and M. Garmendia Mujika, “Influence of geometric parameters of the flow fields on the performance of a PEM fuel cell. A review,” *Int. J. Hydrogen Energy*, vol. 37, no. 20, pp. 15256–15287, 2012.

[26] J. Scholta, G. Escher, W. Zhang, L. K??ppers, L. J??rissen, and W. Lehnert, “Investigation on the influence of channel geometries on PEMFC performance,” *J. Power Sources*, vol. 155, no. 1, pp. 66–71, 2006.

[27] X. Wang, Y. Duan, W. Yan, and X. Peng, “Effects of flow channel geometry on cell performance for PEM fuel cells with parallel and interdigitated flow fields,” *Electrochim. Acta*, vol. 53, pp. 5334–5343, 2008.

[28] L. I. N. Lin, Z. Xinxin, F. Huting, and W. Xiaodong, “Optimization of a serpentine flow field with variable channel heights and widths for

PEM fuel cells," vol. 53, no. 2, pp. 453–460, 2010.

[29] H. C. Liu, W. M. Yan, C. Y. Soong, F. Chen, and H. S. Chu, "Reactant gas transport and cell performance of proton exchange membrane fuel cells with tapered flow field design," vol. 158, pp. 78–87, 2006.

[30] Y. Xu, L. Peng, P. Yi, and X. Lai, "Analysis of the flow distribution for thin stamped bipolar plates with tapered channel shape," *Int. J. Hydrogen Energy*, vol. 41, no. 9, pp. 5084–5095, 2016.

[31] W. Yan, H. Li, P. Chiu, and X. Wang, "Effects of serpentine flow field with outlet channel contraction on cell performance of proton exchange membrane fuel cells," vol. 178, pp. 174–180, 2008.

[32] X. Wang *et al.*, "An inverse geometry design problem for optimization of single serpentine flow field of PEM fuel cell," *Int. J. Hydrogen Energy*, vol. 35, no. 9, pp. 4247–4257, 2010.

[33] S. LEONARDI, P. ORLANDI, R. J. SMALLEY, L. DJENIDI, and R. A. ANTONIA, "Direct numerical simulations of turbulent channel flow with transverse square bars on one wall," *J. Fluid Mech.*, vol. 491, p. S0022112003005500, 2003.

[34] S. A. Isaev, A. I. Leontiev, N. A. Kudryavtsev, and I. A. Pyshnyi, "Numerical Simulation of Vortex Enhancement of Heat Transfer under Conditions of Turbulent Flow Past a Spherical Dimple on the Wall of

a Narrow Channel," *Heat Mass Transf. Phys. Gasdyn.*, vol. 41, no. 2, pp. 229–232, 2003.

[35] X. Wang, Y. Duan, and W. Yan, "Numerical study of cell performance and local transport phenomena in PEM fuel cells with various flow channel area ratios," *J. Power Sources*, vol. 172, pp. 265–277, 2007.

[36] B. Chernyavsky, P. C. Sui, B. S. Jou, and N. Djilali, "Turbulent flow in the distribution header of a PEM fuel cell stack," *Int. J. Hydrogen Energy*, vol. 36, no. 12, pp. 7136–7151, 2011.

[37] B. Dargahi, "The turbulent flow field around a circular cylinder," *Exp. Fluids*, vol. 8, no. 1–2, pp. 1–12, 1989.

[38] É. Fontana *et al.*, "Study of the effects of flow channel with non-uniform cross-sectional area on PEMFC species and heat transfer," vol. 54, pp. 4462–4472, 2011.

[39] L. Peng, X. Lai, P. Hu, and J. Ni, "Flow channel shape optimum design for hydroformed metal bipolar plate in PEM fuel cell," *J. Power Sources*, vol. 178, pp. 223–230, 2008.

[40] D. Chang and S. Wu, "The effects of channel depth on the performance of miniature proton exchange membrane fuel cells with serpentine-type flow fields," *Int. J. Hydrogen Energy*, vol. 40, no. 35, pp. 11659–11667, 2015.

[41] W. Yan, H. Liu, C. Soong, F. Chen, and C. H. Cheng, “Numerical study on cell performance and local transport phenomena of PEM fuel cells with novel flow field designs,” *J. Power Sources*, vol. 161, pp. 907–919, 2006.

[42] X.-D. Wang, Y.-Y. Duan, and W.-M. Yan, “Novel serpentine-baffle flow field design for proton exchange membrane fuel cells,” *J. Power Sources*, vol. 173, no. 1, pp. 210–221, 2007.

[43] M. Rahimi-Esbo, A. A. Ranjbar, A. Ramiar, E. Alizadeh, and M. Aghaee, “Improving PEM fuel cell performance and effective water removal by using a novel gas flow field,” *Int. J. Hydrogen Energy*, vol. 41, no. 4, pp. 3023–3037, 2016.

[44] C. Y. Soong, W. M. Yan, C. Y. Tseng, H. C. Liu, F. Chen, and H. S. Chu, “Analysis of reactant gas transport in a PEM fuel cell with partially blocked fuel flow channels,” *J. Power Sources*, vol. 143, no. 1–2, pp. 36–47, 2005.

[45] H. C. Liu, W. M. Yan, C. Y. Soong, and F. Chen, “Effects of baffle-blocked flow channel on reactant transport and cell performance of a proton exchange membrane fuel cell,” *J. Power Sources*, vol. 142, no. 1–2, pp. 125–133, 2005.

[46] H. Heidary, M. J. Kermani, A. K. Prasad, S. G. Advani, and B. Dabir,

"Numerical modelling of in-line and staggered blockages in parallel flowfield channels of PEM fuel cells," *Int. J. Hydrogen Energy*, vol. 42, no. 4, pp. 2265–2277, 2017.

[47] Y. Qin, X. Li, K. Jiao, Q. Du, and Y. Yin, "Effective removal and transport of water in a PEM fuel cell flow channel having a hydrophilic plate," *Appl. Energy*, vol. 113, pp. 116–126, 2014.

[48] S. Han, N. Choi, and Y. Choi, "Simulation and experimental analysis on the performance of PEM fuel cell by the wave-like surface design at the cathode channel," *Int. J. Hydrogen Energy*, vol. 39, pp. 2628–2638, 2014.

[49] A. Kumar and R. G. Reddy, "Materials and design development for bipolar/end plates in fuel cells," *J. Power Sources*, vol. 129, no. 1 SPEC. ISS., pp. 62–67, 2004.

[50] B. Tsai *et al.*, "Effects of flow field design on the performance of a PEM fuel cell with metal foam as the flow distributor," *Int. J. Hydrogen Energy*, vol. 37, no. 17, pp. 13060–13066, 2012.

[51] F. Zhang, S. Cheng, D. Pant, G. Van Bogaert, and B. E. Logan, "Power generation using an activated carbon and metal mesh cathode in a microbial fuel cell," *Electrochem. commun.*, vol. 11, no. 11, pp. 2177–2179, 2009.

[52] a. K. Srouji, L. J. Zheng, R. Dross, a. Turhan, and M. M. Mench, "Ultra-high current density water management in polymer electrolyte fuel cell with porous metallic flow field," *J. Power Sources*, vol. 239, no. 2013, pp. 433–442, 2013.

[53] a. K. Srouji, L. J. Zheng, R. Dross, a. Turhan, and M. M. Mench, "Performance and mass transport in open metallic element architecture fuel cells at ultra-high current density," *J. Power Sources*, vol. 218, no. 2012, pp. 341–347, 2012.

[54] S. Tanaka and T. Shudo, "Experimental and numerical modeling study of the electrical resistance of gas diffusion layer-less polymer electrolyte membrane fuel cells," *J. Power Sources*, vol. 278, pp. 382–395, 2015.

[55] S. Tanaka and T. Shudo, "Corrugated mesh flow channel and novel microporous layers for reducing flooding and resistance in gas diffusion layer-less polymer electrolyte fuel cells," *J. Power Sources*, vol. 268, pp. 183–193, 2014.

[56] S. Tanaka and T. Shudo, "Significant performance improvement in terms of reduced cathode flooding in polymer electrolyte fuel cell using a stainless-steel microcoil gas flow field," *J. Power Sources*, vol. 248, pp. 524–532, 2014.

[57] S. Asghari, A. Mokmeli, and M. Samavati, “Study of PEM fuel cell performance by electrochemical impedance spectroscopy,” *Int. J. Hydrogen Energy*, vol. 35, no. 17, pp. 9283–9290, 2010.

[58] Z. Xie and S. Holdcroft, “Polarization-dependent mass transport parameters for orr in perfluorosulfonic acid ionomer membranes : an EIS study using microelectrodes,” *J. Electroanal. Chem.*, vol. 568, pp. 247–260, 2004.

[59] A. Dicks and J. Larminie, *Fuel Cell Systems Explained*. New York, 2000.

[60] R. O’Hayre, S.-W. Cha, W. Colella, and F. B. Prinz, *FUEL CELL FUNDAMENTALS*. New York: John Wiley & Sons, 2006.

[61] A. Esposito, A. D. Montello, Y. G. Guezennec, and C. Pianese, “Experimental investigation of water droplet-air flow interaction in a non-reacting PEM fuel cell channel,” *J. Power Sources*, vol. 195, no. 9, pp. 2691–2699, 2010.

[62] A. Theodorakakos, T. Ous, M. Gavaises, J. M. Nouri, N. Nikolopoulos, and H. Yanagihara, “Dynamics of water droplets detached from porous surfaces of relevance to PEM fuel cells,” *J. Colloid Interface Sci.*, vol. 300, no. 2, pp. 673–687, 2006.

[63] Y. Wang, “Porous-Media Flow Fields for Polymer Electrolyte Fuel

Cells," *J. Electrochem. Soc.*, vol. 156, no. 10, pp. 1134–1141, 2009.

[64] W. Kaiser and G. Bo, "Metallic bipolar plates for PEM fuel cells," *J. Power Sources*, vol. 105, pp. 256–260, 2002.

국 문 초 록

고분자 전해질막 연료전지의 상용화를 위해서는 점차 증대되고 있는 고출력과 고효율에 대한 요구를 만족 시킬 수 있는 고출력 고분자 전해질막 연료전지의 개발이 필수적이다. 이를 위해서는 고부하 영역에서 연료전지의 성능을 급격히 감소시키는 물질전달손실을 완화시키는 방안에 대한 연구가 필요하다. 물질전달손실은 플러딩, 산소고갈 등과 같은 원인으로 인하여 발생하며, 이러한 원인을 방지함으로써 물질전달손실을 줄여야 연료전지의 고출력 운전이 가능해진다. 본 연구에서는 연료전지의 고부하 영역 운전에 직접적인 영향을 미치는 물질전달손실을 완화시키기 위하여 새롭게 고안 된 두 가지의 유로를 제안하였다.

먼저 기존의 채널과 달리 유로의 길이에 따라 점차 유로의 깊이가 줄어드는 인클라인드 채널을 고안하여 고분자 전해질막 연료전지의 양극에 적용하였다. 분압 곡선, 출력 곡선, 전기화학 임피던스 측정을 통해 기존의 채널을 이용하는 연료전지와 성능 및 특성을 비교하였으며, 입출구부의 압력강하를 측정하여 주변장치에서 소모되는 일을 고려하여 연료전지의 전체 성능을 평가하였다. 결과적으로 인클라인드 채널을 적용한 연료전지는 기존의 채널을 적용한 연료전지와 비교하여 높은 성능을 나타내었으며, 이는 수학적 분석을 통하여 다시 한번 증명되었다. 인클라인드 채널을 적용할 경우 채널내부에서 막전극접합체로 확산되는 산소의 양이 증가되는 것을 확인 하였으며, 채널 내부의 액적 거동을 분석함으로써 인클라인드 채널이 기존의 채널보다 물 배출에도 용이함을 확인하였다.

메탈폼을 사용하는 새로운 다공성 유로는 기존의 연료전지 유로와는 전혀 다른 형태로, 기존의 유로가 가지는 문제점을 해결할 수 있는 새로운 형태의 유로이다. 기존의 유로가 구조적 문제로 인해 산소의 확산을 막고 생성되는 물을 제대로 배출하지 못하는 문제

점이 있는 반면, 메탈폼 유로는 기체의 확산을 용이하게 하고 생성되는 물을 효과적으로 관리함으로써 연료전지의 성능을 크게 향상시켰다. 이는 분극 곡선과 출력 곡선, 전기화학 임피던스 기법을 통하여 분석되었으며, 단순한 성능 향상뿐만 아니라 출력의 안정성 또한 향상되는 것을 실험을 통해 확인하였다. 더불어, 메탈폼 유로가 적용된 연료전지의 성능 특성을 파악하고, 유동의 위치에 따른 알맞은 유로의 형상을 제시함으로써 두 종류의 메탈폼을 결합한 형태의 새로운 다공성 유로를 고안하였다. 이를 통해 기존의 유로를 사용하는 연료전지의 성능은 물론, 한 종류의 메탈폼을 사용한 다공성 유로보다 높은 출력을 발생시키는 새로운 유로를 제안하였다.

주요어: 고분자 전해질막 연료전지, 양성자 교환막 연료전지, 고출력, 출력향상, 인클라인드채널, 다공성 유로, 메탈폼

학 번: 2014-30290